A Germinal Center Checkpoint of AIRE in B Cells Limits Antibody Diversification

Jordan Z. Zhou[1,2,21], Bihui Huang[1,3,21], Bo Pei,[1], Guang Wen Sun[4], Michael D. Pawlitz[1], Wei Zhang[5], Xinyang Li[5], Kati C. Hokynar[6], Fayi Yao[1,2], Madusha L. W. Perera[7], Shanqiao Wei[7], Simin Zheng[8], Lisa A. Polin[9], Janet M. Poulik[10], Annamari Ranki[11], Kai Krohn[12], Charlotte Cunningham-Rundles[13], Naibo Yang[5,14], Ashok S. Bhagwat[7,15], Kefei Yu[16], Pärt Peterson[17], Kai Kisand[17], Bao Q. Vuong[18], Andrea Cerutti[13,19], Kang Chen[1,8,20,*]

[1]Department of Obstetrics and Gynecology, Wayne State University, Detroit, MI 48201, USA

[2]Center for Molecular Medicine and Genetics, Wayne State University, Detroit, MI 48201, USA

[3]The Seventh Affiliated Hospital of Sun Yat-Sen University, Shenzhen, Guangdong 518107, China

[4]School of Applied Science, Republic Polytechnic, Singapore 738984, Singapore

[5]Beijing Genomics Institute (BGI)-Shenzhen, Guangdong 518083, China

[6]Department of Virology, University of Helsinki, Helsinki 00029, Finland

[7]Department of Chemistry, Wayne State University, Detroit, MI 48202, USA

[8]School of Biological Sciences, Nanyang Technological University, Singapore 636921, Singapore.

[9]Barbara Ann Karmanos Cancer Institute, Department of Oncology, Wayne State University, Detroit, MI 48201, USA

[10]Department of Pathology, Children's Hospital of Michigan, Detroit, MI 48201, USA

[11]Department of Dermatology and Allergic Diseases, University of Helsinki and Helsinki University Hospital, Helsinki 00250, Finland

[12]Helsinki University Hospital Research Institute, Biomedicum, Helsinki 00290, Finland

[13]Immunology Institute, Icahn School of Medicine at Mount Sinai, New York, NY 10029, USA

[14]Complete Genomics Inc., Mountain View, California 94043, USA

[15]Department of Biochemistry, Microbiology and Immunology, Wayne State University, Detroit, MI 48201, USA

[16]Department of Microbiology and Molecular Genetics, Michigan State University, East Lansing, MI 48824, USA

[17]Department of Molecular Pathology, Institute of Biomedicine and Translational Medicine, University of Tartu, Tartu 50411, Estonia

[18]Department of Biology, City College of New York, New York, NY 10031, USA

[19]Mucosal Immunology Studies Team, National Institute of Allergy and Infectious Diseases, National Institutes of Health, Maryland 20892, USA

[20]Lead Contact

[21]These authors contributed equally.

*Correspondence: kang@wayne.edu

SUMMARY

In response to antigens, B cells undergo affinity maturation and class switching mediated by activation-induced cytidine deaminase (AID) in germinal centers (GCs) of secondary lymphoid organs, but uncontrolled AID activity can precipitate autoimmunity and cancer. The regulation of GC antibody diversification is of fundamental importance but not well understood. We found that autoimmune regulator (AIRE), the molecule essential for T cell tolerance, is expressed in GC B cells in a CD40-dependent manner, interacts with AID and negatively regulates antibody affinity maturation and class switching by inhibiting AID function. AIRE deficiency in B cells caused altered antibody repertoire, increased somatic hypermutations, elevated autoantibodies to T helper 17 effector cytokines and defective control of skin *Candida albicans*. These results define a GC B cell checkpoint of humoral immunity and illuminate new approaches of generating high-affinity neutralizing antibodies for immunotherapy.

KEYWORDS

Humoral immunity; checkpoint; B cell; antibody diversification; germinal center; AIRE; AID; immunodeficiency; autoimmunity; immunotherapy

INTRODUCTION

A properly diversified and selected repertoire of antibodies is essential for effective immune defense against diverse pathogens as well as the prevention of autoimmune diseases. After V(D)J recombination in the bone marrow (BM) that generates a primary antibody repertoire, B lymphocytes enter GCs of secondary lymphoid organs, such as the lymph nodes, spleen, tonsils and mucosa-associated lymphoid tissues, to further diversify their antibody repertoire in response

to antigens by undergoing class switch recombination (CSR) and somatic hypermutation (SHM), both of which are mediated by the DNA-cytosine deaminase AID (Muramatsu et al., 2000; Revy et al., 2000). SHM introduces point mutations in immunoglobulin (Ig) variable region exons for selection of higher-affinity antibody clones by antigens, whereas CSR replaces Ig constant region exons encoding IgM and IgD with those encoding IgG, IgA, or IgE to provide antibodies with new effector functions (Murphy and Weaver, 2016b). However, aberrant AID activity in B cells can cause mutations in non-Ig loci to precipitate cancer (Casellas et al., 2016), and AID-mediated GC reaction can generate autoreactive antibodies to drive many autoimmune diseases (Vinuesa et al., 2009). The absence of B cell lymphomas and overt autoimmune diseases in healthy individuals amidst ongoing humoral immune responses reflect the existence of physiological mechanisms that restrain AID-mediated antibody diversification in GC B cells. The details of these mechanisms are of fundamental importance but not fully understood.

Humoral immunity is regulated by cell-mediated immunity, in which the molecule AIRE induces the expression of peripheral tissue-specific antigens (TSAs) in medullary epithelial cells (mTECs) and B cells in the thymus to promote the negative selection of self-reactive T cells or their conversion into regulatory T (Treg) cells (Anderson et al., 2002; Malchow et al., 2013; Yamano et al., 2015). AIRE is also expressed in specialized extrathymic cells (eTACs) that can inactivate self-reactive T cells in the periphery (Gardner et al., 2008; Gardner et al., 2013). Loss-of-function mutations in the *AIRE* gene cause autoimmune polyglandular syndrome type 1 (APS-1) (Finnish-German, 1997; Nagamine et al., 1997) associated with organ-specific autoimmunity, aberrant production of autoantibodies and increased susceptibility to mucocutaneous infection by *Candida albicans*, an otherwise innocuous commensal microbe in humans. Mysteriously, APS-1 patients can produce high-affinity neutralizing antibodies against T helper 17 (T_H17) effector

cytokines, which has been suggested to negatively impact anti-fungal immune defense (Kisand et al., 2010; Meyer et al., 2016; Puel et al., 2010). In light of these findings, we sought to determine whether AIRE has a B cell-intrinsic role in regulating peripheral antibody diversification.

Here we show that AIRE is expressed in GC B cells in a CD40-dependent manner, interacts with AID, and negatively regulates AID-mediated peripheral antibody diversification. AIRE-deficient mouse B cells undergo elevated class switching and affinity maturation after antigenic stimulation, which correlates with enhanced generation of genomic uracil, elevated Ig SHM, augmented AID targeting to Ig switch (S) regions and increased interaction of AID with transcriptionally stalled RNA polymerase II (Pol II). In addition, naive B cells of APS-1 patients undergo increased CSR upon stimulation. Mice with AIRE deficiency in B cells have elevated levels of autoantibodies against T helper 17 (T_H17) effector cytokines and heightened skin *C. albicans* burden after infection, which recapitulates the symptoms of APS-1 patients. Our results define a previously unknown but crucial B cell-intrinsic AIRE-mediated GC checkpoint of peripheral antibody diversification that limits autoimmunity.

RESULTS

GC B Cells Express AIRE

Secondary lymphoid organs are the major sites for peripheral antibody diversification (Murphy and Weaver, 2016a). To determine any roles of AIRE in peripheral antibody diversification, we first examined AIRE expression in B cells of human secondary lymphoid organs using an antibody that detects AIRE in the nuclei of mTECs (**Figure S1A**). We found many $IgD^{-}CD19^{+}$ or $IgD^{-}Pax5^{+}$ B cells inside tonsillar and splenic follicles that harbored nuclear AIRE (**Figure 1A–D**, **Figure S1B** and **C**). Follicular $AIRE^{+}$ B cells expressed the GC B cell-associated

molecule Bcl-6 (**Figure S1C**). In contrast, tonsillar and splenic IgD^+ B cells in the mantle zone and IgD^+ plasmablasts in GCs and extrafollicular areas (Chen et al., 2009) expressed little or no AIRE (**Figure S1B** and **Figure 1D**). Peripheral blood IgD^+CD27^- or $CD24^+CD38^{lo}$ naive, IgD^+CD27^+ circulating marginal zone, IgD^-CD27^+ or $CD24^{hi}CD38^-$ memory, IgD^-CD27^- atypical memory and $CD24^{hi}CD38^{hi}$ transitional B cells as well as $CD24^-CD38^{hi}$ plasma cells (PCs) did not express AIRE either (**Figure S1D**). Consistent with their follicular localization, tonsillar $AIRE^+$ B cells were mostly IgD^-CD38^+ GC B cells, with a small fraction being IgD^+CD38^+ founder GC (FGC) or IgD^-CD38^- memory B cells (**Figure 1E**).

Similar to human B cells, AIRE was found in B cells in the splenic follicles of immunized mice (**Figure S1E** and **F**). Consistently, in the *Aire*^{Adig} reporter mice (Gardner et al., 2008) after intraperitoneal immunizations, B cell AIRE expression was detected in FAS^+GL7^+ GC B cells in the spleen, inguinal lymph nodes (ILNs), mesenteric lymph nodes (MLNs) and Peyer's patches (PPs) and in thymic B cells, but not in FAS^-GL7^- non-GC B cells or $CD138^+$ PCs in these tissues, or in peripheral blood or peritoneal B cells (**Figure 1F** and **G**, **Figure S1G**–**J**). Consistently, *Aire* transcript level was markedly higher in splenic GFP^+ GC B cells than non-GC B cells (**Figure 1H**). Furthermore, AIRE was detected in both $CXCR4^+CD83^-$ dark zone (DZ) and $CXCR4^{lo}CD83^+$ light zone (LZ) B cells in mouse spleens (**Figure 1I**) and DZ and LZ B cells in human tonsils (**Figure 1J** and **K**). Altogether, these data indicate that AIRE expression in GC B cells is a specific and conserved characteristic of human and mouse secondary lymphoid organs.

Follicular B Cell AIRE Expression Requires CD40 Signaling

The induction of T cell-dependent GC B cell responses in secondary lymphoid organs involves B cell antigen presentation to primed cognate T helper (T_H) cells and clonal proliferation upon

receiving T_H cell signals, such as CD40-ligand (CD40L) and interleukin (IL)-4 (Liu et al., 1989; Yusuf et al., 2010). CD40 signaling was previously reported to promote AIRE expression by mTECs and thymic B cells (Akiyama et al., 2008; Yamano et al., 2015). To determine the regulation of AIRE expression in follicular B cells, we examined the tonsillar tissue of a patient with the rare primary immunodeficiency (PID) Hyper-IgM Syndrome type 3 (HIGM3), which is caused by loss-of-function mutations in the *CD40* gene (Durandy et al., 2005). In contrast to the prominent AIRE expression in tonsillar follicular B cells of healthy subjects (**Figure 1A** and **B**, **Figure S1B** and **C**), the tonsil of the HIGM3 patient harbored enlarged follicles containing B cells that had no expression of AIRE and failed to downregulate cell surface IgD (**Figure 2A** and **B**). Of note, tonsillar IgD plasmablasts were absent from the follicles but still present in the extrafollicular area, which is consistent with the existence of T cell-independent pathways for their generation as we reported previously (Chen et al., 2009), and indicates a specific shutdown of the T cell-dependent GC antibody diversification machinery. These results demonstrate a requirement for CD40 signaling in follicular B cell AIRE expression *in vivo*.

To further ascertain a role of CD40 signaling in promoting B cell AIRE expression, we treated mouse splenic naive resting B cells and human peripheral blood IgD^+ mature naive B cells *in vitro* with CD40L alone or in combination with IL-4. Consistent with the above *in vivo* data, these B cells expressed AIRE protein and transcript upon CD40L stimulation (**Figure 2C**–**E**). AIRE induction was abrogated by caffeic acid phenethyl ester (CAPE), a selective inhibitor of nuclear factor-kappa B (NF-κB) (Natarajan et al., 1996), a transcription factor activated by CD40 (**Figure 2C**–**E**). Furthermore, AIRE transcript and protein were also induced in the mouse B cell line CH12 (Nakamura et al., 1996) upon anti-CD40 stimulation (**Figure 2F** and **G**).

Collectively, these results show that CD40 signaling promotes AIRE expression in GC B cells *in vivo* and in B cells and cell lines *in vitro*.

AIRE in B Cells Inhibits CSR and SHM

As GC is the site of antibody diversification, including CSR and SHM (Murphy and Weaver, 2016b), we sought to determine the B cell-intrinsic function of AIRE in CSR and SHM. We employed several alternative and independent experimental approaches to achieve this goal.

Firstly, we engrafted lethally irradiated B cell-deficient μMT mice with the BM of CD45.1$^+$ *Aire*$^{+/+}$ and CD45.2$^+$ *Aire*$^{-/-}$ mice depleted of B220$^+$ cells at a ratio of 1:1 (**Figure S2A**), allowing the donor B cell compartment to develop in the same environment in which the thymic epithelium is *Aire*$^{+/+}$ so that the autoimmune manifestations of AIRE deficiency do not develop. Twenty-eight days later, naive resting splenic unswitched *Aire*$^{+/+}$ and *Aire*$^{-/-}$ B cells from these BM chimeras were adoptively transferred to secondary μMT recipients at a ratio of 1:1 (**Figure S2B**). These secondary μMT recipients were subsequently immunized with the T cell-dependent antigen (4-hydroxy-3-nitrophenylacetyl)$_{32}$-Keyhole Limpet Hemocyanin (NP$_{32}$-KLH) and analyzed the affinity maturation and class switching of NP-specific donor B cells by flow cytometry (**Figure 3A**). After the immunizations, the splenic GC B cell compartment contained more *Aire*$^{-/-}$B cells than *Aire*$^{+/+}$ B cells (**Figure 3B**), and the GC *Aire*$^{-/-}$ B cells had a higher NP$_8$-to-NP$_{36}$ binding ratio and a higher percentage of NP$_8$-binding cells in total NP-specific cells than their *Aire*$^{+/+}$ counterpart (**Figure 3C** and **D**), indicating increased affinity maturation. These data suggest that AIRE inhibits SHM in a B cell-intrinsic manner.

Secondly, we adoptively transferred an equal number of naive resting unswitched B cells from CD45.2$^+$ *Aire*$^{+/+}$ or CD45.2$^+$ *Aire*$^{-/-}$ donor mice into μMT recipients and assessed the CSR and SHM of NP-specific donor B cells after the immunizations by flow cytometry, enzyme-

linked immunosorbent assay (ELISA) and Ig heavy (IgH) chain variable (V) region mutation profiling with next-generation sequencing (**Figure 3E**). The *Aire*$^{+/+}$ and *Aire*$^{-/-}$ donor B cells exhibited a similar phenotype and had a comparable NP_8-to-NP_{36} binding ratio before the transfer (**Figure S2C**–**E**). Following the immunizations, *Aire*$^{+/+}$ and *Aire*$^{-/-}$ donor B cells entered the GC similarly in their respective recipients (**Figure S2F**), and GC *Aire*$^{+/+}$ and *Aire*$^{-/-}$ donor B cells exhibited similar expression of major co-stimulatory and co-inhibitory molecules (**Figure S2G**). µMT recipients of *Aire*$^{+/+}$ or *Aire*$^{-/-}$ B cells had a similar proportion of CXCR5^{+}PD-1^{+} follicular helper T (T_{FH}) cells (**Figure S2H**) and Foxp3^{+}CD25^{+} follicular regulatory T (T_{FR}) cells in the spleen (**Figure S2I**). However, NP-specific *Aire*$^{-/-}$ donor B cells exhibited elevated class switching by harboring a much higher fraction of IgM^{-}IgD^{-} cells than NP-specific *Aire*$^{+/+}$ donor B cells (**Figure 3F**), and underwent increased affinity maturation by producing IgG1, IgG2b and IgG3 of higher NP_4-to-NP_{29} binding ratios (**Figure 3G**). In contrast, a higher NP_4-to-NP_{29} binding ratio was not observed in the IgM compartment (**Figure 3G**). Increased CSR and SHM of donor *Aire*$^{-/-}$ B cells were not a secondary effect of differential AIRE expression by donor B cells in the thymus, because we found a negligible number of B cells in the thymus of the µMT recipient mice and the adoptive transfer did not lead to an increase in B cell numbers in the thymic stroma of the recipients at the end of the experiment, indicating that the donor B cells did not enter the thymus of the recipients during the course of our experiment (**Figure S2J** and **K**). Analysis of the IgH variable region (IgHV) SHM landscape of NP-specific *Aire*$^{+/+}$ and *Aire*$^{-/-}$ donor B cells sorted from the recipient mice (**Figure S2L**) showed that *Aire*$^{-/-}$ NP-specific class-switched IgG and IgE B cells had higher rates of IgHV SHMs in complementarity-determining region 2 (CDR2) and framework region 3 (FR3) than *Aire*$^{+/+}$ NP-specific B cells (**Figure 3H**). Importantly, such an increased SHM profile was not seen in the NP-specific IgM and IgD

compartments (**Figure 3H**). In addition, there was an increased frequency of C-to-T transitions among the SHMs in the IgH V region coding sequences in *Aire*$^{-/-}$ NP-specific B cells compared to *Aire*$^{+/+}$ NP-specific B cells (**Figure 3I**), which is a molecular signature associated with the action of AID in the IgH V region (Maul et al., 2011). *Aire*$^{+/+}$ and *Aire*$^{-/-}$splenic B cells exhibited comparable proliferation and apoptosis upon stimulation *ex vivo* (**Figure S3A–D**). These data suggest that AIRE suppresses CSR and SHM in AID-experienced B cells.

Thirdly, we sorted IgD^{+}CD27^{-} mature naive B cells from the peripheral blood of healthy subjects and APS-1 patients and compared their CSR *in vitro* upon stimulation with T cell-dependent stimuli. Naive B cells of APS-1 patients underwent increased CSR compared to those of healthy subjects by expressing higher levels of the post-switch transcript Iμ-Cγ1 or Iμ-Cγ3 following stimulation with CD40L and IL-4 or CD40L and interferon (IFN)-γ, respectively (**Figure 3J**).

Fourthly, using CRISPR-*Cas9*-mediated gene editing, we disrupted the *Aire* gene in the murine B cell line CH12 that class-switches from IgM to IgA upon stimulation with anti-CD40, TGF-β and IL-4 (Nakamura et al., 1996), and identified 3 *Aire*$^{-/-}$ CH12 clones which were frame-shifted in both *Aire* alleles (**Table S1**, and **Figure S4A** and **B**), devoid of AIRE protein expression (**Figure S4C**) and free from detectable CRISPR off-target effects (data not shown). Upon stimulation, these *Aire*$^{-/-}$ CH12 clones underwent elevated IgA CSR (**Figure 4A** and **B**) with concomitantly increased levels of the Iα-Cμ circle transcript compared to their parental *Aire*$^{+/+}$ CH12 cells (**Figure 4C**). The increased CSR was specific to IgA, as Iγ1-Cμ, the circle transcript of IgG1, an isotype that CH12 cells do not switch to, was not affected by *Aire* deficiency (**Figure 4D**). Exaggerated IgA CSR in *Aire*$^{-/-}$ CH12 cells was not a result of increased induction of AID (**Figure 4E** and **F**) or germline transcription (**Figure 4G**), nor a

result of increased survival (**Figure S4D** and **E**). Remarkably, WT AIRE suppressed cytokine-induced CSR when re-introduced into *Aire*$^{-/-}$ CH12 cells (**Figure 4H**). Collectively, the results obtained from these various experimental systems demonstrate the B-cell intrinsic function of AIRE in inhibiting CSR and SHM.

AIRE Interacts with AID in GC B Cells

We next investigated the mechanism by which AIRE inhibits peripheral antibody diversification. Given AID as the obligatory enzyme that mediates CSR and SHM (Muramatsu et al., 2000), we asked whether AIRE inhibits AID function in B cells. To this end, we first examined whether AIRE and AID interact in GC B cells. AIRE and AID co-localized in the nuclei of tonsillar IgD^{-} CD38^{+} GC B cells (**Figure 5A** and **B**, and **Figure S5A**) but not in IgD^{+}CD38^{-} naive B cells (**Figure S5B**), IgD^{-}CD38^{-} switched memory B cells (**Figure S5C**) or IgD^{-}CD38^{hi} switched PCs (**Figure S5D**), albeit a low level of nuclear AIRE and AID were detected in a small fraction of IgD^{+}CD38^{+} FGC B cells (**Figure S5E**). Using an AID antibody validated for immunoprecipitation (IP) and Chromatin IP (ChIP) (Vuong et al., 2009), we found that AIRE interacted with AID in human tonsillar CD19^{+} and CD19^{+}IgD^{-} cell fractions (**Figure 5C**). AID and AIRE did not interact via DNA in GC B cells as they still co-immunoprecipitated after DNAse I treatment (**Figure S6A**). AIRE also co-immunoprecipitated with AID in splenic B cells of immunized WT but not *Aire*$^{-/-}$ or *Aicda*$^{-/-}$ mice (**Figure 5D** and **Figure S6B**). Based on these data, we conclude that AIRE interacts with AID in GC B cells *in vivo*.

Interaction of AIRE with AID Requires the CARD and NLS domains of AIRE

We subsequently generated a series of deletion mutants of AIRE with C-terminal Myc and His tags to characterize AIRE's interaction with AID (**Figure 5E** and **Table S2A**). AIRE mutants missing the N-terminal caspase activation and recruitment domain (CARD) and/or nuclear

localization signal (NLS) lost the ability to interact with AID (**Figure 5F**), suggesting the requirement for the CARD domain and nuclear localization of AIRE for interaction with AID. Furthermore, using a series of deletion, domain replacement or point mutants of AID with an N-terminal FLAG tag (**Figure 5G** and **Table S2B**), we found that the interaction between AID and AIRE required both the catalytic and APOBEC-like domains of AID, although the catalytic activity of AID was not necessary, as the catalytically inactive AID^{E58A} mutant (Patenaude et al., 2009) still interacted with AIRE (**Figure 5H**). The AID point mutation G23S, which substantially abrogates the SHM but not much CSR activity of AID (Wei et al., 2011), did not affect the interaction with AIRE (**Figure 5H**). Echoing the CARD-dependent interaction of AIRE with AID, a CARD domain deletion mutant of AIRE had impaired ability to suppress CSR when introduced into *Aire*$^{-/-}$ CH12 cells (**Figure 5I**).

AIRE Inhibits the Function of AID during Antibody Diversification

Since AID enzymatically generates uracils in DNA (Bransteitter et al., 2003; Chaudhuri et al., 2003; Sohail et al., 2003), we employed a genomic uracil dot blot assay to directly test the effect of AIRE on the activity of AID (**Figure 6A** and **B**). In CH12 cells, increased uracils were detected in the genome upon stimulation with anti-CD40, TGF-β and IL-4 to undergo IgA CSR, which peaked on day 3 (Shalhout et al., 2014), whereas *Acida*$^{-/-}$ CH12 cells failed to accumulate genomic uracils after stimulation (**Figure 6C**), indicating that the emergence of genomic uracils was mediated by AID. Upon stimulation, *Aire*$^{-/-}$ CH12 cells harbored higher levels of genomic uracil than *Aire*$^{+/+}$ CH12 cells (**Figure 6C** and **D**). This result reflects the inhibition of AID's enzymatic function by AIRE at a step upstream of the deamination reaction.

We further investigated how AIRE may inhibit AID's enzymatic activity. Upstream of DNA deamination by AID is the proper targeting of AID to the IgH S regions at sites of Pol II stalling

(Chaudhuri et al., 2003; Pavri et al., 2010). We hypothesized that AIRE may interfere with the targeting of AID to IgH S regions during CSR. Using ChIP and IP assays, we found increased AID binding to the Sμ, but not Iμ or Sγ1, region (**Figure 6E**) and increased interaction of AID with serine-5 phosphorylated Pol II and its associated factor Spt5 at a promoter-proximal pause site (Peterlin and Price, 2006) in stimulated *Aire*$^{-/-}$ CH12 cells compared to stimulated *Aire*$^{+/+}$ CH12 cells (**Figure 6F** and **Figure S6C**). These data suggest that AIRE inhibits AID function in B cells by interfering with the interaction of AID with transcriptionally paused Pol II and the targeting of AID to its IgH DNA substrate.

AIRE Deficiency in B Cells Engenders Humoral Autoimmunity and Compromises Skin *Candida* Immune Defense

Given that the vast majority of APS-1 patients mysteriously develop chronic mucocutaneous candidiasis (CMC) as an early clinical symptom (Kisand and Peterson, 2015), we sought to determine the functional impact of B cell-intrinsic AIRE in humoral immunity and anti-*Candida* immune defense, and asked whether AIRE deficiency in peripheral B cells could promote APS-1-like CMC. We employed a mouse dermal candidiasis model which allows skin *C. albicans* infection to be established without the use of immunosuppressive agents (Conti et al., 2014). μMT recipient mice reconstituted with either *Aire*$^{+/+}$ or *Aire*$^{-/-}$ B cells were first exposed to heat-killed *C. albicans* pseudohyphae and subsequently infected cutaneously with live *C. albicans* pseudohyphae (**Figure 7A**). Four days after infection, μMT recipient mice of *Aire*$^{-/-}$ B cells had heightened fungal burden in the skin (**Figure 7B** and **C**) and concomitant elevation of circulating autoantibodies to IL-17A, IL-17F and IL-22 as compared to μMT recipients of *Aire*$^{+/+}$ B cells (**Figure 7D** and **Figure S7A**). The sera of μMT recipients of *Aire*$^{-/-}$ B cells contained enhanced blocking activity of the binding of IL-17A, IL-17F and IL-22 to their receptors (**Figure 7E**). In

addition, the dermal infection site of μMT recipients of *Aire*$^{-/-}$ B cells harbored reduced IL-17A- and IL-22-producing T cells (**Figure 7F** and **G**), which was accompanied by diminished neutrophils infiltration into the infected skin tissue (**Figure 7H**). These results are reminiscent of the aberrant production of class-switched neutralizing autoantibodies against T_H17 cytokines in APS-1 patients that may impair anti-*C. albicans* immunity (Kisand et al., 2010; Meyer et al., 2016; Puel et al., 2010), and collectively show that AIRE deficiency in peripheral B cells compromises cutaneous anti-*Candida* immune defense and promotes APS-1-like CMC by engendering humoral autoimmunity.

DISCUSSION

AIRE as A Paradigm of B Cell-Intrinsic Intracellular Immune Checkpoint

The concept and importance of immune checkpoint are now widely appreciated by scientists and clinicians. Immune checkpoints refer to molecules that mediate negative regulation of immune responses and therefore have a crucial role in maintaining immunological self-tolerance and avoiding autoimmunity. Many of the checkpoint molecules can be hijacked by tumors or pathogens for immune evasion and have therefore emerged as therapeutic targets for cancer and infectious diseases. To date, the majority of immune checkpoints under research investigation or clinical development encompass cell surface ligands and receptors that are involved in antigen-presenting cell (APC)–T cell interactions in immune-inductive sites (i.e., secondary lymphoid organs) or immune-effector sites (Sharma and Allison, 2015). Here, we demonstrate AIRE expression in the GC stage of B cell differentiation and its negative regulation on AID-mediated peripheral antibody diversification. Consequently, AIRE deficiency in B cells results in exaggerated antibody diversification and autoimmunity. Importantly, increased SHM of *Aire*$^{-/-}$

donor B cells was only seen in class-switched isotypes but not the IgM or IgD compartment, indicating an effect of AIRE only in AID-experienced B cells. This is not only consistent with the GC-specific AIRE expression in peripheral B cells, but also suggests that the function of AIRE described here is not a secondary effect of thymic B cells. The result from *Aire*$^{+/+}$ and *Aire*$^{-/-}$ B cell chimeras further corroborates this conclusion and confirms the B cell-intrinsic role of AIRE in limiting antibody diversification. Therefore, AIRE represents a paradigmatic B cell-intrinsic intracellular immune checkpoint of humoral immunity (**Figure 7I**).

Functionally Important Levels of AIRE May Have a Broader Expression Pattern

Besides mTECs (Anderson et al., 2002), AIRE protein expression has been previously reported in thymic B cells as well as several normal or malignant cell types of the hematopoietic or non-hematopoietic lineage in the periphery in humans and/or mice (Bianchi et al., 2016; Gardner et al., 2008; Gardner et al., 2013; Hobbs et al., 2015; Lindh et al., 2008; Poliani et al., 2010; Yamano et al., 2015). Intriguingly, little or no AIRE protein was seen in mouse GC B cells in a previous study, which was thought to result from B cell receptor (BCR)-mediated inhibition of AIRE induction; however, mouse B cells still expressed markedly elevated levels (~20 fold) of AIRE transcript when they were stimulated with anti-CD40 in the presence of anti-IgM (Yamano et al., 2015). In contrast, we present evidences obtained using multiple approaches to demonstrate AIRE protein expression in human and mouse GC B cells *in vivo*, and have also found much higher levels of AIRE transcript in mouse GC B cells than in non-GC B cells (data not shown). Therefore, BCR triggering does not completely abolish AIRE induction in GCs under physiological conditions. Consistent with our finding, BCR signaling in the GCs is reduced due to high phosphatase activity (Khalil et al., 2012) and, in some cases, BCR specificity may not be required for entry into GCs (Silver et al., 2018). Nonetheless, the role of

AIRE in inhibiting AID shown here is in line with BCR engagement in facilitating CSR and SHM of antigen-specific B cell clones and their affinity maturation by downregulating AIRE.

We currently do not know if AIRE in GC B cells has a significant impact on TSA expression and Treg induction by these cells as seen in mTECs and B cells in the thymus (Anderson et al., 2002; Malchow et al., 2013; Yamano et al., 2015), or an impact on $CD4^+$ T cell inactivation as seen in eTACs in secondary lymphoid organs (Gardner et al., 2008; Gardner et al., 2013). However, the comparable response of splenic T_{FR} cells in immunized μMT recipients and the similar expression of co-stimulatory and co-inhibitory molecules on donor *Aire*$^{-/-}$ and *Aire*$^{-/-}$ B cells would argue against these possibilities. In agreement with others (Gardner et al., 2013; Yamano et al., 2015), we found that the highest level of AIRE expression in mice appeared to be in mTECs and thymic B cells (data now shown). Hence, a lower level of AIRE expression in GC B cells as compared to thymic mTECs and thymic B cells would allow AIRE to perform unique and different functions, and our demonstration of the function of AIRE in regulating antibody diversification suggests that functionally important levels of AIRE have a broader expression pattern than previously appreciated. Lending further credence to this notion is the example of AID, where a much lower expression level in BM B cell precursors compared to that in GC B cells has a profound effect on B cell repertoire as well as both central and peripheral B cell tolerance in humans and mice (Cantaert et al., 2015; Meyers et al., 2011).

AIRE as a Unique Negative Regulator of AID

Many proteins have been reported to interact with and/or regulate AID in B cells, and they are thought to function at various steps of the molecular cascade of antibody diversification ranging from chromatin remodeling, AID targeting, transcriptional regulation, RNA processing, DNA repair and post-translational protein modification (Casellas et al., 2016; Vaidyanathan et al.,

2014; Xu et al., 2012). To our knowledge, among the AID-interacting partners identified to date, AIRE is the only one which, when deficient, enhances AID function, whereas all others impair AID function when they are missing. This provides a unique way to up-regulate the activity of AID in B cells. Whether AIRE interacts with AID directly or indirectly via other factors remains to be elucidated. Our results suggest the requirement for the CARD and NLS domains of AIRE in the interaction with AID. CARD is critical for AIRE's interaction with bromodomain-containing protein 4 (Brd4) which binds acetylated lysines in CARD and bridges AIRE with the positive transcription elongation factor b (P-TEFb) complex to induce ectopic gene expression in mTECs by promoting Pol II elongation (Giraud et al., 2014; Giraud et al., 2012; Oven et al., 2007; Yoshida et al., 2015). The increased interaction of AID with IgH S region and transcriptionally paused Pol II in *Aire*$^{-/-}$ CH12 cells undergoing CSR is therefore consistent with this body of literature, considering AID is targeted to DNA sites of Pol II pausing (Pavri et al., 2010). The genomic uracil dot blot assay we employed directly detects the product of AID's enzymatic activity, in contrast to conventional methods such as flow cytometry, ELISA and antibody sequencing that measure the final outcome of CSR and SHM as an indirect readout of AID's function. Increased generation of genomic uracils in *Aire*$^{-/-}$ CH12 cells undergoing CSR points to the regulation of AID by AIRE at steps upstream of the deamination reaction, which further agrees with the role of AIRE in restraining AID targeting to its DNA substrate. However, the involvement of other mechanisms upstream or downstream of the deamination reaction, such as the regulation of chromatin availability or DNA repair by AIRE (Abramson et al., 2010; Koh et al., 2018), cannot be discounted.

B Cell-Extrinsic and -Intrinsic AIRE Deficiency May Differentially Contribute to Autoimmunity and Immunodeficiency in APS-1

APS-1 is caused by mutations in a single gene but has emerged as a disease with complex pathogenesis. In fact, it has been classified as a type IV PID, a disease of immune dysregulation (Al-Herz et al., 2011). APS-1-associated CMC amidst the multi-organ autoimmune manifestations indicates the co-occurrence of immunodeficiency and autoimmunity, which are two conditions that are thought to occur usually at the opposite ends of the clinical immune spectrum. Such a seemingly paradoxical feature is now being found in an increasing number of primary and acquired immunodeficiencies and autoimmune diseases, such as selective IgA deficiency (SIgAD), immune dysregulation-polyendocrinopathy-enteropathy-X-linked syndrome (IPEX), severe combined variable immunodeficiency (CVID), acquired immunodeficiency syndrome (AIDS), systemic lupus erythematosus (SLE) and diabetes mellitus (DM) (Bacchetta and Notarangelo, 2013; Grammatikos and Tsokos, 2012; Zandman-Goddard and Shoenfeld, 2002). Our work revealed that, besides the central and peripheral abnormalities in T cell tolerance extrinsic to B cells, APS-1 involves previously unknown B cell-intrinsic dysregulation in peripheral antibody diversification, and this can engender humoral autoimmunity, such as the production of autoreactive antibodies against T_H17 effector cytokines. Our findings offer a plausible mechanistic explanation to the clinical observation of the presence of high affinity autoreactive neutralizing antibodies in these patients (Kisand et al., 2010; Meyer et al., 2016; Puel et al., 2010) and the causes of defective anti-*Candida* immune defense, thereby arguing for the concept that the seemingly contradictory autoimmunity and immunodeficiency can go hand-in-hand if there is an overproduction of autoreactive antibodies that impair protective immunity against pathogens. Of note, B cells were required to cause the multi-organ inflammation in *Aire*$^{-/-}$ mice not by producing autoantibodies, but by mediating early T cell priming and expansion (Gavanescu et al., 2008). This suggests that the multi-organ autoimmunity and CMC-associated

immunodeficiency in APS-1 are differentially contributed by the B cell-extrinsic and -intrinsic consequences of AIRE deficiency. We think that this scenario, if proven to be true, could be a paradigm applicable to understanding many other immunodeficiencies co-presenting with autoimmunity that involve humoral immune dysfunction. Indeed, an interesting example that mirrors this scenario is seen in AID-deficient individuals and mice that suffer from immunodeficiency due to the lack of CSR and SHM in the periphery (Muramatsu et al., 2000; Revy et al., 2000) but also have B cell autoimmunity likely due to missing AID's potential function in purging autoreactive immature B cells in the BM (Cantaert et al., 2015; Meyers et al., 2011). The insights gained from this study, therefore, could potentially offer a new direction for developing therapies that specifically and actively target the various aspects of pathogenesis of APS-1 and these other diseases.

AIRE Ablation as a Potentially New and Effective Approach of Antibody Generation for Immunotherapy

Besides offering new mechanistic insights into the regulation of the GC antibody diversification machinery and the unique production of high-affinity neutralizing autoantibodies in APS-1, our study underscores the important and emerging idea that immune tolerance mechanisms can be barriers to the generation of effective immunity (Khan et al., 2014; Schroeder et al., 2017), and controlled breaching of peripheral tolerance can permit neutralizing antibody responses that can be therapeutically beneficial. Remarkably, we found increased Ig framework region SHMs in class-switched antigen-specific *Aire*$^{-/-}$ B cells. Such an observation is reminiscent of the hallmarks of broadly and potently neutralizing antibodies against certain pathogens such as HIV-1 (Klein et al., 2013), the generation of which remains one of the most important mysteries as well as challenges in immunology. Our findings therefore point to a new effective strategy for

428 producing such antibodies by removing a critical B cell-intrinsic brake of AID, which is AIRE.
429 We envisage that further mechanistic elucidation of how B cell-intrinsic AIRE regulates AID
430 function could assist in cracking the elusive molecular underpinning of the generation of broadly
431 neutralizing antibodies and lead to substantial advances in antibody-based immunotherapies
432 against devastating diseases, such as AIDS and cancer.

433

434 ## STAR★METHODS

435 Detailed methods are provided in the online version of this paper and include the following:

436 - KEY RESOURCES TABLE
437 - CONTACT FOR REAGENTS AND RESOURCE SHARING
438 - EXPERIMENTAL MODEL AND SUBJECT DETAILS
439 - Human subjects
440 - Mice
441 - Primary cell cultures
442 - Cell lines
443 - Microbe strain
444 - METHOD DETAILS
445 - Human blood and tissue sample processing and cell isolation
446 - Mouse blood and tissue cell isolation
447 - Mouse immunization
448 - BM and B cell chimeras
449 - Discrimination of intravascular and tissue leukocytes
450 - Culture and stimulation or primary B cells

- Generation and validation of *Aire*$^{-/-}$ CH12 cells
- Plasmids
- Transfection
- *C. albicans* culture
- Cutaneous *C. albicans* infection
- Immunoprecipitation
- RNA extraction and quantitative real-time polymerase chain reaction
- Chromatin immunoprecipitation and quantitative real-time PCR
- Protein extraction and Western Blot
- Genomic uracil quantitation
- Conventional flow cytometry
- Imaging flow cytometry
- Immunofluorescence analysis
- ELISA
- IgHV repertoire and mutation analysis

- QUANTIFICATION AND STATISTICAL ANALYSIS
  - Statistical analyses
- DATA AND SOFTWARE AVAILABILITY
  - Software availability

AUTHOR CONTRIBUTIONS

B.H., B.P., J.Z.Z. and G.W.S. designed and performed research, and analyzed data. M.D.P., W.Z., X.L., K.C.H., F.Y., M.L.W.P., S.W., S.Z., L.A.P. and Y.P. performed research. J.M.P.,

A.R., K.Kr. and C.C.-R. provided specimens and clinical insights and discussed data. N.Y., A.S.B., K.Y., P.P., K.Ki., B.Q.V. and A.C. provided reagents and discussed data. K.C. designed and directed research, discussed and analyzed data, and wrote the manuscript.

ACKNOWLEDGMENTS

We are grateful to D. Mathis and C. Benoist (Harvard Medical School, USA) for *AIRE* cDNA plasmids, T. Honjo (Kyoto University, Japan) for *Aicda*$^{-/-}$ mice and CH12 cells, M. Anderson (University of California-San Francisco, USA) for *Aire*^{Adig} mice and discussions, T. Hagen (National University of Singapore) for the pcDNA3-eGFP vector, J.X. Ang, G. Lee and Q. Peng (Republic Polytechnic, Singapore) for assistance in creating and validating *Aire*$^{-/-}$ CH12 cells, C. Lim (Republic Polytechnic, Singapore) for assistance in constructing *Aire* mutant plasmids, E. van Buren and J. Back (Microscopy and Flow Cytometry Core of the Barbara Ann Karmanos Cancer Institute, USA) for assistance in cell sorting and imaging flow cytometry, and S. Dzinic, K. White and J. Kushner (Animal Model and Therapeutics Evaluation Core of the Barbara Ann Karmanos Cancer Institute, USA) for assistance in some animal experiments. The Chen laboratory is supported by the US National Institutes of Health (R21AI122256, U01AI95776 Mucosal Immunology Studies Team Young Investigator Award), Burroughs Wellcome Fund (1013738 Preterm Birth Initiative), American Congress of Obstetricians and Gynecologists (Industry Grant in Immunization), China Jiangsu Province Department of Health (Expert of Medical Research Program) and Wayne State University (Office of the Vice President for Research, Perinatal Research Initiative). The Bhagwat laboratory was supported by the National Institutes of Health grant R01GM057200 and Wayne State University Bridge award. S.Z. is supported by the Lee Kuan Yew Postdoctoral Fellowship.

REFERENCES

Abramson, J., Giraud, M., Benoist, C., and Mathis, D. (2010). Aire's partners in the molecular control of immunological tolerance. Cell *140*, 123-135.

Akiyama, T., Shimo, Y., Yanai, H., Qin, J., Ohshima, D., Maruyama, Y., Asaumi, Y., Kitazawa, J., Takayanagi, H., Penninger, J.M., *et al.* (2008). The tumor necrosis factor family receptors RANK and CD40 cooperatively establish the thymic medullary microenvironment and self-tolerance. Immunity *29*, 423-437.

Al-Herz, W., Bousfiha, A., Casanova, J.L., Chapel, H., Conley, M.E., Cunningham-Rundles, C., Etzioni, A., Fischer, A., Franco, J.L., Geha, R.S., *et al.* (2011). Primary immunodeficiency diseases: an update on the classification from the international union of immunological societies expert committee for primary immunodeficiency. Frontiers in immunology *2*, 54.

Anderson, K.G., Mayer-Barber, K., Sung, H., Beura, L., James, B.R., Taylor, J.J., Qunaj, L., Griffith, T.S., Vezys, V., Barber, D.L., *et al.* (2014). Intravascular staining for discrimination of vascular and tissue leukocytes. Nat Protoc *9*, 209-222.

Anderson, M.S., Venanzi, E.S., Klein, L., Chen, Z., Berzins, S.P., Turley, S.J., von Boehmer, H., Bronson, R., Dierich, A., Benoist, C., *et al.* (2002). Projection of an immunological self shadow within the thymus by the aire protein. Science *298*, 1395-1401.

Bacchetta, R., and Notarangelo, L.D. (2013). Immunodeficiency with autoimmunity: beyond the paradox. Frontiers in immunology *4*, 77.

Ballon, G., Chen, K., Perez, R., Tam, W., and Cesarman, E. (2011). Kaposi sarcoma herpesvirus (KSHV) vFLIP oncoprotein induces B cell transdifferentiation and tumorigenesis in mice. The Journal of clinical investigation *121*, 1141-1153.

Bianchi, F., Sommariva, M., De Cecco, L., Triulzi, T., Romero-Cordoba, S., Tagliabue, E., Sfondrini, L., and Balsari, A. (2016). Expression and prognostic significance of the autoimmune regulator gene in breast cancer cells. Cell Cycle *15*, 3220-3229.

Boersma, V., Moatti, N., Segura-Bayona, S., Peuscher, M.H., van der Torre, J., Wevers, B.A., Orthwein, A., Durocher, D., and Jacobs, J.J.L. (2015). MAD2L2 controls DNA repair at telomeres and DNA breaks by inhibiting 5' end resection. Nature *521*, 537-540.

Bransteitter, R., Pham, P., Scharff, M.D., and Goodman, M.F. (2003). Activation-induced cytidine deaminase deaminates deoxycytidine on single-stranded DNA but requires the action of RNase. Proceedings of the National Academy of Sciences of the United States of America *100*, 4102-4107.

Cantaert, T., Schickel, J.N., Bannock, J.M., Ng, Y.S., Massad, C., Oe, T., Wu, R., Lavoie, A., Walter, J.E., Notarangelo, L.D., *et al.* (2015). Activation-Induced Cytidine Deaminase Expression in Human B Cell Precursors Is Essential for Central B Cell Tolerance. Immunity *43*, 884-895.

Cao, A.T., Yao, S., Gong, B., Nurieva, R.I., Elson, C.O., and Cong, Y. (2015). Interleukin (IL)-21 promotes intestinal IgA response to microbiota. Mucosal immunology *8*, 1072-1082.

Casellas, R., Basu, U., Yewdell, W.T., Chaudhuri, J., Robbiani, D.F., and Di Noia, J.M. (2016). Mutations, kataegis and translocations in B cells: understanding AID promiscuous activity. Nature reviews Immunology *16*, 164-176.

Chaudhuri, J., Tian, M., Khuong, C., Chua, K., Pinaud, E., and Alt, F.W. (2003). Transcription-targeted DNA deamination by the AID antibody diversification enzyme. Nature *422*, 726-730.

542 Chen, K., Xu, W., Wilson, M., He, B., Miller, N.W., Bengten, E., Edholm, E.S., Santini, P.A.,
543 Rath, P., Chiu, A., *et al.* (2009). Immunoglobulin D enhances immune surveillance by
544 activating antimicrobial, proinflammatory and B cell-stimulating programs in basophils.
545 Nature immunology *10*, 889-898.
546 Conti, H.R., Huppler, A.R., Whibley, N., and Gaffen, S.L. (2014). Animal models for candidiasis.
547 Curr Protoc Immunol *105*, 19.16.11-19.16.13.
548 Doi, T., Obayashi, K., Kadowaki, T., Fujii, H., and Koyasu, S. (2008). PI3K is a negative
549 regulator of IgE production. International immunology *20*, 499-508.
550 Dudakovic, A., Camilleri, E.T., Xu, F., Riester, S.M., McGee-Lawrence, M.E., Bradley, E.W.,
551 Paradise, C.R., Lewallen, E.A., Thaler, R., Deyle, D.R., *et al.* (2015). Epigenetic Control of
552 Skeletal Development by the Histone Methyltransferase Ezh2. J Biol Chem *290*, 27604-
553 27617.
554 Durandy, A., Revy, P., Imai, K., and Fischer, A. (2005). Hyper-immunoglobulin M syndromes
555 caused by intrinsic B-lymphocyte defects. Immunological reviews *203*, 67-79.
556 Finnish-German, A.C. (1997). An autoimmune disease, APECED, caused by mutations in a
557 novel gene featuring two PHD-type zinc-finger domains. Nature genetics *17*, 399-403.
558 Gardner, J.M., Devoss, J.J., Friedman, R.S., Wong, D.J., Tan, Y.X., Zhou, X., Johannes, K.P., Su,
559 M.A., Chang, H.Y., Krummel, M.F., *et al.* (2008). Deletional tolerance mediated by
560 extrathymic Aire-expressing cells. Science *321*, 843-847.
561 Gardner, J.M., Metzger, T.C., McMahon, E.J., Au-Yeung, B.B., Krawisz, A.K., Lu, W., Price,
562 J.D., Johannes, K.P., Satpathy, A.T., Murphy, K.M., *et al.* (2013). Extrathymic Aire-
563 expressing cells are a distinct bone marrow-derived population that induce functional
564 inactivation of CD4(+) T cells. Immunity *39*, 560-572.

565 Gavanescu, I., Benoist, C., and Mathis, D. (2008). B cells are required for Aire-deficient mice to
566 develop multi-organ autoinflammation: A therapeutic approach for APECED patients.
567 Proceedings of the National Academy of Sciences of the United States of America *105*,
568 13009-13014.
569 Giraud, M., Jmari, N., Du, L., Carallis, F., Nieland, T.J., Perez-Campo, F.M., Bensaude, O., Root,
570 D.E., Hacohen, N., Mathis, D., *et al.* (2014). An RNAi screen for Aire cofactors reveals a
571 role for Hnrnpl in polymerase release and Aire-activated ectopic transcription. Proceedings
572 of the National Academy of Sciences of the United States of America *111*, 1491-1496.
573 Giraud, M., Yoshida, H., Abramson, J., Rahl, P.B., Young, R.A., Mathis, D., and Benoist, C.
574 (2012). Aire unleashes stalled RNA polymerase to induce ectopic gene expression in thymic
575 epithelial cells. Proceedings of the National Academy of Sciences of the United States of
576 America *109*, 535-540.
577 Grammatikos, A.P., and Tsokos, G.C. (2012). Immunodeficiency and autoimmunity: lessons
578 from systemic lupus erythematosus. Trends in molecular medicine *18*, 101-108.
579 Hobbs, R.P., DePianto, D.J., Jacob, J.T., Han, M.C., Chung, B.M., Batazzi, A.S., Poll, B.G., Guo,
580 Y., Han, J., Ong, S., *et al.* (2015). Keratin-dependent regulation of Aire and gene expression
581 in skin tumor keratinocytes. Nature genetics *47*, 933-938.
582 Hsu, P.D., Scott, D.A., Weinstein, J.A., Ran, F.A., Konermann, S., Agarwala, V., Li, Y., Fine,
583 E.J., Wu, X., Shalem, O., *et al.* (2013). DNA targeting specificity of RNA-guided Cas9
584 nucleases. Nat Biotechnol *31*, 827-832.
585 Khalil, A.M., Cambier, J.C., and Shlomchik, M.J. (2012). B cell receptor signal transduction in
586 the GC is short-circuited by high phosphatase activity. Science *336*, 1178-1181.

587 Khan, I.S., Mouchess, M.L., Zhu, M.L., Conley, B., Fasano, K.J., Hou, Y., Fong, L., Su, M.A.,
588 and Anderson, M.S. (2014). Enhancement of an anti-tumor immune response by transient
589 blockade of central T cell tolerance. The Journal of experimental medicine *211*, 761-768.
590 Kisand, K., Boe Wolff, A.S., Podkrajsek, K.T., Tserel, L., Link, M., Kisand, K.V., Ersvaer, E.,
591 Perheentupa, J., Erichsen, M.M., Bratanic, N., *et al.* (2010). Chronic mucocutaneous
592 candidiasis in APECED or thymoma patients correlates with autoimmunity to Th17-
593 associated cytokines. The Journal of experimental medicine *207*, 299-308.
594 Kisand, K., and Peterson, P. (2015). Autoimmune polyendocrinopathy candidiasis ectodermal
595 dystrophy. Journal of clinical immunology *35*, 463-478.
596 Klein, F., Diskin, R., Scheid, J.F., Gaebler, C., Mouquet, H., Georgiev, I.S., Pancera, M., Zhou,
597 T., Incesu, R.B., Fu, B.Z., *et al.* (2013). Somatic mutations of the immunoglobulin
598 framework are generally required for broad and potent HIV-1 neutralization. Cell *153*, 126-
599 138.
600 Koh, A.S., Miller, E.L., Buenrostro, J.D., Moskowitz, D.M., Wang, J., Greenleaf, W.J., Chang,
601 H.Y., and Crabtree, G.R. (2018). Rapid chromatin repression by Aire provides precise
602 control of immune tolerance. Nature immunology *19*, 162-172.
603 Lindh, E., Lind, S.M., Lindmark, E., Hassler, S., Perheentupa, J., Peltonen, L., Winqvist, O., and
604 Karlsson, M.C. (2008). AIRE regulates T-cell-independent B-cell responses through BAFF.
605 Proceedings of the National Academy of Sciences of the United States of America *105*,
606 18466-18471.
607 Liu, Y.J., Joshua, D.E., Williams, G.T., Smith, C.A., Gordon, J., and MacLennan, I.C. (1989).
608 Mechanism of antigen-driven selection in germinal centres. Nature *342*, 929-931.

609 Malchow, S., Leventhal, D.S., Nishi, S., Fischer, B.I., Shen, L., Paner, G.P., Amit, A.S., Kang,
610 C., Geddes, J.E., Allison, J.P., *et al.* (2013). Aire-dependent thymic development of tumor-
611 associated regulatory T cells. Science *339*, 1219-1224.
612 Maul, R.W., Saribasak, H., Martomo, S.A., McClure, R.L., Yang, W., Vaisman, A., Gramlich,
613 H.S., Schatz, D.G., Woodgate, R., Wilson, D.M., 3rd, *et al.* (2011). Uracil residues
614 dependent on the deaminase AID in immunoglobulin gene variable and switch regions.
615 Nature immunology *12*, 70-76.
616 Meyer, S., Woodward, M., Hertel, C., Vlaicu, P., Haque, Y., Karner, J., Macagno, A., Onuoha,
617 S.C., Fishman, D., Peterson, H., *et al.* (2016). AIRE-Deficient Patients Harbor Unique
618 High-Affinity Disease-Ameliorating Autoantibodies. Cell *166*, 582-595.
619 Meyers, G., Ng, Y.S., Bannock, J.M., Lavoie, A., Walter, J.E., Notarangelo, L.D., Kilic, S.S.,
620 Aksu, G., Debre, M., Rieux-Laucat, F., *et al.* (2011). Activation-induced cytidine deaminase
621 (AID) is required for B-cell tolerance in humans. Proceedings of the National Academy of
622 Sciences of the United States of America *108*, 11554-11559.
623 Muramatsu, M., Kinoshita, K., Fagarasan, S., Yamada, S., Shinkai, Y., and Honjo, T. (2000).
624 Class switch recombination and hypermutation require activation-induced cytidine
625 deaminase (AID), a potential RNA editing enzyme. Cell *102*, 553-563.
626 Murphy, K.M., and Weaver, C. (2016a). Basic Concepts in Immunology. In Janeway's
627 Immunobiology (Garland Science), pp. 1-36.
628 Murphy, K.M., and Weaver, C. (2016b). The Humoral Immune Response. In Janeway's
629 Immunobiology (Garland Science), pp. 399-441.

Nagamine, K., Peterson, P., Scott, H.S., Kudoh, J., Minoshima, S., Heino, M., Krohn, K.J., Lalioti, M.D., Mullis, P.E., Antonarakis, S.E., *et al.* (1997). Positional cloning of the APECED gene. Nature genetics *17*, 393-398.

Nakamura, M., Kondo, S., Sugai, M., Nazarea, M., Imamura, S., and Honjo, T. (1996). High frequency class switching of an IgM+ B lymphoma clone CH12F3 to IgA+ cells. International immunology *8*, 193-201.

Natarajan, K., Singh, S., Burke, T.R., Jr., Grunberger, D., and Aggarwal, B.B. (1996). Caffeic acid phenethyl ester is a potent and specific inhibitor of activation of nuclear transcription factor NF-kappa B. Proceedings of the National Academy of Sciences of the United States of America *93*, 9090-9095.

Nowak, U., Matthews, A.J., Zheng, S., and Chaudhuri, J. (2011). The splicing regulator PTBP2 interacts with the cytidine deaminase AID and promotes binding of AID to switch-region DNA. Nature immunology *12*, 160-166.

Oven, I., Brdickova, N., Kohoutek, J., Vaupotic, T., Narat, M., and Peterlin, B.M. (2007). AIRE recruits P-TEFb for transcriptional elongation of target genes in medullary thymic epithelial cells. Mol Cell Biol *27*, 8815-8823.

Patenaude, A.M., Orthwein, A., Hu, Y., Campo, V.A., Kavli, B., Buschiazzo, A., and Di Noia, J.M. (2009). Active nuclear import and cytoplasmic retention of activation-induced deaminase. Nat Struct Mol Biol *16*, 517-527.

Pavri, R., Gazumyan, A., Jankovic, M., Di Virgilio, M., Klein, I., Ansarah-Sobrinho, C., Resch, W., Yamane, A., Reina San-Martin, B., Barreto, V., *et al.* (2010). Activation-induced cytidine deaminase targets DNA at sites of RNA polymerase II stalling by interaction with Spt5. Cell *143*, 122-133.

Peterlin, B.M., and Price, D.H. (2006). Controlling the elongation phase of transcription with P-TEFb. Molecular cell *23*, 297-305.

Poliani, P.L., Kisand, K., Marrella, V., Ravanini, M., Notarangelo, L.D., Villa, A., Peterson, P., and Facchetti, F. (2010). Human peripheral lymphoid tissues contain autoimmune regulator-expressing dendritic cells. The American journal of pathology *176*, 1104-1112.

Puel, A., Doffinger, R., Natividad, A., Chrabieh, M., Barcenas-Morales, G., Picard, C., Cobat, A., Ouachee-Chardin, M., Toulon, A., Bustamante, J., *et al.* (2010). Autoantibodies against IL-17A, IL-17F, and IL-22 in patients with chronic mucocutaneous candidiasis and autoimmune polyendocrine syndrome type I. The Journal of experimental medicine *207*, 291-297.

Ran, F.A., Hsu, P.D., Wright, J., Agarwala, V., Scott, D.A., and Zhang, F. (2013). Genome engineering using the CRISPR-Cas9 system. Nat Protoc *8*, 2281-2308.

Revy, P., Muto, T., Levy, Y., Geissmann, F., Plebani, A., Sanal, O., Catalan, N., Forveille, M., Dufourcq-Labelouse, R., Gennery, A., *et al.* (2000). Activation-induced cytidine deaminase (AID) deficiency causes the autosomal recessive form of the Hyper-IgM syndrome (HIGM2). Cell *102*, 565-575.

Schroeder, K.M.S., Agazio, A., Strauch, P.J., Jones, S.T., Thompson, S.B., Harper, M.S., Pelanda, R., Santiago, M.L., and Torres, R.M. (2017). Breaching peripheral tolerance promotes the production of HIV-1-neutralizing antibodies. The Journal of experimental medicine *214*, 2283-2302.

Shalhout, S., Haddad, D., Sosin, A., Holland, T.C., Al-Katib, A., Martin, A., and Bhagwat, A.S. (2014). Genomic uracil homeostasis during normal B cell maturation and loss of this balance during B cell cancer development. Mol Cell Biol *34*, 4019-4032.

676 Sharma, P., and Allison, J.P. (2015). The future of immune checkpoint therapy. Science *348*, 56-
677 61.
678 Silver, J., Zuo, T., Chaudhary, N., Kumari, R., Tong, P., Giguere, S., Granato, A., Donthula, R.,
679 Devereaux, C., and Wesemann, D.R. (2018). Stochasticity enables BCR-independent
680 germinal center initiation and antibody affinity maturation. The Journal of experimental
681 medicine *215*, 77-90.
682 Sohail, A., Klapacz, J., Samaranayake, M., Ullah, A., and Bhagwat, A.S. (2003). Human
683 activation-induced cytidine deaminase causes transcription-dependent, strand-biased C to U
684 deaminations. Nucleic acids research *31*, 2990-2994.
685 Steuerwald, N., Cohen, J., Herrera, R.J., and Brenner, C.A. (2000). Quantification of mRNA in
686 single oocytes and embryos by real-time rapid cycle fluorescence monitored RT-PCR. Mol
687 Hum Reprod *6*, 448-453.
688 Vaidyanathan, B., Yen, W.F., Pucella, J.N., and Chaudhuri, J. (2014). AIDing Chromatin and
689 Transcription-Coupled Orchestration of Immunoglobulin Class-Switch Recombination.
690 Frontiers in immunology *5*, 120.
691 Vinuesa, C.G., Sanz, I., and Cook, M.C. (2009). Dysregulation of germinal centres in
692 autoimmune disease. Nature reviews Immunology *9*, 845-857.
693 Vuong, B.Q., Lee, M., Kabir, S., Irimia, C., Macchiarulo, S., McKnight, G.S., and Chaudhuri, J.
694 (2009). Specific recruitment of protein kinase A to the immunoglobulin locus regulates
695 class-switch recombination. Nature immunology *10*, 420-426.
696 Wang, S., Huang, J., Lyu, H., Lee, C.K., Tan, J., Wang, J., and Liu, B. (2013). Functional
697 cooperation of miR-125a, miR-125b, and miR-205 in entinostat-induced downregulation of
698 erbB2/erbB3 and apoptosis in breast cancer cells. Cell Death Dis *4*, e556.

699 Wei, M., Shinkura, R., Doi, Y., Maruya, M., Fagarasan, S., and Honjo, T. (2011). Mice carrying
700 a knock-in mutation of Aicda resulting in a defect in somatic hypermutation have impaired
701 gut homeostasis and compromised mucosal defense. Nature immunology *12*, 264-270.
702 Wei, S., Perera, M.L.W., Sakhtemani, R., and Bhagwat, A.S. (2017). A novel class of chemicals
703 that react with abasic sites in DNA and specifically kill B cell cancers. PLoS One *12*,
704 e0185010.
705 Wei, S., Shalhout, S., Ahn, Y.H., and Bhagwat, A.S. (2015). A versatile new tool to quantify
706 abasic sites in DNA and inhibit base excision repair. DNA Repair (Amst) *27*, 9-18.
707 Xu, G., Chapman, J.R., Brandsma, I., Yuan, J., Mistrik, M., Bouwman, P., Bartkova, J., Gogola,
708 E., Warmerdam, D., Barazas, M., *et al.* (2015). REV7 counteracts DNA double-strand break
709 resection and affects PARP inhibition. Nature *521*, 541-544.
710 Xu, Z., Zan, H., Pone, E.J., Mai, T., and Casali, P. (2012). Immunoglobulin class-switch DNA
711 recombination: induction, targeting and beyond. Nature reviews Immunology *12*, 517-531.
712 Yamano, T., Nedjic, J., Hinterberger, M., Steinert, M., Koser, S., Pinto, S., Gerdes, N., Lutgens,
713 E., Ishimaru, N., Busslinger, M., *et al.* (2015). Thymic B Cells Are Licensed to Present Self
714 Antigens for Central T Cell Tolerance Induction. Immunity *42*, 1048-1061.
715 Yoshida, H., Bansal, K., Schaefer, U., Chapman, T., Rioja, I., Proekt, I., Anderson, M.S., Prinjha,
716 R.K., Tarakhovsky, A., Benoist, C., *et al.* (2015). Brd4 bridges the transcriptional regulators,
717 Aire and P-TEFb, to promote elongation of peripheral-tissue antigen transcripts in thymic
718 stromal cells. Proceedings of the National Academy of Sciences of the United States of
719 America *112*, E4448-4457.
720 Yusuf, I., Kageyama, R., Monticelli, L., Johnston, R.J., Ditoro, D., Hansen, K., Barnett, B., and
721 Crotty, S. (2010). Germinal center T follicular helper cell IL-4 production is dependent on

722 signaling lymphocytic activation molecule receptor (CD150). Journal of immunology *185*,
723 190-202.
724 Zandman-Goddard, G., and Shoenfeld, Y. (2002). HIV and autoimmunity. Autoimmunity
725 reviews *1*, 329-337.
726 Zhang, W., Du, Y., Su, Z., Wang, C., Zeng, X., Zhang, R., Hong, X., Nie, C., Wu, J., Cao, H., *et*
727 *al.* (2015). IMonitor: A Robust Pipeline for TCR and BCR Repertoire Analysis. Genetics
728 *201*, 459-472.

729

FIGURE LEGENDS

Figure 1. GC B Cells Express AIRE.

(A and B) Immunofluorescence analysis of the tonsillar tissue of a healthy donor for IgD, CD19, AIRE and DAPI-stained DNA. The dotted line outlines the follicles. Bars: 100 μm (A) or 25 μm (B).

(C and D) Immunofluorescence analysis of tissues of a healthy donor for IgD, AIRE, CD19 and DNA. Arrow heads indicate follicular IgD^+ plasmablasts. Dotted lines mark the boundary between follicular mantle zone and the follicle. Bars: 40 μm (C) and 15 μm (D).

(E) Flow cytometric analysis of AIRE expression in tonsillar total $CD19^+$ B cells, IgD^+CD38^- naive B cells, IgD^+CD38^+ founder GC (FGC) B cells, IgD^-CD38^+ GC B cells and IgD^-CD38^- memory B cells. The data represent 5 donors.

(F and G) Flow cytometric and statistical analyses of Aire (GFP) expression in splenic and ILN viable $CD19^+B220^+FAS^+GL7^+$ GC B cells, $CD19^+B220^+FAS^-GL7^-$ non-GC B cells and $CD19^{lo}B220^{lo}CD138^+$ PCs of B6 mice (shaded histograms, $n = 5$ for spleen and $n = 4$ for ILN) or B6.$Aire^{Adig}$ mice (colored histograms, $n = 5$ for spleen and $n = 4$ for ILN) after 4 i.p. immunizations with NP_{32}-KLH with CFA and subsequently with IFA. Data are represented as mean ± SEM. $^{**}P < 0.01$, $^{***}P < 0.001$, by 1-way ANOVA with Tukey's post hoc test.

(H) qPCR analysis of *Aire* transcript levels in $CD19^+B220^+FAS^-GL7^-$ non-GC B cells ($n = 5$) and $CD19^+B220^+FAS^+GL7^+GFP^+$ Aire-expressing GC B cells ($n = 4$) of $Aire^{Adig}$ mice after 1 i.p. immunization with SRBC and CFA. Data are represented as mean ± SEM. $^{***}P < 0.001$, by 2-tailed unpaired *t*-test.

(I) Flow cytometric and statistical analyses of $CD83^{+}CXCR4^{lo}$ LZ and $CD83^{-}CXCR4^{hi}$ DZ B cells in splenic total GC and GFP^{+} GC B cells of immunized B6.*Aire*^{Adig} mice, by 2-tailed paired *t*-test.

(J and K) Immunofluorescence analysis of the tonsillar tissue of a healthy donor for IgD, CD23, Pax5 and AIRE. The dotted line outlines the follicles and delineates the border between LZ and DZ. Bars: 200 μm (J) or 30 μm (K).

Figure 2. Follicular B Cell AIRE Expression Requires CD40 Signaling.

(A and B) Immunofluorescence analysis of tonsillar tissues of a HIGM3 patient for IgD, AIRE, CD19 and DNA. The area outlined in A is shown with a higher magnification in B. The dotted line outlines the follicles. Bars: 100 μm (A) or 25 μm (B).

(C) Flow cytometric analysis of Aire (GFP) expression in splenic B cells of a B6 or B6.*Aire*^{Adig} mouse treated for 3 d with medium or CD40L with or without IL-4 in the absence (vehicle) or presence of CAPE. The data represent the results from 3 B6 and 3 B6.*Aire*^{Adig} mice.

(D and E) qRT-PCR and Western Blot analyses of *AIRE* transcript and protein levels, the protein levels of total and Ser536-phosphorylated NF-κB p65, as well as total and Thr202/Tyr204-phosphorylated Erk1/2 in human peripheral blood IgD^{+} B cells treated with medium or CD40L, or CD40L and IL-4, in the presence of vehicle or CAPE for 3 d. Data are represented as mean ± SEM. ***$P < 0.001$, by 2-tailed unpaired *t*-test.

(F and G) qRT-PCR and Western Blot analyses of *Aire* transcript and Aire protein levels in mouse CH12 cells treated with anti-CD40, TGF-β and 100 ng/ml IL-4 for 3 d. Data are represented as mean ± SEM. $P < 0.001$, by 2-tailed unpaired *t*-test.

Figure 3. AIRE Inhibits CSR and SHM in B cells.

(A) The generation and immunization of *Aire*$^{+/+}$ and *Aire*$^{-/-}$ BM and B cell chimeric mice.

(B) The percentage of CD45.1^{+} *Aire*$^{+/+}$ and CD45.2^{+} *Aire*$^{-/-}$ B cells in the splenic GC B cells of the secondary μMT recipient mice (n = 6) after the immunizations. ***P < 0.001, by 2-tailed paired t-test.

(C and D) Flow cytometric and statistical analyses of the ratio of NP_8- to NP_{36}-binding (C) and NP_8- to total NP-binding (D) GC B cells after immunizations of the secondary μMT recipient mice (n = 6). **P < 0.05, **P < 0.01, by 2-tailed paired t-test.

(E) The generation and immunization of *Aire*$^{+/+}$ and *Aire*$^{-/-}$ B cell chimeric mice.

(F) Flow cytometric analysis of surface IgD and IgM on NP_{36}-binding B cells in μMT recipients of *Aire*$^{+/+}$ or *Aire*$^{-/-}$ B cells immunized with NP_{32}-KLH. The result represents 3 age- and sex-matched μMT recipients each of B cells from 3–5 age- and sex-matched littermate donor *Aire*$^{+/+}$ or *Aire*$^{-/-}$ mice.

(G) The ratios of the titers of circulating NP_4-binding to NP_{29}-binding IgM, IgG1, IgG2b and IgG3 in immunized μMT recipient mice of *Aire*$^{+/+}$ or *Aire*$^{-/-}$ B cells. The results represent 4 experiments, each consisting of B cells from 3–5 age- and sex-matched littermate donor mice and 6–8 age- and sex-matched littermate μMT recipient mice. *P < 0.05, **P < 0.01, by 2-tailed unpaired t-test.

(H) The SHM landscape across IgHV, including FR2, CDR2, FR3, CDR3 and FR4, of NP_{36}-binding IgM^{-}IgD^{-} or IgM^{+}IgD^{+} *Aire*$^{+/+}$ and *Aire*$^{-/-}$ donor B cells in μMT recipients after immunizations with NP_{32}-KLH. The result represents 3 μMT recipients of *Aire*$^{+/+}$ donor B cells and 3 μMT recipients of *Aire*$^{-/-}$ donor B cells.

(I) Frequencies of C-to-T transitions in SHMs in IgHV of NP-specific IgG^+, IgA^+ or IgE^+ splenic B cells from μMT recipient mice of *Aire*$^{+/+}$ or *Aire*$^{-/-}$ B cells after immunizations with NP_{32}-KLH. Data are represented as median ± upper/lower quartile. **P* < 0.05, ***P* < 0.01, by 1-tailed unpaired *t*-test.

(J) qRT-PCR analysis of the fold induction of Iμ-Cγ1 and Iμ-Cγ3 post-switch transcript levels in peripheral blood IgD^+CD27^- naïve B cells from healthy subjects (*n* = 5) or APS-1 patients (*n* = 5) stimulated for 3 d with CD40L and IL-4 or IFN-γ over the respective unstimulated control B cells. **P* < 0.05, by 1-tailed unpaired *t*-test (upper panel) or 1-tailed Mann-Whitney *U* test (lower panel).

Figure 4. *Aire*$^{-/-}$ CH12 Cells Undergo Elevated CSR.

(A and B) Flow cytometric and statistical analyses of IgA CSR in WT and *Aire*$^{-/-}$ CH12 cells treated with medium (Control) or anti-CD40, TGF-β and IL-4 for 3 d. Data in **F** was determined as the difference between the percentages of IgA^+IgM^- cells in stimulated samples to unstimulated samples. The results (mean ± SEM) represent or compare 16 experiments involving WT CH12 cells, 8 experiments involving clones 43, 6 experiments involving clone 53, and 13 experiments involving clone 69. ***P* < 0.01, ****P* < 0.001, by 2-tailed unpaired *t*-test.

(C) qRT-PCR analysis of the Iα-Cμ circle transcript levels (mean ± SEM) in WT and *Aire*$^{-/-}$ CH12 cells treated with medium (Control) or anti-CD40, TGF-β and IL-4 for 3 d. The results compare 3 experiments. **P* < 0.05, ***P* < 0.01, by 1-tailed unpaired *t*-test.

(D) qRT-PCR analysis of the Iγ1-Cμ circle transcript level in *Aire*$^{+/+}$ CH12 cells and *Aire*$^{-/-}$ CH12 cell clones 43, 53 and 69 that were either unstimulated or stimulated with anti-CD40,

818 TGF-β and IL-4 for 3 d. The result was normalised using the respective *Actb* transcript level and
819 expressed as fold of induction (mean ± SEM) relative to unstimulated *Aire*$^{+/+}$ CH12 cells.
820 (E and F) Western Blot analysis of AID in WT and *Aire*$^{-/-}$ CH12 cells that were either
821 unstimulated or stimulated with anti-CD40, TGF-β and IL-4 for 3 d. Lamin B1 and GAPDH
822 were used as the control for nuclear and cytoplasmic proteins, respectively. The data are
823 presented as mean ± SEM and represent 3 experiments.
824 (G) qRT-PCR analysis of *Aicda* and the Iμ-Cμ and Iα-Cα germline transcript levels (mean ±
825 SEM) in *Aire*$^{+/+}$ CH12 cells and *Aire*$^{-/-}$ CH12 cell clones 43, 53 and 69 that were either
826 unstimulated or stimulated with anti-CD40, TGF-β and IL-4 for 3 d.
827 (H) Flow cytometric analysis of IgA CSR in *Aire*$^{-/-}$ CH12 cells (clone 69) transfected with a plasmid
828 expressing WT (AIRE^{WT}-GFP) AIRE-GFP and treated with medium (Control) or anti-CD40, TGF-β
829 and IL-4 for 3 d. The results represent 3 experiments.
830

831 **Figure 5. AIRE Interacts with AID in GC B Cells.**

832 (A and B) Imaging flow cytometric analysis of AIRE and AID in tonsillar IgD^{-}CD38^{+} GC B
833 cells of a healthy donor. Bars: 7 μm (A). The results represent 3 donors.
834 (C and D) Co-IP of AIRE and AID in tonsillar CD19^{+} total, IgD^{+} naive and FGC and CD19^{+}IgD^{-}
835 GC and memory B cells of a healthy donor, and in splenic CD19^{+} B cells of a B6 mouse after 3
836 doses of immunization with SRBCs. The results are representative of tonsils of 4 donors and
837 spleens of 3 mice.
838 (E) The domain structures of recombinant WT and mutant human AIRE and AID molecules.
839 Dotted lines indicated the deleted regions in the mutant proteins.

(F) Co-IP of WT AID and WT or mutant AIRE in HKB-11 cells 24 h after transfection of plasmid(s) encoding WT AID and WT or mutant AIRE proteins.

(G) The domain structures of recombinant WT and mutant human AID proteins.

(H) Co-IP of WT AIRE and WT or mutant AID in HKB-11 cells 24 h after transfection of plasmid(s) encoding WT AIRE and WT or mutant AID proteins. The results in E and G are representative of 3 experiments.

(I) Flow cytometric analysis of IgA CSR in *Aire*$^{-/-}$ CH12 cells (clone 69) transfected with a plasmid expressing either WT (Aire^{WT}-GFP) or CARD-deficient (Aire$^{\Delta CARD}$-GFP) AIRE-GFP and treated with medium (Control) or anti-CD40, TGF-β and IL-4 for 3 d. The results represent 3 experiments.

Figure 6. AIRE Inhibits AID Function by Interfering with AID Targeting to Its IgH DNA Substrate.

(A and B) The principle, chemistry and calibration of the dot blot assay for the quantitation of genomic uracil content.

(C) The genomic uracil levels in WT, *Aire*$^{-/-}$, *Aicda*$^{-/-}$, or *Ung*$^{-/-}$ CH12 cells after 72 h of treatment without or with anti-CD40, TGF-β and IL-4. The results are presented as mean ± SEM and represent 3 experiments. ***$P < 0.001$, by 2-tailed unpaired *t*-test. Bisulfite-treated *E. coli* DNA was included as a positive control.

(D) The genomic uracil content in WT and *Aire*$^{-/-}$ CH12 cells after 48 or 72 h of treatment without or with anti-CD40, TGF-β and IL-4. The results are presented as mean ± SEM and represent 3 experiments. **$P < 0.01$, ***$P < 0.001$, by 2-tailed unpaired *t*-test.

(E) ChIP-qPCR analysis for the interaction of AID with Sμ, Iμ and Sγ1 regions in WT and *Aire*$^{-/-}$ CH12 cells after 72 h of treatment without or with anti-CD40, TGF-β and IL-4. The results are presented as mean ± SEM and represent 3 experiments. **P* < 0.05, by 2-tailed unpaired *t*-test.

(F) Co-IP of AID with pSer5-Pol II, total Pol II, Spt5 and Aire in WT and *Aire*$^{-/-}$ CH12 cells after 72 h of treatment without or with anti-CD40, TGF-β and IL-4. The results represent 3 experiments.

Figure 7. Aire Deficiency in B Cells Promotes Humoral Autoimmunity and Compromises Cutaneous Anti-*Candida* Defense.

(A) The cutaneous candidiasis infection model.

(B and C) GMS stain of cutaneous *C. albicans* and skin fungal burden (CFU per mg of tissue) (mean ± SEM) in μMT recipient mice of *Aire*$^{+/+}$ or *Aire*$^{-/-}$ donor B cells 4 d after infection. Bars: 1 mm (B, upper panels) or 100 μm (B, lower panels). ***P* < 0.01, by 1-tailed unpaired *t*-test.

(D) ELISA of the levels (mean ± SEM) of autoantibodies binding to IL-17A, IL-17F and IL-22 in the sera of μMT recipient mice of *Aire*$^{+/+}$ or *Aire*$^{-/-}$ donor B cells 4 d after infection. **P* < 0.05, ***P* < 0.01, by 1-tailed unpaired *t*-test.

(E) ELISA of the levels (mean ± SEM) of blocking activity of IL-17A, IL-17F and IL-22 to their receptors in the sera of μMT recipient mice of *Aire*$^{+/+}$ or *Aire*$^{-/-}$ donor B cells 4 d after infection. **P* < 0.05, ***P* < 0.01, ****P* < 0.001, by 1-way ANOVA with Tukey's post hoc test.

(F and G) Flow cytometric and statistical analyses of IL-17A and IL-22 expression in cutaneous T cells of μMT recipient mice of *Aire*$^{+/+}$ or *Aire*$^{-/-}$ donor B cells (*n* = 4 in each group) 4 d after infection and after *ex vivo* re-stimulation. The data are represented as mean ± SEM. **P* < 0.05, by 1-tailed unpaired *t*-test.

(H) Immunofluorescence analysis of Ly-6G (red) and DNA (blue) in cutaneous tissues surrounding the *C. albicans* infection site in μMT recipient mice of *Aire*$^{+/+}$ or *Aire*$^{-/-}$ donor B cells 4 d after infection. The results in B–H represent 2 experiments, with 4 mice per group in each experiment. Bars: 160 μm (upper panels) or 40 μm (lower panels).

(I) A simplified schematic of AIRE-mediated GC checkpoint of antibody diversification in B cells. At the T–B cell border of secondary lymphoid organs, B cells present antigens to and receive co-stimulation from DC-activated T cells, which also induce AIRE expression in B cells via CD40. The activated B cells enter the GC DZ and undergo SHM, proliferation and subsequent affinity selection by interacting with antigens on the surface of follicular dendritic cells (FDCs) in LZ. Low-affinity B cells will undergo apoptosis, whereas high-affinity B cells receive help from T follicular helper (T_{FH}) cells to undergo CSR, and subsequently either re-enter the SHM–proliferation cycle in the DZ or exit the GC as plasma cells or memory B cells. AIRE in B cells limits autoantibody generation by restraining excessive AID activity in the GC.

SUPPLEMENTAL INFORMATION

SUPPLEMENTAL TABLES

899 **Table S1. *Aire*$^{-/-}$ CH12 Cell Clones, Related to Figure 4 and Figure 5.**

Clone	Mutation(s) and alleles	Sequencing histogram
43	Allele 1	
	Allele 2	

53	Allele 1 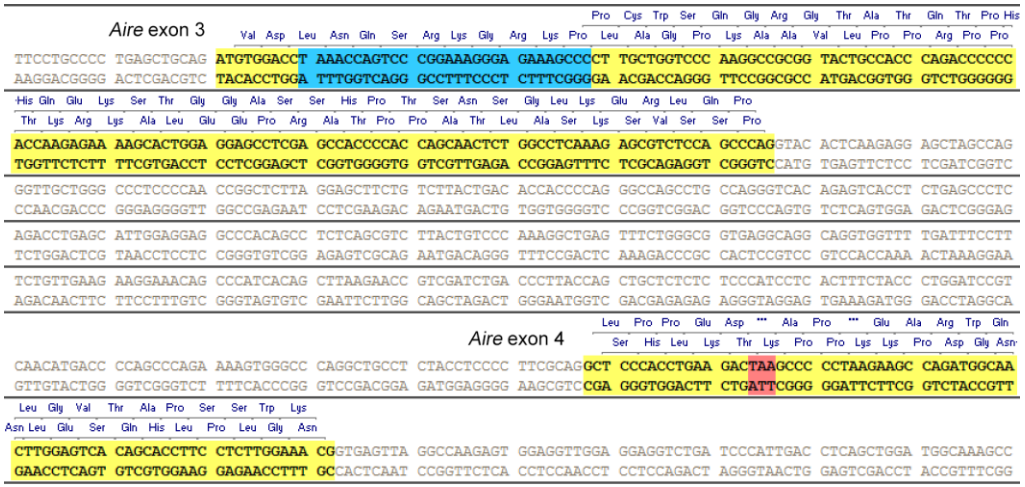	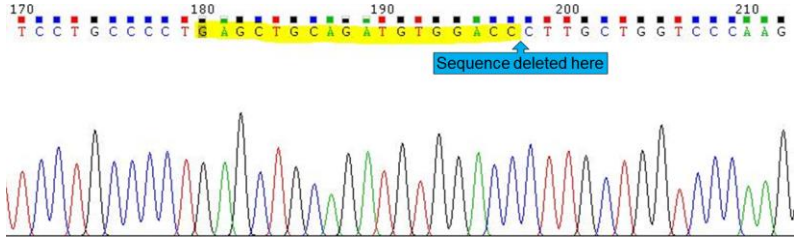
	Allele 2 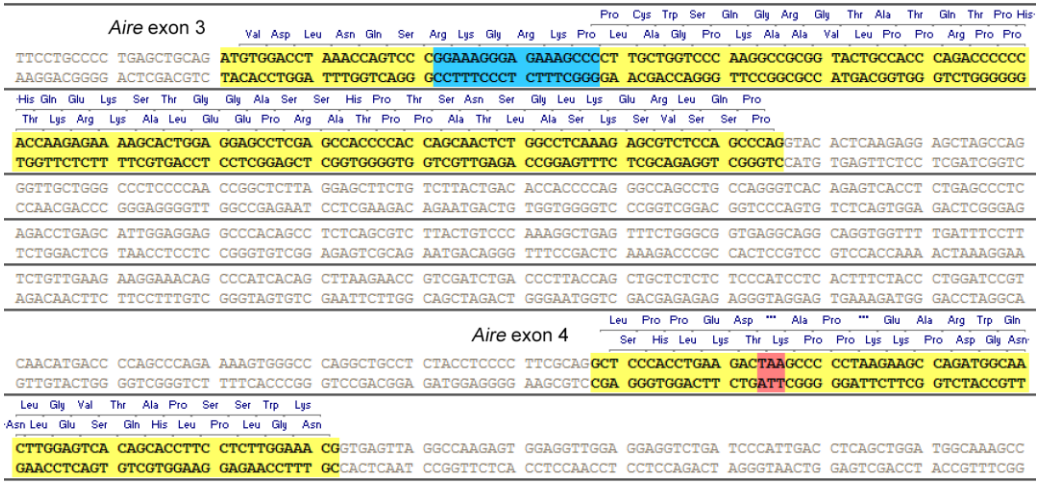	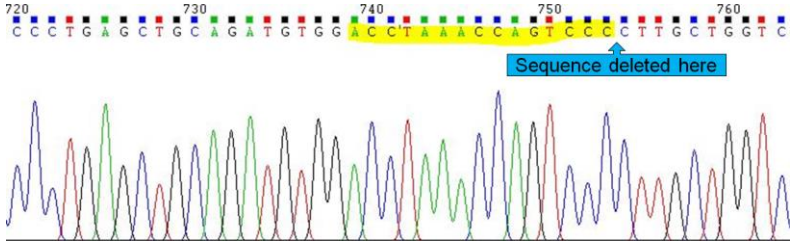

69	Both alleles 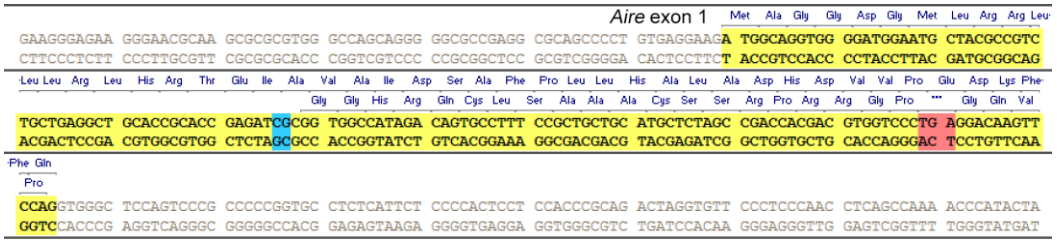	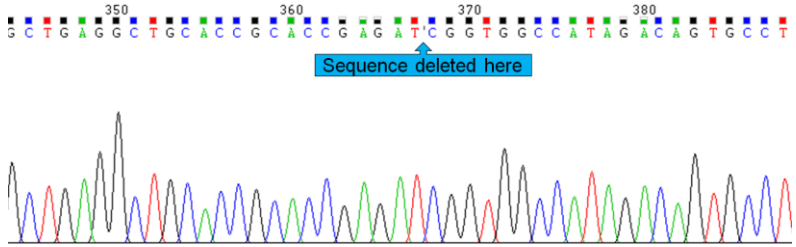

900

Table S2. Human AIRE and AID Constructs, Related to Figure 4 and Figure 5.

(**A**) Human AIRE constructs in pcDNA3.1(**–**)/Myc-His

Name	Description	Remaining region	MW with tag (kDa)
WT	Full length	1-545	60.7
M1	ΔPHD2	1-430	48.8
M2	ΔPHD1, PHD2	1-298	35
M3	ΔSAND, PHD1, PHD2	1-181	23
M4	ΔCARD	101-545	49
M5	ΔCARD, ΔNLS	181-545	41
M6	ΔNLS	1-100, 181-545	52.5
M7	NLS only	101-181	12

(**B**) Human AID constructs in pFLAG-CMV2

Name	Description	Remaining region	MW with tag (kDa)
WT	Full length	1-198	26.3
M1	E58A	1-198	26.3
M2	NLS of AID replaced with NLS of nucleoplasmin	1-198	26.3
M3	ΔCatalytic domain	1-54, 95-198	21.4
M4	ΔAPOBEC-like and ΔNES domains	1-94	13.8
M5	ΔNLS	1-8, 27-198	24
M6	G23S	1-198	26.3

Table S3. Cloning Primers Used to Generate *Aire*$^{-/-}$ CH12 Clones and AIRE and AID Mutant Molecules, Related to Figure 4 and Figure 5.

(A) Primers for cloning human AIRE constructs into pcDNA3.1(–)/Myc-His

Name	Description	Primer name and sequence (5'-3')
WT	Full length	–
M1	ΔPHD2	D430_R AGGAGCCAGGTTCTGCTGACC Hind-Myc_F GAAAGCTTTCTAGAACAAAAACTCATCTCA
M2	ΔPHD1, PHD2	D298_R CTCGTCCTCATTCTTCTGGTGGAG Hind-Myc_F GAAAGCTTTCTAGAACAAAAACTCATCTCA
M3	ΔSAND, PHD1, PHD2	D181_R AATCCCGTTCCCGAGTGGAAG Hind-Myc_F GAAAGCTTTCTAGAACAAAAACTCATCTCA
M4	ΔCARD	EcoRV-ATG_R CATGGTGAATTCTGCAGATATCCAGC D101_F CCCAAAGATGTGGACCTCAGCC
M5	ΔCARD, ΔNLS	EcoRV-ATG_R CATGGTGAATTCTGCAGATATCCAGC D181_F ATTCAGACCATGTCAGCTTCAGTCCA
M6	ΔNLS	D100_R GAAGCTGTCCAGGATGGGCTG D181_F ATTCAGACCATGTCAGCTTCAGTCCA
M7	NLS only	D181_R AATCCCGTTCCCGAGTGGAAG Hind-Myc_F GAAAGCTTTCTAGAACAAAAACTCATCTCA

(B) Primers for cloning human AID constructs into pFLAG-CMV2

Name	Description	Primer name and sequence (5'-3')
M1	E58A	AID_F ATGGACAGCCTCTTGATGAACCG AID_R AAGTCCCAAAGTACGAAATGCGTC
M2	NLS of AID replaced with NLS of nucleoplasmin	npNLS_top AAAAGGCCGGCGGCCACGAAAAAGGCCGGCCAGGCAAAAAAGAAAAAG npNLS_bottom CTTTTTCTTTTTTGCCTGGCCGGCCTTTTTCGTGGCCGCCGGCCTTTT (npNLS_top and npNLS_bottom were annealed together before ligation with the PCR product of the primer pair AID8_R and AID27_F.)
M3	ΔCatalytic domain	AID54_R GCCGTTCTTATTGCGAAGATAACCA AID95_F GCCGACTTTCTGCGAGGGA
M4	ΔAPOBEC-like and ΔNES domains	AID94_R CACATGTCGGGCACAGTCGTAG TAG_F TAGACTGAAACTTTTTTGGGGGAGGG

M5	ΔNLS	AID8_R CCGGTTCATCAAGAGGCTGTCC AID27_F ACCTACCTGTGCTACGTAGTGAAGAGGC
M6	G23S	AID22_R CTTAGCCCAGCGGACATTTTTGA AIDS23_F AGTCGGCGTGAGACCTACCTGTG

(C) Cloning primers for generating pCMV-Tag1-mAire-GFP plasmids

Description	**Primer name and sequence (5'-3')**
Full length Aire	–
AireΔNLS	D106_R GTCCACATCTTTTGGGAAGCCG D182_F ATTCAGACCATGGCAGCTTCTGTC
Full length eGFP	GFP_F ATGGTGAGCAAGGGCGAGGAG GFP_R CTTGTACAGCTCGTCCATGCCG
Aire of AireΔNLS in pCMV-Tag1 vector	TGA-SalI_F TGATGACAGGTCGACCTCGAGC AIRE_R GGAAGAGAAGGGTGGTGTCTCGG

(D) Oligos used to clone sgRNA into targeting vectors

Description	**Oligo name and sequence (5'-3')**
Aire$^{-/-}$ CH12 clone 69	_Top CACCGGCACCGCACCGAGATCGCGG
	_Bottom AAACCCGCGATCTCGGTGCGGTGCC
Aire$^{-/-}$ CH12 clones 43 and 53	_Top CACCGACCTAAACCAGTCCCGGAAA
	_Bottom AAACTTTCCGGGACTGGTTTAGGTC

SUPPLEMENTAL FIGURE LEGENDS

Figure S1. AIRE Is Expressed Specifically in GC B Cells of Human and Mouse Secondary Lymphoid Organs, Related to Figure 1.

(A) Immunofluorescence analysis of the thymus of a healthy donor for EpCAM, AIRE and DNA. Bars: 20 μm.

(B and C) Immunofluorescence analysis of tonsillar tissues of healthy donors for IgD, AIRE, CD19, Pax5, Bcl-6 and DNA. The dotted lines mark the boundary between tonsil follicular mantle zone and the follicle. Arrow heads point to follicular IgD^+ plasmablasts (B) and $Pax5^+Bcl\text{-}6^+AIRE^+$ GC B cells (C). Bars: 15 μm (B) and 30 μm (C).

(D) Flow cytometric analysis of AIRE expression in human peripheral blood naive (IgD^+CD27^-), MZ (IgD^+CD27^+), switched memory (IgD^-CD27+), double-negative (IgD^-CD27^-) B cells, and transitional ($CD24^{hi}CD38^{hi}$), mature ($CD24^{int}CD38^{int}$), memory ($CD24^{hi}CD38^-$) B cells and plasma cells ($CD24^-CD38^{hi}$).

(E) Immunofluorescence analysis of the thymic tissue of a B6 mouse for UEA-1, AIRE and DNA, and the splenic tissue of a B6 mouse immunized with 3 doses of sheep red blood cells (SRBCs) for IgD, Aire, CD19 and DNA, and Bar: 20 μm.

(G) Flow cytometric gating strategy for identifying mouse splenic non-GC ($CD19^+B220^+GL7^-FAS^-$), GC ($CD19^+B220^+GL7^+FAS^+$) B cells and plasma cells ($CD19^{lo}B220^{lo}CD138^+$).

(H) Genotypes and Aire expression in ILN, splenic, peripheral blood and peritoneal B cells of a litter of *Aire*^{Adig} mice after 1 dose of i.p. SRBC immunization with or without CFA.

(I) Percentage of GFP^+ B cells (mean ± SEM) in splenic GC B cells of *Aire*^{Adig} transgene-positive mice (n = 5) after 1 dose of i.p. SRBC immunization with CFA. The dotted line indicates of mean value of GFP^+ B cells in splenic non-GC B cells of these mice.

(J) AIRE expression in mouse peripheral blood, splenic, MLN, PP, peritoneum and thymic B cells of B6.*Aire*^{Adig} mice after 1 dose of i.p. SRBC immunization without CFA. The data are representative of 6 B6.*Aire*^{Adig} and 6 B6 mice that were age- and sex-matched and housed in the same SPF room.

Figure S2. *Aire*$^{+/+}$ and *Aire*$^{-/-}$ Donor BM and B Cells Had a Similar Phenotype Before Transfer, Related to Figure 3.

(A) Flow cytometric analysis of CD45.1$^+$ *Aire*$^{+/+}$ and CD45.2$^+$ *Aire*$^{-/-}$ donor BM before and after B220 cell depletion.

(B) Flow cytometry analysis of splenic naive resting B cells that were purified from the spleens of primary μMT chimeras of CD45.1$^+$ *Aire*$^{+/+}$ and CD45.2$^+$ *Aire*$^{-/-}$ BM and used as donor B cells for the secondary μMT chimeric hosts. The ratio of CD45.2$^+$ *Aire*$^{+/+}$ and CD45.2$^+$ *Aire*$^{-/-}$ splenic B cells were adjusted to be 1:1 prior to the secondary transfer.

(C) Representative purity of CD45.2$^+$ *Aire*$^{+/+}$ and CD45.2$^+$ *Aire*$^{-/-}$ littermate donor B cells before adoptive transfer into μMT hosts.

(D) Cell surface expression of CD21, CD23, CD38, CD40, CD62L, CD80, CD86, CD93, I-A^b, BAFF-R and IgM and IgD on purified CD45.2$^+$ *Aire*$^{+/+}$ and CD45.2$^+$ *Aire*$^{-/-}$ littermate donor B cells before adoptive transfer, as determined by flow cytometry.

(E) NP_8-to-NP_{36} binding ratios (mean ± SEM) of pre-immune splenic naive resting donor B cells of CD45.2$^+$ *Aire*$^{-/-}$, CD45.2$^+$ *Aire*$^{+/+}$ and CD45.1$^+$ *Aire*$^{+/+}$ mice, by 1-way ANOVA with Tukey's post hoc test.

(F) Percentage of $GL7^+FAS^+$ GC B cells in the spleens of μMT recipients of either *Aire*$^{+/+}$ or *Aire*$^{-/-}$ B cells that were immunized i.p. with NP_{32}-KLH. Flow cytometry was performed 4 d after the last immunization.

(G) Cell surface expression of the co-stimulatory or co-inhibitory molecules CD80, CD86, PD-L1, PD-L2 and ICOSL on $GL7^+FAS^+$ GC B cells in the spleens of μMT recipients after immunizations. Shaded histograms indicate the staining using isotype-matched control antibodies.

(H and I) Percentage of splenic PD-1^+CXCR5^+ T_{FH} cells and PD-$1^+CXCR5^+Foxp3^+CD25^+$ T_{FR} cells in the spleens of immunized μMT recipients. The results shown represent 4 experiments, each consisting of B cells from 3–5 age- and sex-matched littermate donor mice and 6–8 age- and sex-matched littermate μMT recipient mice.

(J and K) Flow cytometric and statistical analyses of the percentages of total and intravascular B cells in thymic cells of μMT mice that received donor B cells after all the immunizations with NP_{32}-KLH. Age and sex-matched unimmunized μMT mice were included as controls. The data are represented as mean ± SEM.

(L) The sorting and sequencing strategies for *Aire*$^{+/+}$ and *Aire*$^{-/-}$ donor B cells in μMT recipients after immunizations with NP_{32}-KLH. NP-specific B cells were sorted based on NP_{36} binding.

Figure S3. *Aire*$^{+/+}$ and *Aire*$^{-/-}$B Cells Showed Similar Proliferation and Apoptosis *in vitro*, Related to Figure 3.

(A and B) CFSE dilution in purified splenic B cells from age- and sex-matched littermate donor *Aire*$^{+/+}$ and *Aire*$^{-/-}$ mice treated with medium (Control) or 5 μg/ml anti-CD40 and 100 ng/ml IL-4 for 4 or 6 d. Non-viable cells were excluded from the analysis.

(C) Statistical comparison of the percentage (mean ± SEM) of CFSE^{lo} *Aire*$^{+/+}$ vs. *Aire*$^{-/-}$ splenic B cells (n = 3) after 4 or 6 days of stimulation with 5 μg/ml anti-CD40 and 100 ng/ml IL-4, by 2-tailed unpaired *t*-test. The results represent 3 independent experiments.

(D) Apoptosis of *Aire*$^{+/+}$ or *Aire*$^{-/-}$ B cells treated with medium (Control) or 500 ng/ml CD40L and 100 ng/ml IL-4 for 3 or 7 d, as determined by Annexin V and 7-AAD staining by flow cytometry. All results shown are representative of 3 experiments, each consisting of cells from 2–3 age- and sex-matched littermate *Aire*$^{+/+}$ and *Aire*$^{-/-}$ mice.

Fig. S4. Validation of *Aire*$^{-/-}$ CH12 Cell Clones, Related to Figure 4.

(A) Verification of *Aire* mutations in CH12 clones by PCR using primers that only anneal to the WT sequence, giving no amplification in clones 43, 47 and 53. Clone 47 has a 3-bp deletion in both *Aire* alleles causing a single amino acid deletion, and hence was not used in experiments.

(B) Verification of *Aire* mutations in both alleles of CH12 clone 69 by PCR showing no amplification using primer pair #2 which anneals to the WT but not the mutated sequence. Primer pair #1 amplifies a sequence immediately downstream of the mutation site, and primer pair #3 is specific for the single-stranded repair template used in CRISPR.

(C) Western Blot analysis of AIRE protein expression in WT and *Aire*$^{-/-}$ CH12 cells.

(D) Flow cytometric analysis of apoptosis by Annexin V and 7-AAD staining of WT and *Aire*$^{-/-}$ CH12 cells treated with medium (Control) or anti-CD40, TGF-β1 and IL-4 for 3 d.

(E) Percentages of late (Annexin V^{+}7-AAD^{+}) and early (Annexin V^{+}7-AAD^{-}) apoptotic cells (mean ± SEM) in WT and *Aire*$^{-/-}$ CH12 cells treated with medium (Control) or anti-CD40, TGF-β1 and IL-4 for 3 d. *P < 0.05, by 2-tailed *t*-test. The data in D and E represent 4 experiments.

Fig. S5. AIRE and AID Co-localize in the Nuclei of GC B Cells, Related to Figure 5.

(A–E) Imaging flow cytometry of AIRE and AID in tonsillar $IgD^{-}CD38^{+}$ GC, $IgD^{+}CD38^{-}$ naive, $IgD^{-}CD38^{-}$ switched memory B cells, $IgD^{-}CD38^{hi}$ switched PCs and $IgD^{+}CD38^{+}$ founder GC (FGC) B cells of a healthy donor. DNA was counter stained with DAPI. Samples stained with isotype-matched control antibodies were used to define the fluorescence baseline for AIRE and AID. Four representative cells in each population stained with AIRE and AID or with isotype control antibodies were shown. Bars: 7 μm.

Figure S6. AID Interacts with AIRE in B Cells, Related to Figure 5 and Figure 6.

(A) Co-IP of AIRE and AID in tonsillar $CD19^{+}$ total, IgD^{+} naive, and FGC and $CD19^{+}IgD^{-}$ GC and memory B cells of a healthy donor after treatment of the cell lysates with DNAse I. PCR amplification of β-Actin gDNA in DNAse I-treated or untreated cells was also performed.

(B) Co-IP of AIRE and AID in splenic B cells of immunized WT or *Aicda*$^{-/-}$ mice. The data represent 2 experiments.

(C) Co-IP of AID with pSer5-Pol II, total Pol II, Spt5 and Aire in WT and *Aire*$^{-/-}$ CH12 cells after 72 h of treatment without or with anti-CD40, TGF-β and IL-4. The results represent 3 experiments.

Figure S7. AIRE Deficiency in B Dells Impairs Skin T_H17 Immunity against *C. albicans*, Related to Figure 7.

(A) Levels of autoantibodies (mean ± SEM) binding to IL-17A, IL-17F and IL-22 in the sera of μMT recipient mice of *Aire*$^{+/+}$ or *Aire*$^{-/-}$ donor B cells 4 d after infection. $*P < 0.05$, $**P < 0.01$, by 1-tailed unpaired *t*-test.

(B) Flow cytometric gating strategy for identifying mouse skin viable T cells after *ex vivo* re-stimulation. T cells downregulation CD3 or TCR after *ex vivo* stimulation with PMA and ionomycin; thus $CD3^+$ or $TCR\beta^+$ events were gated for analysis. This gate also included $TCR\gamma\delta^+$ T cells, which were $CD3^+$.

STAR★METHODS

KEY RESOURCES TABLE

REAGENT or RESOURCE	SOURCE	IDENTIFIER
Antibodies against human antigens		
Rat monoclonal anti-AID, unconjugated (mAID-2)	eBioscience	Cat#14-5959
Rabbit polyclonal anti-AID, unconjugated	Jayanta Chaudhuri	(Vuong et al., 2009)
Rat monoclonal anti-AID, AF647 (EK2-5G9)	BD	Cat#565785
Mouse monoclonal anti-AIRE, unconjugated (C-2)	Santa Cruz	Cat#sc-373703
Human recombinant anti-AIRE, APC (REA352)	Miltenyi Biotec	Cat#130-105-401
Rat monoclonal anti-AIRE, eF570 (TM-724)	eBioscience	Cat#41-9534
Human recombinant anti-AIRE, APC (REA352)	Miltenyi Biotec	Cat#130-105-359
Mouse monoclonal anti-Bcl6, unconjugated (GI191E/A8)	Ventana	Cat# 227M
Mouse monoclonal anti-CD19, Biotin (HIB19)	Biolegend	Cat#302204
Mouse monoclonal anti-CD19, eF450 (HIB19)	Tonbo	Cat#75-0199-T100
Mouse monoclonal anti-CD19, PE (4G7)	BD	Cat#349209
Mouse monoclonal anti-CD19, PE (HIB19)	BD	Cat#555413
Mouse monoclonal anti-CD19, PE-CF594 (HIB19)	BD	Cat#562321
Mouse monoclonal anti-CD23, FITC (9P25)	Beckman	Cat#IM0529
Mouse monoclonal anti-CD19, PE-Cy7 (HIB19)	eBioscience	Cat#25-0199
Mouse monoclonal anti-CD19, QDot655 (SJ25C1)	Thermo Fisher	Cat#Q10179
Mouse monoclonal anti-CD19, BV786 (SJ25C1)	BD	Cat#563326
Mouse monoclonal anti-CD24, APC-eF780 (eBioSN3)	eBioscience	Cat#47-0247
Mouse monoclonal anti-CD27, AF647 (O323)	Biolegend	Cat#302812
Mouse monoclonal anti-CD38, APC (HIT2)	Biolegend	Cat#303510
Mouse monoclonal anti-CD38, PE-Cy7 (HIT2)	Biolegend	Cat#303516
Mouse monoclonal anti-CD45, eF450 (2D1)	eBioscience	Cat#48-9459
Mouse monoclonal anti-CD45, PE-Cy7 (HI30)	Tonbo	Cat#60-0459
Mouse monoclonal anti-EpCAM, AF488 (9C4)	Biolegend	Cat#324210
Rabbit monoclonal anti-Hsp90, unconjugated (C45G5)	Cell Signaling	Cat#4877
Goat polyclonal $F(ab)_2$ anti-IgD, Biotin	Southern Biotech	Cat#2032-08
Goat polyclonal $F(ab)_2$ anti-IgD, FITC	Southern Biotech	Cat#2032-02
Mouse monoclonal anti-IgD, FITC (IA6-2)	BD	Cat#555778
Rabbit polyclonal anti-Lamin B1, unconjugated (H-90)	Santa Cruz	Cat#sc-20682
Rat monoclonal anti-Pax5, AF594 (1H9)	BioLegend	Cat#649711
Mouse monoclonal anti-β-Actin, unconjugated (AC-15)	Sigma-Aldrich	Cat#A5441
Antibodies against mouse antigens		
Rat monoclonal anti-AID, unconjugated (mAID-2)	eBioscience	Cat#14-5959
Rabbit polyclonal anti-AID, unconjugated	Jayanta Chaudhuri	(Vuong et al., 2009)
Rabbit polyclonal anti-AIRE, unconjugated (H-300)	Santa Cruz	Cat#sc-33188
Goat polyclonal anti-AIRE, unconjugated (D-17)	Santa Cruz	Cat#sc-17986
Rat monoclonal anti-AIRE, unconjugated (5H12)	eBioscience	Cat#14-5934
Rat monoclonal anti-AIRE, eF660 (5H12)	eBioscience	Cat#50-5934
Human recombinant anti-AIRE, APC (REA352)	Miltenyi Biotec	Cat#130-105-359
Rat monoclonal anti-B220, APC-Cy7 (RA3-6B2)	Biolegend	Cat#103224
Rat monoclonal anti-B220, Biotin (RA3-6B2)	Biolegend	Cat#103204

Rat monoclonal anti-BAFF-R, APC (eBio7H22-E16)	eBioscience	Cat#17-5943
Rat monoclonal anti-CD138, Biotin (281-2)	Biolegend	Cat#142514
Rat monoclonal anti-CD138, PE-Cy7 (281-2)	Biolegend	Cat#142511
Rat monoclonal anti-CD16/CD32, unconjugated (2.4G2)	Tonbo	Cat#70-0161
Rat monoclonal anti-CD16/CD32, unconjugated (2.4G2)	BD	Cat#553141
Rat monoclonal anti-CD19, Biotin (1D3)	BD	Cat#553784
Rat monoclonal anti-CD19, BV650 (6D5)	Biolegend	Cat#115541
Rat monoclonal anti-CD19, FITC (1D3)	Tonbo	Cat#35-0193
Rat monoclonal anti-CD19, Pacific Blue (6D5)	Biolegend	Cat#115523
Rat monoclonal anti-CD19, PE-CF594 (1D3)	BD	Cat#562291
Rat monoclonal anti-CD21, APC (7G6)	BD	Cat#558658
Rat monoclonal anti-CD23, PE (B3B4)	BD	Cat#553139
Rat monoclonal anti-CD25, APC (PC61.5)	Tonbo	Cat#20-0251
Rat monoclonal anti-CD3, APC-Cy7 (17A2)	Tonbo	Cat#25-0032
Rat monoclonal anti-CD38, PE-Cy7 (90)	Biolegend	Cat#102717
Rat monoclonal anti-CD4, unconjugated (GK1.5)	Biolegend	Cat#100401
Rat monoclonal anti-CD4, FITC (GK1.5)	Biolegend	Cat#100406
Rat monoclonal anti-CD4, FITC (GK1.5)	BD	Cat#553729
Rat monoclonal anti-CD4, PE (GK1.5)	Biolegend	Cat#100408
Rat monoclonal anti-CD4, PerCP-Cy5.5 (GK1.5)	Biolegend	Cat#100434
Hamster monoclonal anti-CD40, unconjugated (HM40-3)	eBioscience	Cat#16-0402
Hamster monoclonal anti-CD40, FITC (H40-3)	BD	Cat#553723
Rat monoclonal anti-CD45, violetFluor450 (30-F11)	Tonbo	Cat#75-0451
Rat monoclonal anti-CD45, biotin (30-F11)	eBioscience	Cat#13-0451-85
Rat monoclonal anti-CD62L, PE-Cy7 (MEL-14)	BD	Cat#560516
Hamster monoclonal anti-CD80, PerCP-Cy5.5 (16-10A1)	BD	Cat#560526
Rat monoclonal anti-CD83, BV650 (Michel-19)	Biolegend	Cat#121515
Rat monoclonal anti-CD86, APC (GL-1)	BD	Cat#558703
Rat monoclonal anti-CD93, PE (AA4.1)	Biolegend	Cat#136503
Rat monoclonal anti-CXCR4, Biotin (2B11)	eBioscience	Cat#13-9991
Rat monoclonal anti-CXCR5, PE (L138D7)	Biolegend	Cat#145504
Hamster monoclonal anti-FAS, PE (Jo2)	BD	Cat#554258
Rat monoclonal anti-Foxp3, V450 (MF23)	BD	Cat#561293
Rabbit monoclonal anti-GAPDH, unconjugated (14C10)	Cell Signaling	Cat#2188
Rat monoclonal anti-GL7, AF647 (GL7)	BD	Cat#561529
Rabbit monoclonal anti-Hsp90, unconjugated (C45G5)	Cell Signaling	Cat#4877
Rat monoclonal anti-I-A^b, PerCP-Cy5.5 (AF6-120.1)	Biolegend	Cat#116416
Rat monoclonal anti-ICOSL, PE (HK5.3)	Biolegend	Cat#107405
Rat monoclonal anti-IgA, FITC (C10-3)	BD	Cat#559354
Goat polyclonal anti-IgA, HRP	Bethyl	Cat#A90-103P
Rat monoclonal anti-IgD, PE-Cy7 (11-26c.2a)	Biolegend	Cat#405727
Rat monoclonal anti-IgD, PE-Cy7 (11-26c)	eBioscience	Cat#25-5993
Horse polyclonal anti-IgG, ALP	Vector Laboratories	Cat#AP-2000

Goat polyclonal anti-IgG1, HRP	Jackson Immuno	Cat#115-035-205
Rat monoclonal anti-IgG1, PE-CF594 (A85-1)	BD	Cat#562559
Goat polyclonal anti-IgG2b, HRP	Jackson Immuno	Cat#115-035-207
Goat polyclonal anti-IgG3, HRP	Jackson Immuno	Cat#115-035-209
Goat polyclonal $F(ab)_2$ anti-IgM, unconjugated	Southern Biotech	Cat#1022-01
Rat monoclonal anti-IgM, APC (RMM-1)	Biolegend	Cat#406509
Goat polyclonal anti-IgM, HRP	Bethyl	Cat#A90-101P
Rat monoclonal anti-IL-17A, BV650 (TC11-18H10)	Biolegend	Cat#506929
Goat polyclonal anti-IL-22, AF647 (Poly5164)	Biolegend	Cat#516406
Rat monoclonal anti-Ly6G, AF647 (1A8)	Biolegend	Cat#127610
Hamster monoclonal anti-PD-1, FITC (J43)	eBioscience	Cat#11-9985
Hamster monoclonal anti-PD-1, PE-Cy7 (J43)	eBioscience	Cat#25-9985
Rat monoclonal anti-PD-L1, PE-Cy7 (10F.9G2)	Biolegend	Cat#124314
Rat monoclonal anti-PD-L2, PE (TY25)	BD	Cat#557796
Goat polyclonal anti-Pol II, unconjugated	Bethyl	Cat#A303-835A
Rabbit polyclonal anti-Pol II Ser5, unconjugated	Bethyl	Cat#A304-408A
Rabbit polyclonal anti-Spt5, unconjugated	Santa Cruz	Cat#sc-28678
Hamster monoclonal anti-TCRβ, PerCP-Cy5.5 (H57-597)	Biolegend	Cat#109227
Hamster monoclonal anti-TCRγδ, BV421 (GL3)	Biolegend	Cat#118119
Mouse monoclonal anti-β-Actin, unconjugated (AC-15)	Sigma-Aldrich	Cat#A5441
Mouse monoclonal anti-IL17A, unconjugated (eBioMM17F3)	eBioscience	Cat#16-7173-81
Mouse monoclonal anti-IL17F, unconjugated (RN17)	eBioscience	Cat#16-7473-82
Mouse monoclonal anti-IL22, unconjugated (IL22JOP)	eBioscience	Cat#16-7222-82
Antibodies against protein tags		
Mouse monoclonal anti-6xHis, unconjugated (J099B12)	Biolegend	Cat#652502
Mouse monoclonal anti-c-Myc, unconjugated (9E10)	Biolegend	Cat#626802
Rabbit polyclonal anti-FLAG, unconjugated	Cell Signaling	Cat#2368
Mouse monoclonal anti-FLAG, magnetic beads (M2)	Sigma-Aldrich	Cat#F3165
Isotype control antibodies		
Goat polyclonal IgG, unconjugated	Santa Cruz	Cat#sc-2028
Goat polyclonal IgG, AF647 (Poly24030)	Biolegend	Cat#403006
Goat polyclonal $F(ab)_2$ IgG, Biotin	Southern Biotech	Cat#0110-08
Goat polyclonal $F(ab)_2$ IgG, FITC	Southern Biotech	Cat#0110-02
Hamster monoclonal IgG2, PE (B81-3)	BD	Cat#550085
Hamster monoclonal IgG2, PerCP-Cy5.5 (B81-3)	BD	Cat#560562
Hamster monoclonal IgM, FITC (G235-1)	BD	Cat#553960
Mouse monoclonal IgG1, AF647 (MOPC-21)	Biolegend	Cat#400155
Mouse monoclonal IgG1, APC (MOPC-21)	BD	Cat#555751
Mouse monoclonal IgG1, APC (MOPC-21)	Biolegend	Cat#400120
Mouse monoclonal IgG1, Biotin (MOPC-21)	Biolegend	Cat#400103
Mouse monoclonal IgG1, PE (MOPC-21)	BD	Cat#555749
Mouse monoclonal IgG1, PE-Cy7 (MOPC-21)	BD	Cat#555872

Mouse monoclonal IgG1, PE-Cy7 (MOPC-21)	Biolegend	Cat#400126
Mouse monoclonal IgG2a, FITC (X39)	BD	Cat#349051
Rabbit polyclonal IgG, unconjugated	Santa Cruz	Cat#sc-2027
Rabbit polyclonal IgG, unconjugated	R&D	Cat#AF-008
Rat monoclonal IgG1, BV650 (RTK2071)	Biolegend	Cat#400437
Rat monoclonal IgG2a, unconjugated (RTK2758)	Biolegend	Cat#400501
Rat monoclonal IgG2a, APC (RTK2758)	Biolegend	Cat#400511
Rat monoclonal IgG2a, Biotin (eBR2a)	eBioscience	Cat#13-4321
Rat monoclonal IgG2a, eF570 (eBR2a)	eBioscience	Cat#41-4321
Rat monoclonal IgG2a, PE (eBR2a)	eBioscience	Cat#12-4321
Rat monoclonal IgG2a, PerCP-Cy5.5 (RTK2758)	Biolegend	Cat#400531
Rat monoclonal IgG2a, PE-Cy7 (RTK2758)	Biolegend	Cat#400521
Rat monoclonal IgG2b, unconjugated (eB149/10H5)	eBioscience	Cat#14-4031
Rat monoclonal IgG2b, AF647 (A95-1)	BD	Cat#557691
Rat monoclonal IgG2b, Biotin (RTK4530)	Biolegend	Cat#400603
Rat monoclonal IgG2b, eF660 (eB149/10H5)	eBioscience	Cat#50-4031
Rat monoclonal IgG2b, PE (A95-1)	BD	Cat#553989
Rat monoclonal IgG2b, PE-Cy7 (RTK4530)	Biolegend	Cat#400617
Human recombinant IgG, APC (REA293)	Miltenyi Biotec	Cat#130-104-615
Human recombinant IgG, PE (REA293)	Miltenyi Biotec	Cat#130-104-613
Secondary antibodies		
Mouse monoclonal anti-Biotin, magnetic microbeads	Miltenyi Biotec	Cat#130-090-485
Donkey polyclonal anti-goat IgG, HRP	Santa Cruz	Cat#sc-2020
Donkey polyclonal anti-mouse IgG, AF546	Thermo Fisher	Cat#A10036
Donkey polyclonal anti-mouse IgG, CF647	Sigma-Aldrich	Cat#SAB4600176
Donkey polyclonal anti-mouse IgG, HRP	Santa Cruz	Cat#sc-2318
Donkey polyclonal F(ab')$_2$ anti-rat IgG, HRP	Jackson Immuno	Cat#712-036-153
Goat polyclonal F(ab')$_2$ anti-mouse IgG, Cy3	Jackson Immuno	Cat#115-166-006
Goat polyclonal F(ab')$_2$ anti-mouse IgG, FITC	Southern Biotech	Cat#1032-02
Goat polyclonal F(ab')$_2$ anti-rabbit IgG, Cy3	Jackson Immuno	Cat#111-166-047
Goat polyclonal anti-rabbit IgG, HRP	Santa Cruz	Cat#sc-2004
Bacterial, Fungal and Viral Strains		
Candida albicans	ATCC	Cat#MYA-2876
Heat Inactivated *C. albicans* pseudohyphae	Made in house	This paper
Live *C. albicans* pseudohyphae	Made in house	This paper
Biological Samples		
Human blood	American Red Cross	This paper
Human spleen	Children's Hospital of Michigan	This paper
Human thymus	Children's Hospital of Michigan	This paper
Human tonsil, healthy	Children's Hospital of Michigan	This paper

Human tonsil, HIGM3	Mount Sinai Medical Center	This paper
Sheep red blood cell	Innovative	Cat#IC100-0210
Chemicals, Peptides, and Recombinant Proteins		
NP_8, FITC	BioSearch	Cat#N-5050F
NP_{36}, PE	BioSearch	Cat#N-5070-1
NP_{32}, KLH	BioSearch	Cat#N-5060
NP_4, BSA	BioSearch	Cat#N-5050L-10
NP_{29}, BSA	BioSearch	Cat#N-5050H-10
UEA-1, Biotin	Vector Laboratories	Cat#B-1065
Streptavidin, AF488	Thermo Fisher	Cat#S11223
Streptavidin, AF546	Thermo Fisher	Cat#S11225
Streptavidin, PerCP-Cy5.5	BD	Cat#551419
Streptavidin, BV605	Biolegend	Cat#405229
Streptavidin, BV785	Biolegend	Cat#405249
Streptavidin, Qdot605	Thermo Fisher	Cat#Q10101MP
Aldehyde Reactive Probe	Cayman Chemical	Cat#10009350
RNase A	Sigma	Cat# R6513
Proteinase K	Qiagen	Cat# 9133
HaeIII	New England Biolabs	Cat# R0108S
O-Allylhydroxylamine hydrochloride (AA7)	Sigma	Cat# 05983
Methoxyamine hydrochloride	Sigma	Cat# 226904
Alkoxyamine-6 (AA6)	Ashok Bhagwat	(Wei et al., 2017)
Alkoxyamine-3 (AA3)	Ashok Bhagwat	(Wei et al., 2015)
DBCO -Cy5	Click Chemistry Tools	Cat# A130-1
Cy5 Azide	Lumiprobe	Cat# A3330
Copper bromide	Sigma	Cat# 254185
TBTA Tris[(1-benzyl-1H-1,2,3-triazol-4-yl)methyl]amine	Sigma	Cat# 678937
DNA Clean and Concentrator kit	Zymo research	Cat# D4014
SYBR Gold nucleic acid gel stain	Invitrogen	Cat# S11494
Zeta probe membrane	Bio-Rad	Cat# 1620165
Complete Freund's Adjuvant	Thermo Fisher	Cat#77140
Incomplete Freund's Adjuvant	Thermo Fisher	Cat#77145
Histopaque-1077	Sigma-Aldrich	Cat#10771
Ammonium-Chloride-Potassium (ACK) Lysis Buffer	Thermo Fisher	Cat#A1049201
Collagenase II	Worthington	Cat#LS004177
Collagenase V	Sigma-Aldrich	Cat#C9263-1G
DNase I	Roche	Cat#11284932001
CD40L (Human)	Peprotech	Cat#310-02
IL-4 (Human)	Peprotech	Cat#200-21
IFN-γ (Human)	Peprotech	Cat#300-02
CD40L (Mouse)	Peprotech	Cat#315-15
IL-4 (Mouse)	Peprotech	Cat#214-14
IL-4 (Mouse)	R&D	Cat#404-ML
IL-17A (Mouse)	Peprotech	Cat#210-17
IL-17F (Mouse)	Peprotech	Cat#210-17F
IL-17RA homodimer (Mouse)	R&D	Cat# 4481-MR-100

IL-21 (Mouse)	Peprotech	Cat#210-21
IL-22 (Mouse)	Peprotech	Cat#210-22
IL-22Rα1 (Mouse)	R&D	Cat# 4294-MR-050
TGF-β1 (Mouse)	R&D	Cat#7666-MB/CF
AIRE and AID WT and mutant proteins, **Table S2**	Kang Chen	This paper
Caffeic Acid Phenethyl Ester (CAPE)	Cayman	Cat#70750
Carboxyfluorescein Succinimidyl Ester (CFSE)	Biolegend	Cat#422701
Lipofectamine 3000	Thermo Fisher	Cat#L3000015
Protease Inhibitor Cocktail	Sigma-Aldrich	Cat#P8340
TRIzol	Thermo Fisher	Cat#15596026
RNALater	Thermo Fisher	Cat#AM7020
RNAProtect	QIAGEN	Cat#76526
NP-40	Sigma-Aldrich	Cat#I8896
4-20% Bis-Tris Gel	GeneScript	Cat#M42012
10% Tris-Glycine Gel	Bio-Rad	Cat#4561034
Polyvinylidene fluoride (PVDF) Membrane	Bio-Rad	Cat#1620177
Nitrocellulose Membrane	Bio-Rad	Cat#1620115
ECL Substrate	Bio-Rad	Cat#170-5061
Western Blotting Chemiluminescence Luminol Reagent	Santa Cruz	Cat#sc-2048
Fc Blocking Reagent	Miltenyi Biotec	Cat#130-059-901
Fc Blocking Reagent	Tonbo Biosciences	Cat#70-0161
CytoFix/CytoPerm	BD	Cat#554722
Transcription Factor Buffer	BD	Cat#562725
7-aminoactinomycin D (7AAD)	Tonbo Biosciences	Cat#13-6993-T500
7-aminoactinomycin D (7AAD)	BD	Cat#559925
Ghost Dye Violet 510 (GV510)	Tonbo Biosciences	Cat#13-0870-T500
Anti-Biotin Magnetic Microbeads	Miltenyi Biotec	Cat#130-090-485
4’,6-diamidine-2’-phenylindole dihydrochloride (DAPI)	Sigma-Aldrich	Cat#D9542
BluePhos Phosphate Substrate	KPL	Cat#50-88-02
BbsI restriction enzyme	Thermo Fisher	Cat#ER1011
Ficoll-Paque	GE Healthcare	Cat#17-1440-03
Golgi Plug	BD	Cat#55029
PMA	Sigma-Aldrich	Cat#P1585-1MG
Ionomycin	Thermo Fisher	Cat#I24222
Quick T4 Ligase	New Engl. Biolabs	Cat#M2200L
Opti-MEM	Thermo Fisher	Cat#31985070
Protein G Beads	Cell Signaling	Cat#8740
Protein G Beads	Thermo Fisher	Cat#88847
CelLytic M Buffer	Sigma-Aldrich	Cat#C2978
Halt Phosphatase Inhibitor	Thermo Fisher	Cat#78426
FluorSave mounting medium	EMD Millipore	Cat#345789
HRP conjugation kit	Abcam	Cat#Ab102890
Image-iT FX Signal Enhancer	Thermo Fisher	Cat#I36933
Critical Commercial Assays		
Mouse B Cell Isolation kit	Miltenyi Biotec	Cat#130-090-862
Click-iT EdU Flow Cytometry Assay kit	Thermo Fisher	Cat#C10418
Phusion Site-Directed Mutagenesis kit	Thermo Fisher	Cat#F541

Amaxa Cell Line Nucleofector Kit V	Lonza	Cat#VCA-1003
BCA Protein Assay kit	Thermo Fisher	Cat#23225
iTaq Universal SYBR Green One-Step kit	Bio-Rad	Cat#172-5150
Cells-to-C_T 1-step SYBR Green kit	Thermo Fisher	Cat#A25601
ChIP Assay kit	EMD Millipore	Cat#17-295
Mouse IgA ELISA	Bethyl	Cat#E90-103
Superscript III First Strand Synthesis	Thermo Fisher	Cat#18808051
PowerSYBR Green Master Mix	Thermo Fisher	Cat#4367660
Experimental Models: Cell Lines		
CH12F3, WT	Tasuku Honjo	(Nakamura et al., 1996)
CH12F3, *Aire*$^{-/-}$ (clones 43, 53 and 69)	Kang Chen	This Paper
CH12F3, *Acida*$^{-/-}$	Kefei Yu	This Paper
CH12F3, *Ung*$^{-/-}$	Ashok Bhagwat	This Paper
HKB-11	ATCC	Cat#12568
Experimental Models: Organisms/Strains		
C57BL/6J	Jackson	Cat#000664
Aire$^{+/-}$ (B6.129S2-Aire$^{tm1.1Doi}$/J)	Jackson	Cat#004743
µMT (B6.129S2-*Ighm*^{tm1Cgn}/J)	Jackson	Cat#002288
B6.*Aire*^{Adig} reporter	Mark Anderson	(Gardner et al., 2008)
Aicda$^{-/-}$	Tasuku Honjo	(Muramatsu et al., 2000)
CD45.1 (B6.SJL-*Ptprc*^{a} *Pepc*^{b}/BoyJ)	Jackson	Cat#002014
Oligonucleotides		
A) qRT-PCR Primers		
Human Primers:		
ACTB: _F: AGAGCTACGAGCTGCCTGAC _R: AGCACTGTGTTGGCGTACAG	Sigma-Aldrich	(Wang et al., 2013)
Iµ_F: GTGATTAAGGAGAAACACTTTGAT	Sigma-Aldrich	(Chen et al., 2009)
Cγ1_R: CCAGGGCTGCTGTGCCCCCA	Sigma-Aldrich	This Paper
Cγ3_R: CCAGGGCCGCTGTGCCCCCA	Sigma-Aldrich	This Paper
AIRE: _F: CCAGGCTCTCAACTGAAGGC _R: GAATCCCGTTCCCGAGTGG	Sigma-Aldrich	(Dudakovic et al., 2015)
Mouse Primers:		
Actb _F: TGCGTGACATCAAAGAGAAG _R: CGGATGTCAACGTCACACTT	Sigma-Aldrich	(Steuerwald et al., 2000)
Aicda _F: GAAAGTCACGCTGGAG _R: TCTCATGCCGTCCCTT	Sigma-Aldrich	(Xu et al., 2015)
Aire (B6.129S2-Aire$^{tm1.1Doi}$/J)*:* _F: GACAAGTTCCAGGAGACGCT _R: AAGCCGTCCAGGATGCTATG	Sigma-Aldrich	This Paper

Iα-Cμ circle transcript: Iα_F: CCAGGCATGGTTGAGATAGAGATAG Cμ_R: AATGGTGCTGGGCAGGAAGT	Sigma-Aldrich	(Cao et al., 2015)
Iγ1-Cμ circle transcript: Iγ1_F: GGCCCTTCCAGATCTTTGAG Cμ_R: AATGGTGCTGGGCAGGAAGT	Sigma-Aldrich	(Doi et al., 2008)
Iμ-Cμ germline transcript: Iμ_F: CTCTGGCCCTGCTTATTGTTG Cμ'_R: GAAGACATTTGGGAAGGACTG	Sigma-Aldrich	(Muramatsu et al., 2000)
Iα-Cα germline transcript: Iα_F: CCTGGCTGTTCCCCTATGAA Cα_R: GAGCTCGTGGGAGTGTCAGTG	Sigma-Aldrich	(Boersma et al., 2015)
Sμ (after ChIP): Sμ_F: TAGTAAGCGAGGCTCTAAAAAGCAT Sμ_R: AGAACAGTCCAGTGTAGGCAGTAGA	Sigma-Aldrich	(Nowak et al., 2011)
Iμ (after ChIP): Iμ_F: GCTCAGCCTGGACTTTCGGTTTGGT Iμ_R: GGAGTCAAGATGGCCGATCAGAACC	Sigma-Aldrich	(Nowak et al., 2011)
Sγ1 (after ChIP): Sγ1_F: TATGATGGAAAGAGGGTAGCATTCACC Sγ1_R: CTCCTTCCCAATCTCCCGTG	Sigma-Aldrich	(Nowak et al., 2011)
sgRNA (CH12 mutant 69): GCACCGCACCGAGATCGCGG (PAM:TGG)	Feng Zhang	http://crispr.mit.edu
sgRNA (CH12 mutants 43 and 53): ACCTAAACCAGTCCCGGAAA (PAM:GGG)	Feng Zhang	http://crispr.mit.edu
B) Primers for screening CRISPR mutants		
CH12 Mutant 69: _F: CTTTCCCGCTTCCTCTATCC _R: ACTGTCTATGGCCACCGC	Sigma-Aldrich	This paper
CH12 Mutant 43: _F1: ACCTAAACCAGTCCCGGAAA _F2 (Second Mutation): CCATTGTTCCTGCCCCTG _R: ACCGTTTCCAAGAGGAAGGT	Sigma-Aldrich	This paper
CH12 Mutant 53: _F: ACCTAAACCAGTCCCGGAAA _R: ACCGTTTCCAAGAGGAAGGT	Sigma-Aldrich	This paper
C) Primers used to generate *AIRE* and *AICDA* mutants, Table S3	Sigma-Aldrich	This paper
D) Oligos used to clone sgRNA for CH12 CRISPR mutants, Table S3	Sigma-Aldrich	This paper
E) Primers to amplify β-Actin gDNA after DNAse I treatment		
*ACTB*_gDNA: _F: CAAGGCCAACCGCGAGAAGA _R: TGTGCTGGGGTCTTGGGATG	Sigma-Aldrich	This paper
Recombinant DNA		
pSpCas9(BB)-2A-Puro	Addgene	Cat#48139
pFLAG-CMV2	Sigma-Aldrich	Cat#E7033
pcDNA3.1(–)	Thermo Fisher	Cat#V38520
pcDNA3-eGFP	Thilo Hagen	N/A

pCMV-Tag1	Agilent Technologies	Cat#211170
Software and Algorithms		
FlowJo 7 and 10	Tree Star	N/A
Adobe Photoshop CS6	Adobe	N/A
Prism 6	GraphPad	N/A
StepOne RT-PCR software	Applied Biosystems	N/A
IDEAS 6.1	Amnis	N/A
VectorNTI 10	Thermo Fisher	N/A
ImageQuant TL 8.1	GE Healthcare	N/A
IMonitor 1.1.0	Wei Zhang	(Zhang et al., 2015)

CONTACT FOR REAGENT AND RESOURCE SHARING

Further information and requests for resources and reagents should be directed to and will be fulfilled by the Lead Contact, Kang Chen (kang@wayne.edu).

EXPERIMENTAL MODEL AND SUBJECT DETAILS

Human subjects

Autoimmune polyglandular syndrome type 1 (APS-1) patients with loss-of-function mutations in the *AIRE* gene were enrolled in the study with an approved protocol of the Ethics Committee of Medicine of the Hospital District of Helsinki and Uusimaa (HUS), Finland. Hyper-IgM syndrome type 3 (HIGM3) patients with loss-of-function mutations in the *CD40* gene were enrolled in the study with an approved Institutional Review Board (IRB) protocol of the Icahn School of Medicine at Mount Sinai. Peripheral blood leukocytes of anonymous healthy donors were obtained from the American Red Cross with a protocol approved by the IRB of Wayne State University (WSU) and the Detroit Medical Centre (DMC). Tonsil, thymus and spleen tissues were obtained after pediatric tonsillectomy, cardiac surgery and splenectomy, respectively, from the Children's Hospital of Michigan with an IRB protocol approved by WSU and DMC.

Mice

C57BL/6J mice, *Aire*$^{+/-}$ and μMT were purchased from the Jackson Laboratory. *Aire*^{Adig} mice in C57BL/6 background were previously reported (Gardner et al., 2008). *Aicda*$^{-/-}$ mice (Muramatsu et al., 2000) were generously provided by Dr. Tasuku Honjo (Kyoto University, Japan). These mice were maintained in the same room at the specific pathogen-free (SPF) facility of the Division of Laboratory Animal Resources (DLAR) at Wayne State University. *Aire*$^{-/-}$ mice were generated by mating *Aire*$^{+/-}$ mice. Age- and sex-matched *Aire*$^{+/+}$ littermates were randomly assigned to experimental groups or used as controls for *ex vivo* and *in vivo* experiments. Prior to any experiment, all *Aire* and *Aire*^{Adig} mice were genotyped by PCR to ensure the correctness of the genotype. All breeding and experimental protocols were approved by Wayne State University Institutional Animal Care and Use Committee (IACUC).

Primary cell cultures

Peripheral blood IgD^{+}CD27^{-} naive B cells of healthy subjects or APS-1 patients were sorted and stored in RNALater. Primary blood, spleen and tonsil IgD^{+} B cells were purified by MACS and cultured in RPMI-1640 medium. Mouse cells purified from spleen and lymph nodes were extracted via B cell isolation kit and cultured in RPMI-1640 medium further supplemented with 5% (v/v) NCTC-109 and 50 μM β-mercaptoethanol.

Cell lines

The human embryonic kidney cell/Burkitt's lymphoma fusion cell line HKB-11 was cultured in DMEM/F12 supplemented with 2 mM L-glutamine, 100 U/ml penicillin, 100 μg/ml streptomycin, 0.25 μg/ml amphotericin B and 10% FBS. WT, *Aire*$^{-/-}$, *Acida*$^{-/-}$ and *Ung*$^{-/-}$ CH12 cells (generated in house) were cultured in RPMI-1640 medium further supplemented with 5% (v/v) NCTC-109 and 50 μM β-mercaptoethanol.

Microbe strain

The *C. albicans* strain SC5314 was purchased from the ATCC, streak plates were made on YPD agar and incubated at 30°C overnight. Plates were then stored at 4°C. For experiments, single colonies were cultured in YPD broth at 30°C for 16 h with shaking at 220 rpm prior to induction of virulent pseudohyphae formation.

METHOD DETAILS

Human blood and tissue sample processing and cell isolation

Peripheral blood mononuclear cells (PBMCs) of APS-1 patients and healthy controls were purified using Ficoll-Paque Plus. Live ($7AAD^-$ or Ghost Violet 510^-) naive B cells ($CD19^+IgD^+CD27^-$) and class-switched memory B cells ($CD19^+IgD^-CD27^+$) were sorted from the PBMCs to a purity of ≥ 99% on a FACSAria II sorter (BD). PBMCs of anonymous healthy donors were isolated using a Histopaque-1077 gradient following the manufacturer's instruction. Red blood cells (RBCs) were lysed using an ammonium-chloride-potassium (ACK) lysing buffer. Human tonsil and spleen tissues were minced into small pieces, meshed through 100 μm cell strainers, and pelleted at 600 g for 5 min at 4°C. Spleen cells were treated with an ACK buffer to remove erythrocytes and filtered through 40 μm cell strainers. Tonsil and spleen cells were then washed with phosphate-buffered saline (PBS). IgD^+ B cells were purified from tonsil cells by magnetic-activated cell sorting (MACS) with a biotinylated goat $F(ab')_2$ anti-human IgD antibody and anti-biotin magnetic microbeads as previously reported (Chen et al., 2009). $CD19^+$ B cells were similarly obtained using a biotinylated mouse anti-human CD19 (clone HIB19) antibody. The $CD19^+IgD^-$ fraction was obtained by selecting for $CD19^+$ cells from the IgD^- fraction by MACS. Thymic cell suspensions were obtained by mincing human thymus tissues

into small pieces and mechanically removing thymocytes followed by 2 rounds of digestion with 0.2% (w/v) Collagenase V and 0.1 mg/ml DNase I in Hank's Balanced Salt Solution (HBSS) for 45 min at 37°C with shaking. The digested samples were filtered through 70 μm cell strainers and washed with PBS.

Mouse blood and tissue cell isolation

Blood was collected from mice before euthanasia. spleen, inguinal lymph nodes, mesenteric lymph node and Peyer's patches were collected after euthanasia. Adjacent fat and other tissues were removed before single cells suspensions were prepared, filtered through 100 μm cell strainer. RBCs from blood were removed by centrifugation on Histopaque 1077, and those in spleens were lysed using an ACK buffer. The cells were washed in PBS and counted before cell sorting, flow cytometry or purification by MACS. Resting B cells were isolated from the spleens of age- and sex-matched *Aire*$^{+/+}$ or *Aire*$^{-/-}$ littermates by MACS using a B Cell Isolate Kit. The purity of the isolated B cells ranged from 97–99.6% as determined by flow cytometry based on CD19 and B220 staining.

Mouse immunization

2.5×10^7 purified *Aire*$^{+/+}$ or *Aire*$^{-/-}$ B cells were introduced via the tail vein into each recipient μMT littermate mouse. One day after the adoptive transfer, each recipient was intraperitoneally (i.p.) immunized with 1 dose of 100 μg NP_{32}-KLH in Complete Freund's Adjuvant and 3 doses of 100 μg NP_{32}-KLH in Incomplete Freund's Adjuvant once every week. Four days after the last immunization, mice were sacrificed, and blood and spleens were collected for ELISA, flow cytometry or cell sorting. In some experiments, mice were immunized 3 times, each with 200 μl of 2% sheep red blood cells in CFA for the initial immunization and IFA for the following

immunizations. For **Figure S1H**, mice were immunized i.p. with 4×10^8 SRBCs in PBS in a final volume of 200 µl/mouse with or without CFA.

BM chimeras and B cell chimeras

BM cells were isolated from the tibias and femurs of age- and sex-matched CD45.1 *Aire*$^{+/+}$ and CD45.2 *Aire*$^{-/-}$ mice by flushing the BM cells with serum-free RPMI-1640 using 27G needles. Following RBC lysis, B220$^+$ BM cells were depleted by MACS after labeling the BM cells with a biotinylated anti-mouse B220 antibody and anti-biotin microbeads. The B220$^-$ cells from CD45.1 *Aire*$^{+/+}$ and CD45.2 *Aire*$^{-/-}$ BMs were mixed at the ratio of 1:1 and adoptively transferred via the tail vein into sex-matched primary µMT littermate recipients 1 d after these recipients received 10 Gy total body irradiation, with each recipient receiving a total of 1.5×10^7 cells. BM reconstitution was allowed to proceed for 28 days. Splenic resting naive B cells were isolated from these primary µMT recipients by MACS using a B Cell Isolation Kit similarly as described above. Purified splenic B cells were counted, adjusted to a ratio of 1:1 and adoptively transferred via the tail vein into sex-matched secondary µMT littermate recipients, with each recipient receiving a total of 1.5×10^7 cells. Mice were then immunized with NP_{32}-KLH and adjuvants as described above.

Discrimination of intravascular and tissue leukocytes

A published method was used to distinguish intravascular and tissue leukocytes in mice (Anderson et al., 2014). In this method, mice were intravenously administered with 6 µg biotinylated anti-CD45 antibody 2–3 minutes prior to anesthesia and cardiac perfusion with PBS, followed by immediate tissue harvest and digestion. Intravascular cells were subsequently stained with fluorochrome-conjugated streptavidin in combination with other cell surface markers before analysis by flow cytometry.

Culture and stimulation or primary B cells

Peripheral blood $IgD^{+}CD27^{-}$ naive B cells of healthy subjects or APS-1 patients were stimulated with 500 ng/ml soluble CD40L (sCD40L) and 100 ng/ml IL-4 or 100 ng/ml IFN-γ. Purified mouse splenic B cells were stimulated with 500 ng/ml sCD40L with or without 100 ng/ml IL-4, 100 ng/ml IL-21 or 25 μM CAPE. In some experiments, sCD40L was replaced with 5 μg/ml anti-CD40. To determine cell proliferation, the cells were labelled with carboxyfluorescein succinimidyl ester (CFSE) according to the manufacture's protocol prior to culture. Alternatively, 10 μM 5-ethynyl-2'-deoxyuridine (EdU) was added to the culture medium for 6 hours before EdU incorporation was determined by flow cytometry using a Click-iT EdU Flow Cytometry Assay Kit according to the manufacturer's protocol.

Generation and validation of *Aire*$^{-/-}$ CH12 cells

Several clones of *Aire*$^{-/-}$ CH12 cells were generated by targeting the *Aire* gene using the CRISPR/Cas9 system as described previously (Ran et al., 2013). Single guide RNAs (sgRNA) targeting exon 1 or exon 3 of mouse *Aire* gene (GenBank AJ007715.1) were designed using the online tool at http://crispr.mit.edu. Sequences with the highest score for the respective region were selected. To express sgRNAs, pairs of oligonucleotides were synthesized and cloned into pSpCas9(BB)-2A-Puro plasmid as reported (Ran et al., 2013). The sgRNA expression plasmid was then transfected into CH12 cells using electroporation (square wave pulse at 200 V for 30 ms) in serum-free RPMI-1640 with 5 mM glutathione in a 4-mm cuvette. 24 hours after transfection, cells were resuspended in 125 ng/ml puromycin for 48 hours. After a brief expansion in puromycin-free media, single cell clones from transfected cells were screened for loss of the sgRNA targeting site using PCR. Clones with deletions in both alleles were identified by PCR. To determine the exact genomic modifications in each clone, the sgRNA-targeting sites

were amplified with primer pairs spanning the targeting sites, and PCR products were sequenced directly using the respective forward primer. In addition, PCR products from clones 43 and 53 were cloned into the pGEM-T Easy vector and sequenced with T7 primer. All three mutant clones used were confirmed to harbor frameshift mutations on both alleles, resulting in termination shortly after the frameshift site. The potential off-target sites in the mouse genome for each guide were identified by the same online tool (http://crispr.mit.edu). Cas9 generally does not tolerate more than 3 mismatches (Hsu et al., 2013). All off-target sites in a potential gene-coding region with non-zero scores (up to 4 mismatches) were verified by sequencing to be intact. The lack of AIRE protein expression in these clones was finally confirmed by Western Blot.

Plasmids

Full-length human *AIRE* cDNA sequence was cloned into pcDNA3.1(–) with tandem C-terminal Myc and 6-Histidine tag. Sequences coding various domains of AIRE were deleted using a Phusion Site-Directed Mutagenesis Kit using appropriate primers. Briefly, to delete a specific section of *AIRE* in the vector, a pair of outward primers was designed to amplify the remaining region together with the plasmid backbone. PCR product was then phosphorylated at 5' end and ligated with Quick T4 ligase to recircularize it. Human AID was obtained by cloning full-length *AICDA* into pFLAG-CMV2 vector with an N-terminal FLAG tag. Domain-specific deletion mutants and G23S and E58A point mutants of AID were generated using the Phusion Site-Directed Mutagenesis kit using appropriate primers. The full-length *Egfp* sequence from pcDNA3-eGFP (from Dr. Thilo Hagen, National University of Singapore) was then cloned in frame to the C-terminus of mouse *Aire*, *AireΔNLS*, or *AireΔCARD* using blunt end ligation of PCR-amplified fragments.

Transfection

10^6 seeded HKB-11 cells were cultured to 70–90% confluence and transfected with 4 μg plasmid DNA using Lipofectamine 3000 in Opti-MEM by following the manufacturer's instruction. CH12 cells were transfected using the Amaxa cell line nucleofector kit V (Lonza). Cells were pelleted at 100 g for 10 min and resuspended in the electroporation buffer according to the manual. 10^6 cells in 100 μl were mixed with 2 μg of target plasmids. The mixture was transferred to cuvettes for electroporation with Nucleofactor 2b (Lonza) using the program D-023. After electroporation, complete medium was immediately added to promote recovery. The electroporated cells were subsequently divided equally into 2 wells, with one well left unstimulated and the other stimulated with 1 μg/ml anti-CD40, 1 ng/ml TGF-β1 and 12.5 ng/ml IL-4 for 3 d.

C. albicans culture

A single colony of *C. albicans* was cultured in YPD broth at 30 ºC for 16 h with shaking at 220 rpm. *C. albicans* existed in the blastospore form after the 16 h culture. The concentration of the culture was quantitated using a hemocytometer. The culture was then diluted 1:10 with fresh YPD broth containing 10% (v/v) heat-inactivated FBS and grown at 37 ºC for 3 h with shaking at 220 rpm. An aliquot of the culture was removed and examined under the microscope to ensure that 95% of blastospores switched to the virulent pseudohyphal form. The culture was pelleted by centrifugation at 4,000 rpm for 10 minutes, washed with PBS twice and resuspended in PBS at the concentration of 5×10^6 CFU per 50 μl based on the quantitation of the culture 3 h ago. The pseudohyphae samples were used for either intradermal infection of mice or the preparation of heat-killed samples by treatment at 95 ºC for 2 h followed by 3 rounds of sonication on ice at 30% maximum power for 5 seconds per round using a sonifier.

Cutaneous *C. albicans* infection

5×10^7 purified *Aire*$^{+/+}$ or *Aire*$^{-/-}$ B cells were introduced via the tail vein into each recipient μMT mouse littermate. Starting from the day of adoptive transfer, 5 doses each of 10^6 CFU heat-killed *C. albicans* pseudohyphae were given intraperitoneally to each recipient mouse every 4 d. Four days after the last injection, mice were infected with 5×10^6 CFU live *C. albicans* pseudohyphae in 50 μl PBS per spot at the deep dermis of the shaved dorsal region (Conti et al., 2014). The actual dose of infection was determined by immediately plating serial dilutions of the inoculum on YPD agar in triplicate, incubating the plates at 28 ºC for 24 h and colony enumeration. The inoculum size per spot ranged between $3.8–12.3\times10^6$ CFU in various experiments. Four days after the infection, blood was obtained prior to sacrificing the mice. The entire dermal injection site was excised for histological evaluation of fungal burden by Grocott's methenamine silver (GMS) stain or by plating, or for determination of effector T cell response by flow cytometry. For GMS stain, the tissues were immediately fixed in 10% formalin overnight and embedded in paraffin before sectioning. For plating, each tissue was weighed, minced, grounded thoroughly and resuspended in sterile PBS. Serial dilutions of the suspensions were plated on YPD agar in triplicate and incubated at 28 ºC for 24 h before colony enumeration. The fungal load was calculated as CFU per mg of tissue. For flow cytometry, the tissues were washed in FBS-free RPMI-1640 twice, minced and digested in FBS-free RPMI-1640 containing 0.7 mg/ml collagenase II, 2 mM EDTA and 25 mM HEPES at 37 ºC for 1 h. The digested samples were passed through a 70 μm cell strainer, washed twice with RPMI-1640 containing 10% FBS, 2 mg/ml glutamine, 100 U/ml penicillin, 100 μg/ml streptomycin and 25 μg/ml amphotericin B. The samples were then cultured in this medium further supplemented with 500 ng/ml PMA, 500

ng/ml ionomycin and 1 μg/ml GolgiPlug at 37 ºC for 5 h before being harvested for flow cytometric analysis.

Immunoprecipitation

Cultured cells were harvested, washed with cold PBS twice and lysed with a CelLytic M buffer containing 1× protease inhibitor cocktail and 1× Halt phosphatase Inhibitor for 60 minutes on ice. The lysates were centrifuged at 18,000 g for 15 minutes at 4 ºC. Protein concentration in the supernatants was determined by a BCA Protein Assay Kit. Equal amounts of lysate supernatants were used for immunoprecipitation with specific or isotype control antibodies using protein G magnetic beads (Cell Signaling 8740 or Thermo Fisher Scientific 88847) according to the manufacturers' instructions.

RNA extraction and quantitative real-time polymerase chain reaction

RNA was extracted from cells or tissues other than those from the APS-1 patients using TRIzol. cDNA synthesis was performed using the Superscript III first strand synthesis system in a thermocycler (Bio-Rad T100). qRT-PCR was performed with PowerSYBR Green Master Mix on a StepOnePlus instrument (Applied Biosystems) using pairs of sense and anti-sense primers targeting the genes of interest. For APS-1 patients' peripheral blood $IgD^{+}CD27^{-}$ B cells, following stimulation, the cells were washed and stored in RNAlater. Prior to RNA isolation, cells were pelleted at 5,000 g for 5 min and the RNAlater was removed. The cells were washed once with ice-cold PBS. RNA was isolated using the lysis and stop solutions in a Cells-to-C_T 1-step SYBR Green kit (Thermo Fisher Scientific A25601) and amplified using an iTaq Universal SYBR Green One-Step kit (Bio-Rad 172-5150) on a StepOnePlus instrument using pairs of sense and anti-sense primers targeting the genes of interest. The *ACTB* (*Actb*) gene was used as an internal control for normalization.

Chromatin immunoprecipitation and quantitative real-time PCR

ChIP was performed using a ChIP assay kit based on the manufacturer's instructions with slight modifications. Following 3 d of stimulation of 10^6 CH12 cells as described above, formaldehyde was added to the culture to the final concentration of 1% and incubated for 10 minutes at 37 ºC to crosslink chromatin. The cells were pelleted, washed twice in PBS, resuspended in an SDS lysis buffer (1% SDS, 10 mM EDTA, 50 mM Tris, pH 8.1) for 10 minutes on ice. DNA was sheared by 3 rounds of sonication on ice at 30% maximum power for 3 seconds per round using a sonifier (Thermo Fisher Scientific Q500). After centrifugation at 13,000rpm for 10 minutes, the supernatants were harvested, diluted 10-fold in a ChIP dilution buffer (0.01% SDS, 1.1% Triton X-100, 1.2 mM EDTA, 16.7 mM Tris-HCl, 167 mM NaCl, pH 8.1) containing protease inhibitors, and precleared with 50% protein A agarose/salmon sperm DNA slurry for 30 minutes at 4 ºC with rotation. After setting aside an aliquot as input, An AID or control antibody was then added and incubated overnight at 4 ºC with rotation, followed by the addition of 50% protein A agarose/salmon sperm DNA slurry for 1 h at 4 ºC with rotation. The agarose was then pelleted and sequentially washed once with the low salt wash buffer, once with the high salt wash buffer, once with the LiCl wash buffer and twice with TE buffer, all of which were components of the kit. DNA in the bound chromatin was eluted from the beads using an elution buffer (1% SDS, 0.1 M $NaHCO_3$, pH 8.0), reverse-crosslinked from proteins by incubation at 65 ºC for 4 h in the presence of 200 mM NaCl, cleaned by 20 μg/ml RNase A treatment for 30 minutes at 37 ºC followed by 40 μg/ml proteinase K treatment for 1 h at 45 ºC, purified using phenol/chloroform extraction followed by ethanol precipitation with carrier glycogen according to the kit's manual and resuspended in TE buffer for quantitative real-time PCR analysis using PowerSYBR Green Master Mix on a StepOnePlus instrument (Applied Biosystems). The fold enrichment of DNA

was calculated using the $\Delta\Delta C_T$ method with control antibody-precipitated samples as an internal reference, and further compared among different CH12 cells and treatments.

Protein extraction and Western Blot

Cells were pelleted and washed twice with ice-cold PBS, lysed with a pH 8.0 protein extraction buffer containing 20 mM Tris-HCl, 150 mM NaCl, 1% IGEPAL CA-630 (NP-40, Sigma-Aldrich I8896), 0.1% sodium dodecyl sulfate (SDS), 1 mM EDTA and protease and phosphatase inhibitor cocktail for 30 minutes on ice. Supernatants were collected after centrifugation, heated at 98 ºC in SDS sample buffer with 4% β-mercaptoethanol for 5 minutes to denature proteins. Proteins were resolved in 4–20% Bis-Tris gels or 10% Tris-Glycine gels and transferred to 0.2 µm polyvinylidene fluoride (PVDF) membranes. The membranes were blocked with 5% (w/v) non-fat milk in Tris-buffered saline with Tween-20 for 30 minutes to 1 h, incubated with primary antibodies overnight at 4 ºC and subsequently with secondary antibodies conjugated to HRP. Signals were visualized with clarity western-blot ECL substrate and exposed on autoradiograph films.

Genomic uracil quantitation

The uracils in genomic DNA were quantified using AA6 as described previously (Wei et al., 2017; Wei et al., 2015). CH12 cells were harvested by centrifugation and lysed by incubating for 1 h at 37°C in Tris-EDTA buffer (TE) containing 2 µg/ml RNase A (Sigma-Aldrich R6513) and 0.5% SDS, followed by incubation with 100 µg/ml Proteinase K (Qiagen 19131) at 56°C for 3 h. DNA was isolated by phenol:chloroform (1:1) extraction and ethanol precipitation and dissolved in TE. The DNA was then digested with HaeIII (New England BioLabs R0108) and purified as described above. Digested genomic DNA was incubated with 10 mM O-Allylhydroxylamine hydrochloride (Sigma-Aldrich 05983) for 1 h at 37°C to block the pre-existing aldehydic lesions

and the DNA was ethanol precipitated. The DNA was then treated with *E. coli* uracil DNA-glycosylase for 30 min at 37°C to excise uracils and create new abasic sites. The resulting abasic sites were labeled with 2 mM AA6 for 1 hour at 37°C and DNA was re-purified and dissolved in ddH_2O. AA6-tagged DNA was labeled with 1.7 µM DBCO-Cy5 (Click Chemistry Tools A130) under Cu-free conditions by shaking the reaction mixture for 2 h at 37°C. Labeled DNA was purified using the DNA Clean and Concentrator kit (Zymo research D4014). Genomic DNA from *E. coli* CJ236 strain served as the uracil standard. WT and bisulfite-treated *E. coli* DNA served respectively as the negative and the positive controls. DBCO-Cy5-labeled DNA was spotted onto a positively charged zeta probe membrane (Bio-Rad 1620153) using a vacuum filtration apparatus and the membrane was scanned using a Typhoon 9210 phosphor imager (GE Healthcare). Cy5 fluorescence was analyzed using the ImageQuant software.

Conventional flow cytometry

Cells were incubated with an Fc blocking reagent (Miltenyi Biotec 130-059-901 or Tonbo Biosciences 70-0161) and stained in PBS at 4°C with antibodies to various cell surface antigens. In the experiments that used NP_8-FITC and NP_{36}-PE to measure B cell affinity maturation, NP_8-FITC was added to the cells and incubated for 15 min before NP_{36}-PE was added. For the staining of intracellular molecules, cells were subsequently fixed and permeabilized using a CytoFix/CytoPerm kit or a Transcription Factor Buffer set. Isotype-matched control antibodies were used to define the baseline staining for the molecules of interest. Cells or beads stained with each fluorochrome were used to establish fluorescent compensation. 7-aminoactinomycin D (7-AAD, Tonbo Biosciences 13-6993-T500 or BD 559925) or Ghost Dye Violet 510 (GV510) was used to identify and exclude non-viable cells from the analysis. Events were acquired on an LSR II or LSR Fortessa flow cytometer (BD) and analyzed using FlowJo version 7 or 10 (Tree Star).

Imaging flow cytometry

$CD19^+$ B cells were purified from tonsillar cell suspensions by MACS with a biotinylated anti-CD19 antibody and anti-biotin microbeads. The cells were then incubated with an Fc blocking reagent and stained at 4°C with antibodies to surface IgD and CD38, fixed and permeabilized, and stained for AID and AIRE or with isotype control antibodies. Nuclei were counter stained with 4',6-diamidine-2'-phenylindole dihydrochloride (DAPI). Tonsillar cells stained with each fluorochrome were used to establish fluorescent compensation. Cells were imaged on an ImageStream X Mark II imaging flow cytometer (Amnis) and data were analyzed using IDEAS 6.1 (Amnis).

Immunofluorescence analysis

Frozen human tissues were stored at −80°C before 6-7 μm tissue sections were made using a cryostat (Leica CM1950). Sections were fixed with 4% paraformaldehyde, permeabilized in PBS containing 0.2% Triton X-100, incubated with Image-iT FX signal enhancer solution, blocked with PBS containing 1% BSA, 0.1% Triton X-100, 100 μg/ml human IgG (for human tissues only) and 10% serum from the source of the fluorochrome-conjugated antibodies, and stained with various combinations of primary antibodies against the molecules of interest, followed by appropriate fluorochrome-conjugated secondary antibodies. For Bcl-6 staining, the antibody used was not diluted and, instead, a large enough volume was used to cover the tissue section. For AIRE staining, a 1:25 dilution of the Miltenyi Biotec anti-AIRE-APC conjugated antibody was used. Nuclei were visualized with DAPI. Following washing, slides were mounted using a FluoroSave reagent and imaged on a confocal microscope (Zeiss LSM 780 or Leica TCS SP5). Pseudocolor images were processed using Photoshop CS6 (Adobe).

ELISA

ELISA to determine NP-specific antibody affinity maturation was performed as previously described (Ballon et al., 2011) with minor modifications in the reagents. Briefly, each serum sample was titrated on both NP_{29}-BSA- and NP_4-BSA-coated microtiter plates. The ratio of binding to NP_4-BSA and NP_{29}-BSA is an indicator of relative Ig affinity maturation. Bound antibodies were detected using horseradish peroxidase (HRP)-conjugated goat-anti-mouse IgG1, IgG2b or IgG. The colorimetric reaction was terminated with the addition of an equal volume of 1 M H_2SO_4 and quantitated on a microplate reader (BioTek Epoch) at 450 nm. ELISA to determine IgG1 and IgA secretion by *ex vivo* stimulated mouse B cells was performed using a mouse IgG1 or IgA quantitation set. Anti-IL-17A, IL-17F and IL-22 autoantibodies in the mouse sera were measured using microtiters plates coated with 1 μg/ml recombinant murine IL-17A, IL-17F or IL-22. The plates were blocked with 10% BSA in PBS, washed, incubated with mouse serum samples, washed and then incubated with an alkaline phosphatase (ALP)-conjugated horse-anti-mouse IgG antibody (1:500). Following washing, the colorimetric reaction was developed using the BluePhos phosphatase substrate system and quantitated on a microplate reader (BioTek Epoch) at 620 nm. For the measurement of autoantibodies that block the binding of IL-17A, IL-17F and IL-22 to their receptors, mouse sera were incubated at 4°C overnight with HRP-conjugated IL-17A, IL-17F or IL-22 of the optimized concentrations, and the mixtures were added to microtiter plates coated with IL-17RA homodimer or IL-22Rα1 after the plates were blocked with 10% BSA in PBS. The plates were then incubated at room temperature for 1 hour and washed. The colorimetric reaction was developed and terminated with the addition of an equal volume of 1 M H_2SO_4 and quantitated on a microplate reader at 450 nm.

IgHV repertoire and mutation analysis

Live (7-AAD$^-$) unswitched (IgM$^+$IgD$^+$) or switched (IgM$^-$IgD$^-$) NP-specific B cells (CD19$^+$B220$^+$NP$_{36}^+$) in the spleens of immunized μMT recipients were sorted using a SONY SH800 cell sorter (SONY Biotechnology) and resuspended in RNAProtect solution. High-throughput IgHV repertoire profiling by RNA-Seq was performed iRepertoire, Inc. (Huntsville, AL, USA). The raw sequences were processed and analyzed using the IMonitor 1.1.0 pipeline (Zhang et al., 2015). With this pipeline tool, each sequence was mapped to the *Mus musculus* germline V-D-J sequences (IMGT, http://www.imgt.org/vquest/refseqh.html) to identify the V, D and J gene segments and the CDRs, which were also used for clonal clustering. The sequences observed only once in a sample were filtered off to reduce the sequencing error. Subsequently, the sequences were normalized according to the number of cells in each sample. By comparing the sequence of each clone with the germline sequence, the mismatches of nucleotides were regarded as potential mutations. To eliminate PCR noise and sequencing errors, the first 25 bp of the sequences corresponding to the primer-binding site were excluded from the analysis, and the sequences were filtered if 3 successive mismatches were observed in them. Finally, the mutation rate for each IMGT position in the IgHV was calculated if the sequencing depth for that position was ≥10, and the frequency of each type of nucleotide substitution at these mutated positions were computed for each Ig isotype.

QUANTIFICATION AND STATISTICAL ANALYSIS

Statistical Analyses

All statistical analyses were performed using Excel or Prism. Graphs represent data from at least 2 independent experiments, each consisting of at least 3 biological replicates. The exact number of the biological replicates (*n*) in the presented data set are indicated in the figure legends.

Results are expressed as mean ± SEM. Pair-wise statistical difference was assessed by the parametric *t*-test or the non-parametric Mann-Whitney *U* test depending on the distribution of the data, which is stated in the figure legends. Multiple group comparisons were performed using 1-way ANOVA with Tukey's post hoc test. Differences were considered significant when *P* values were < 0.05. *P* values > 0.05 are either not shown, marked with NS (not significant), or indicated in the figure if they are close to 0.05. **P* < 0.05, ***P* < 0.01, ****P* < 0.001.

DATA AND SOFTWARE AVAILABILITY

Software Availability

All software used for the data analysis in this study is commercially or freely available. The IMonitor software used for immune repertoire analysis has been published (Zhang et al., 2015) and can be downloaded at https://github.com/zhangwei2015/IMonitor.

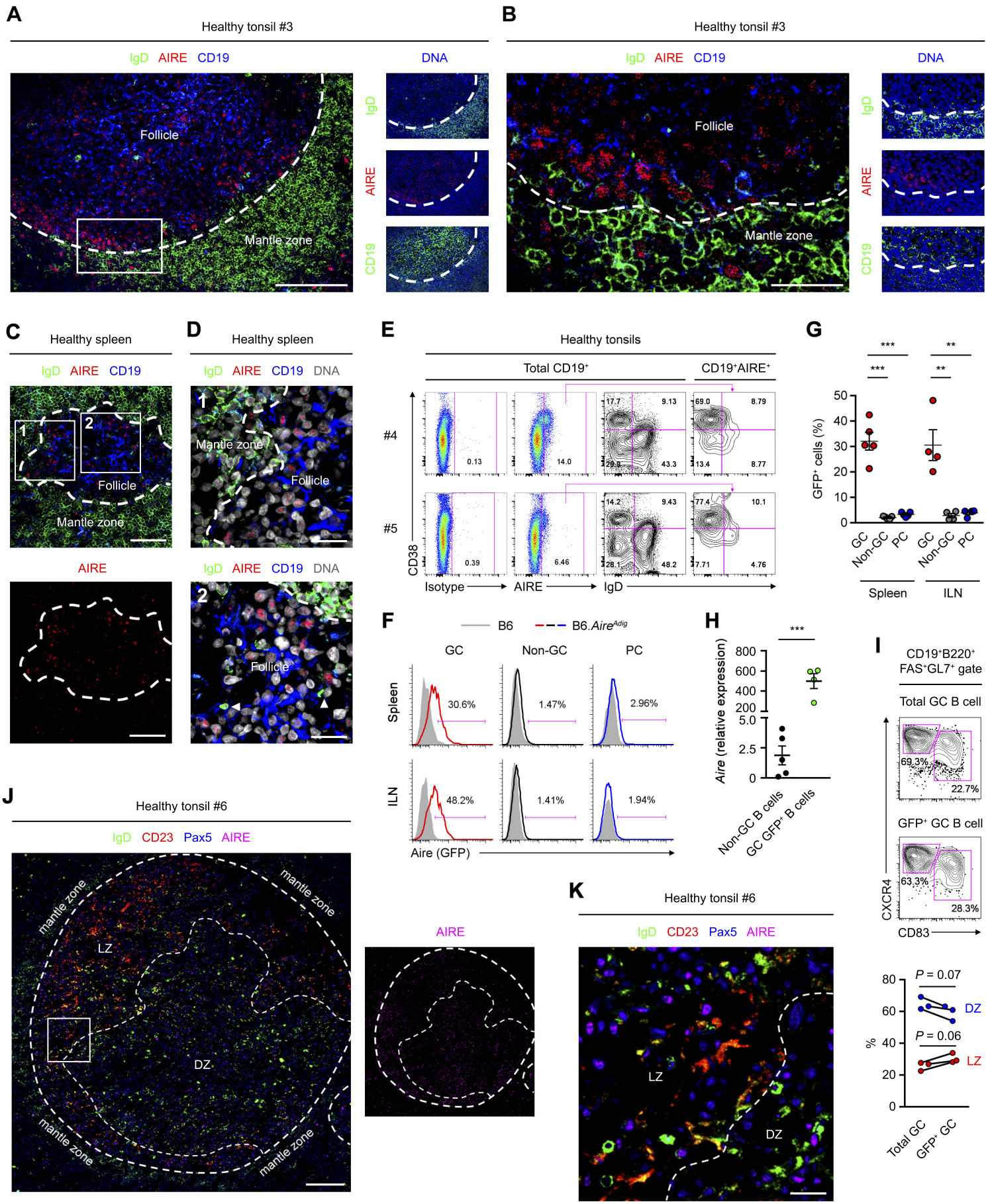

Figure 1

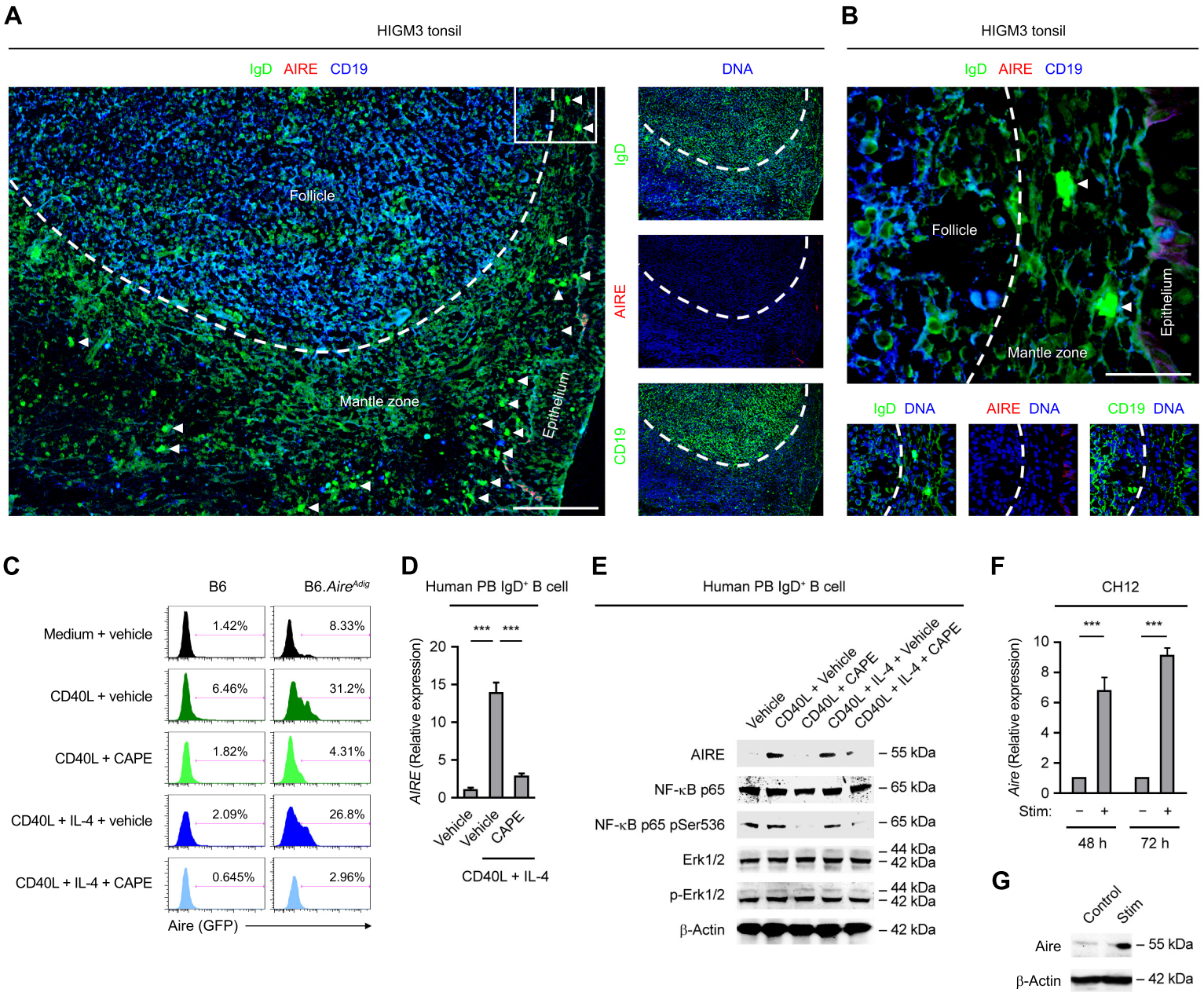

Figure 2

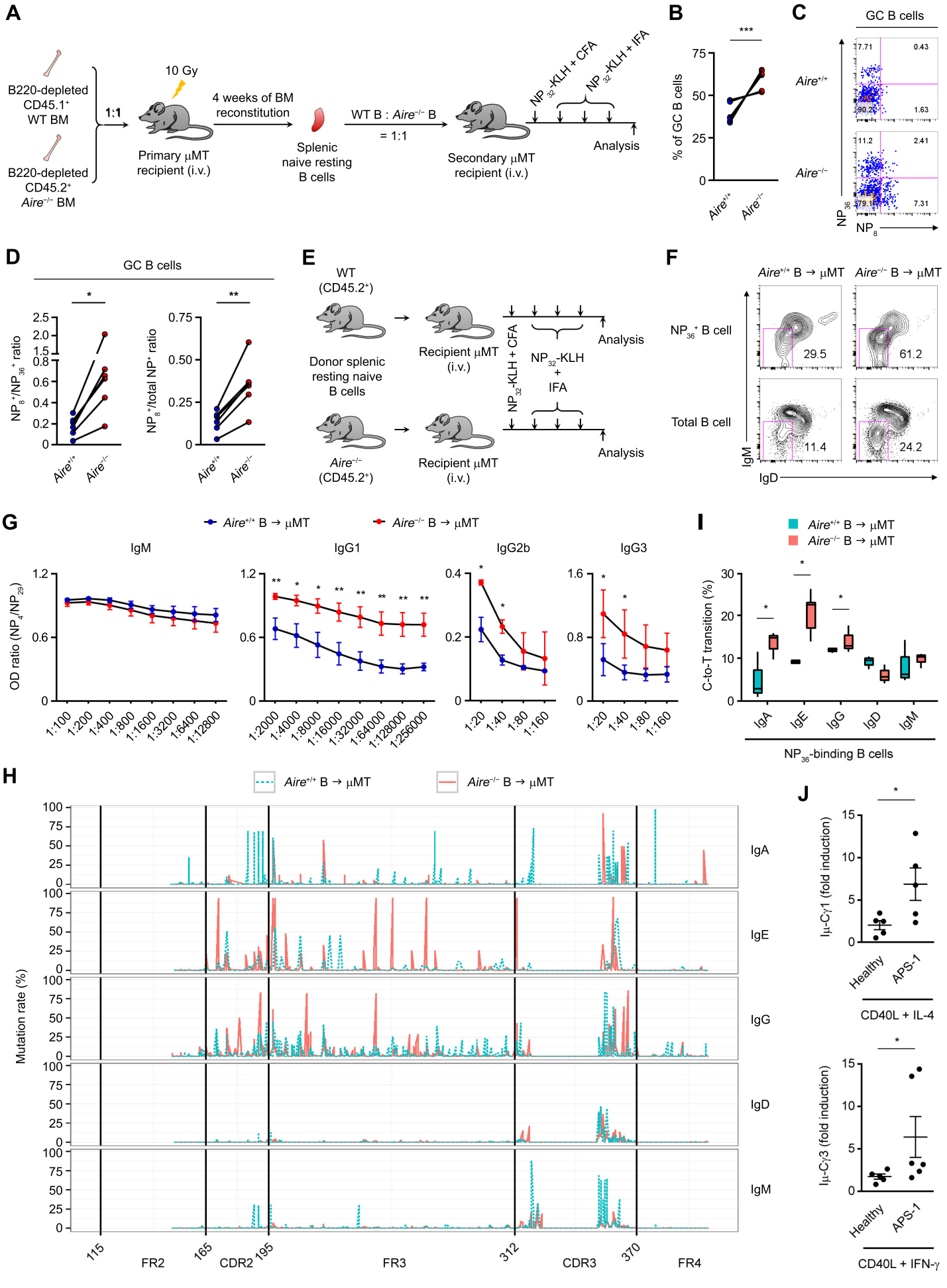

Figure 3

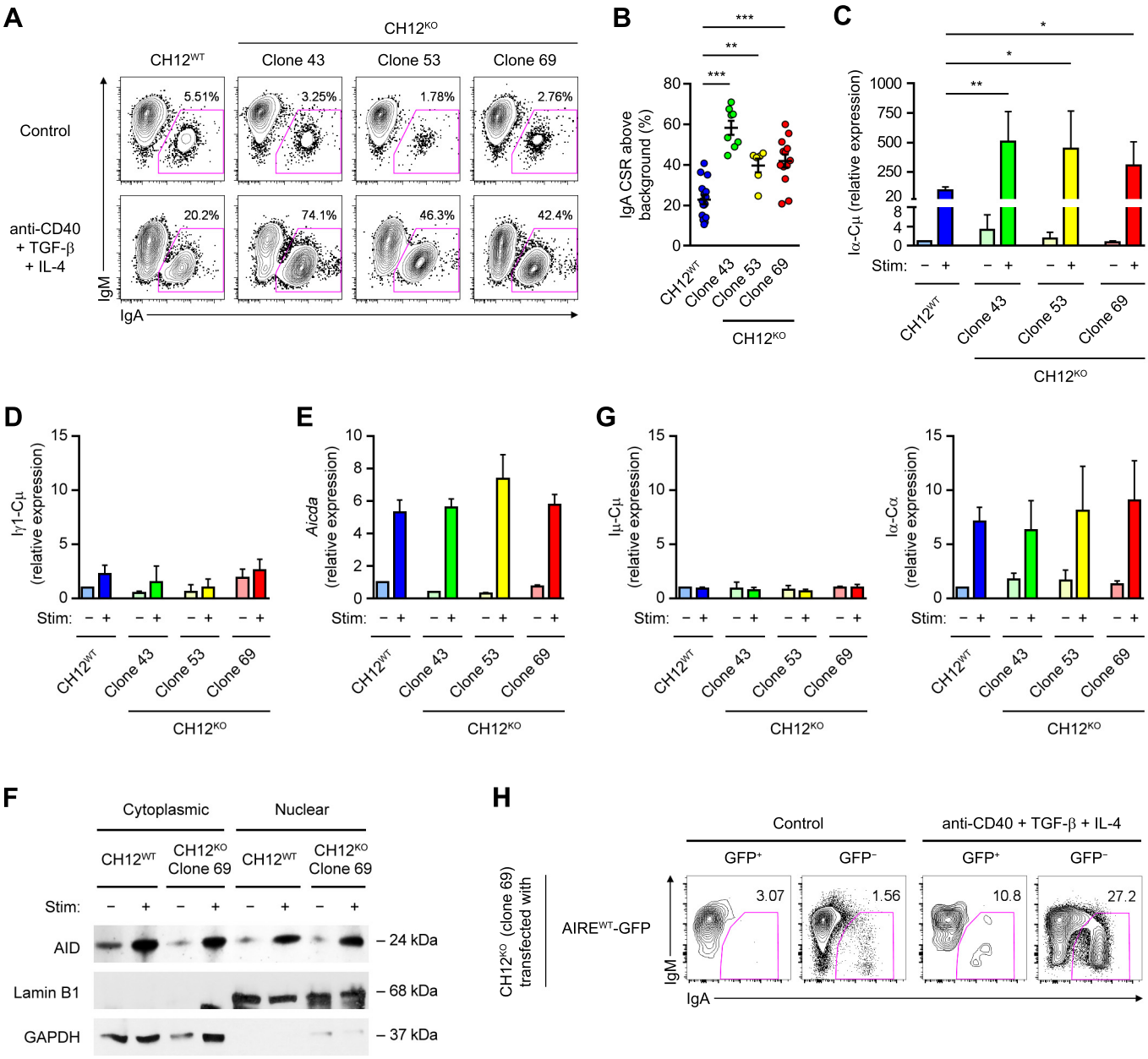

Figure 4

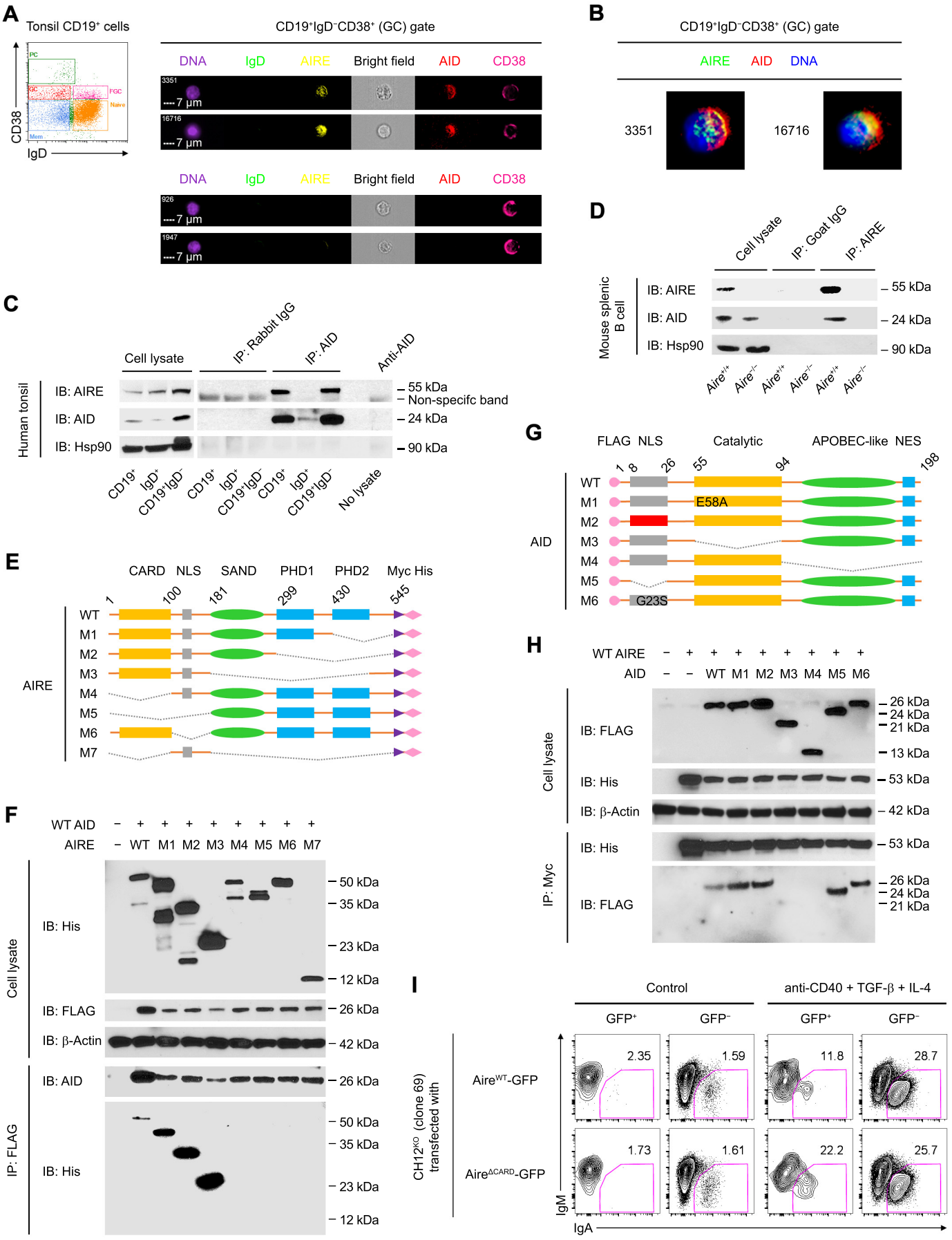

Figure 5

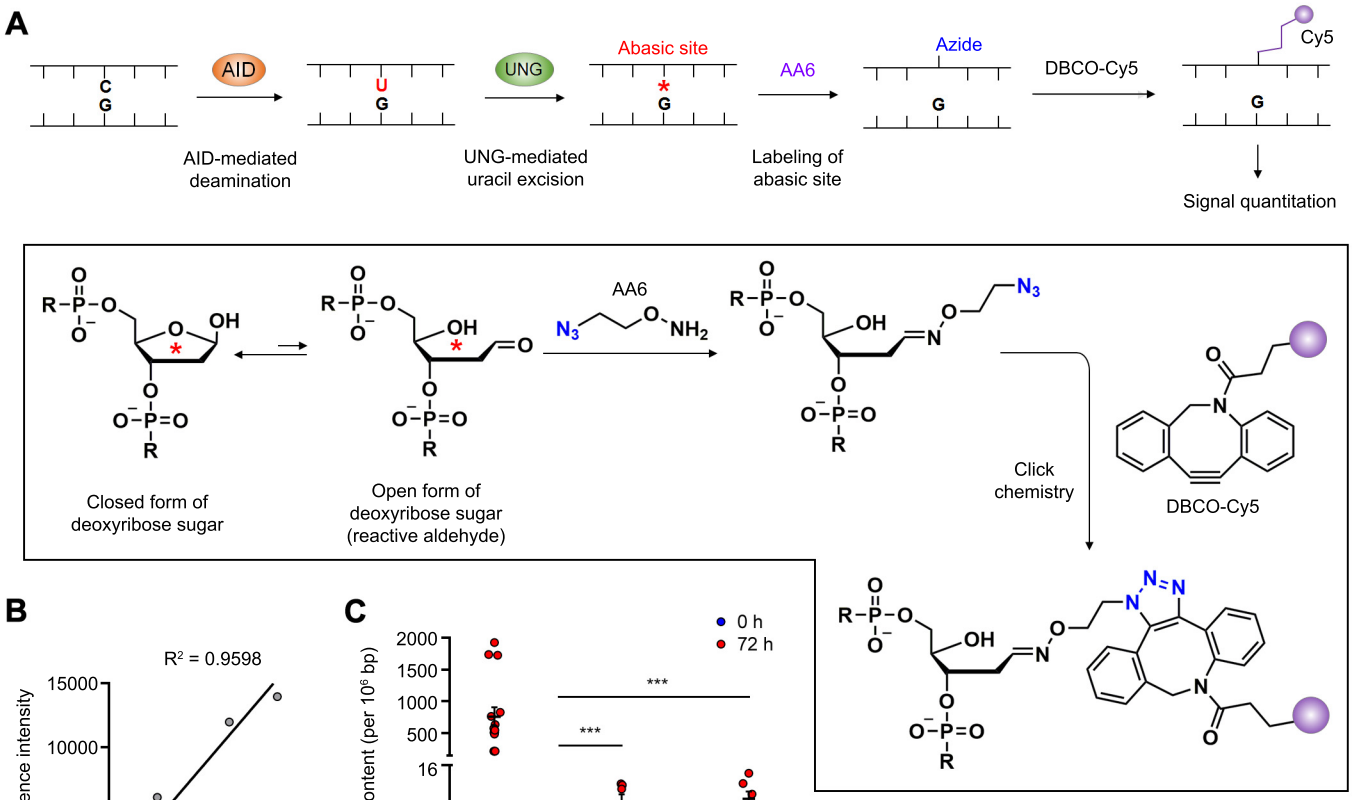

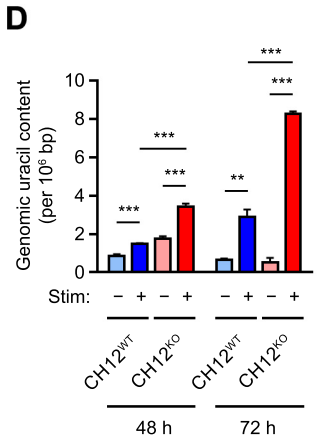

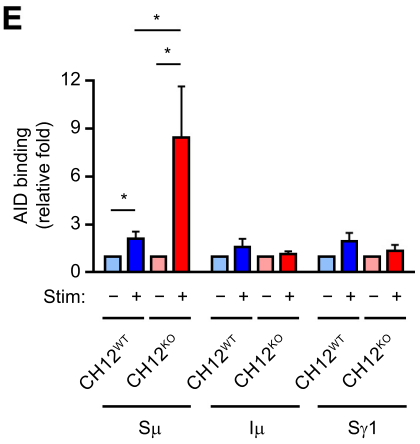

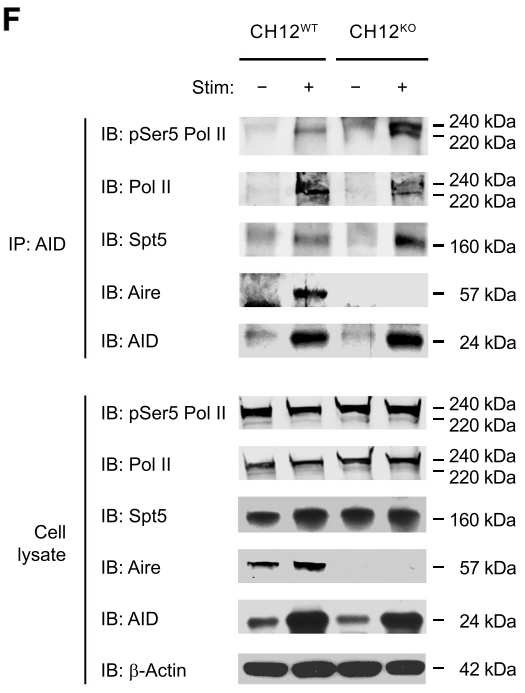

Figure 6

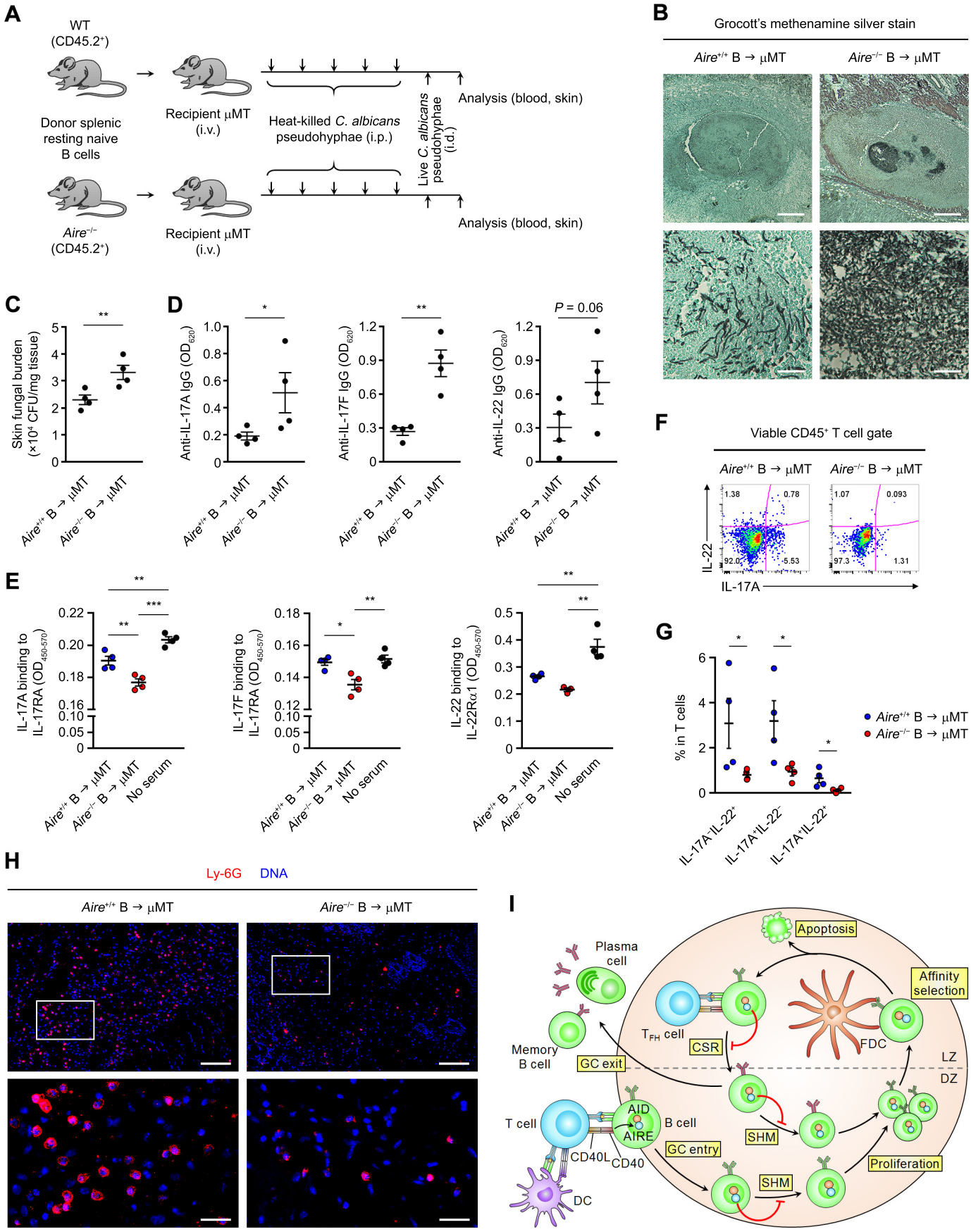

Figure 7

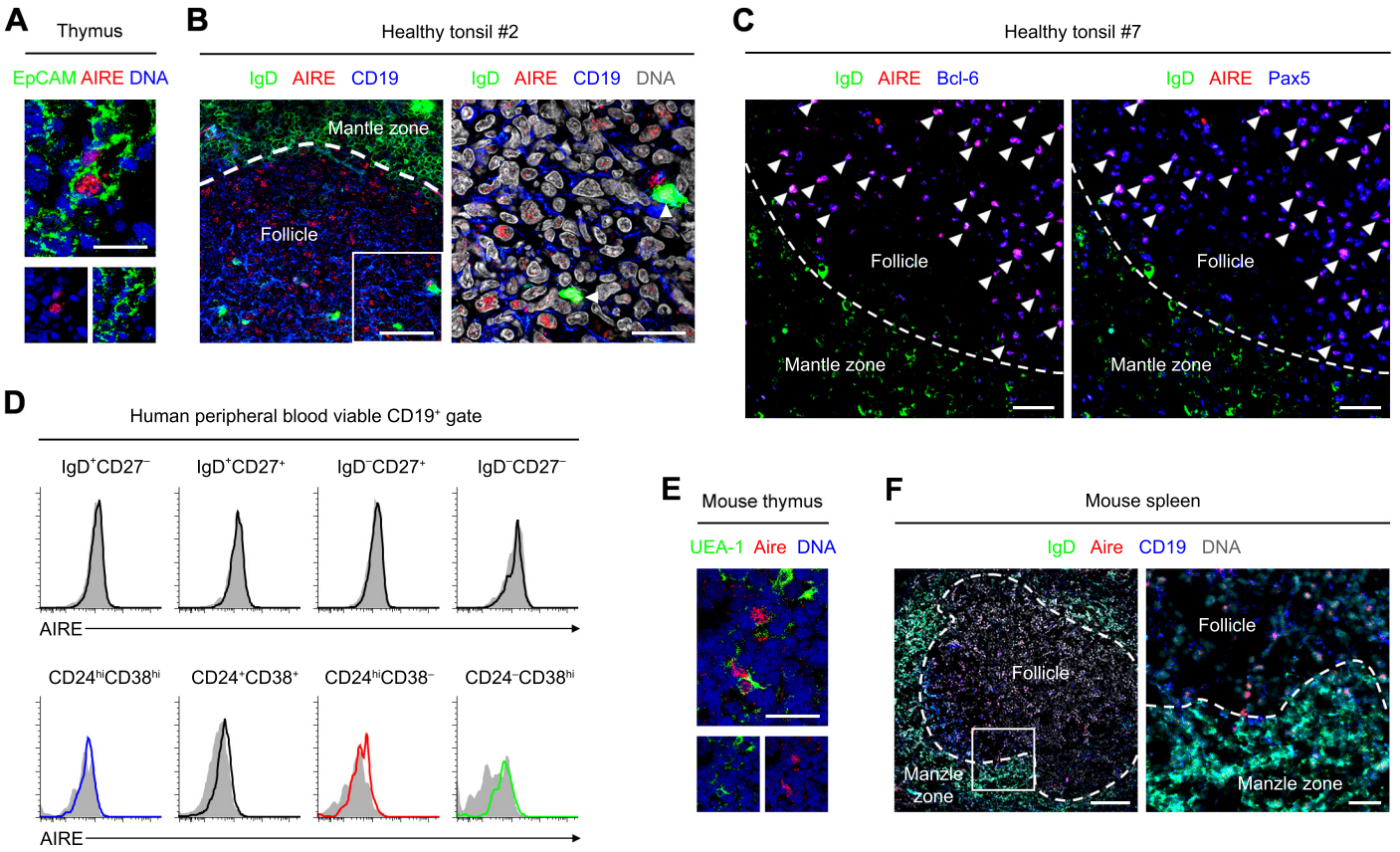

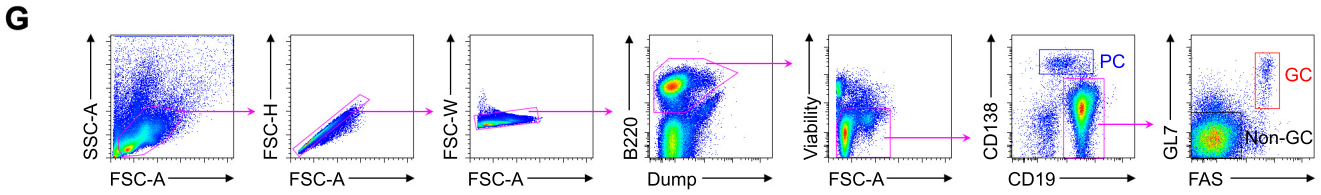

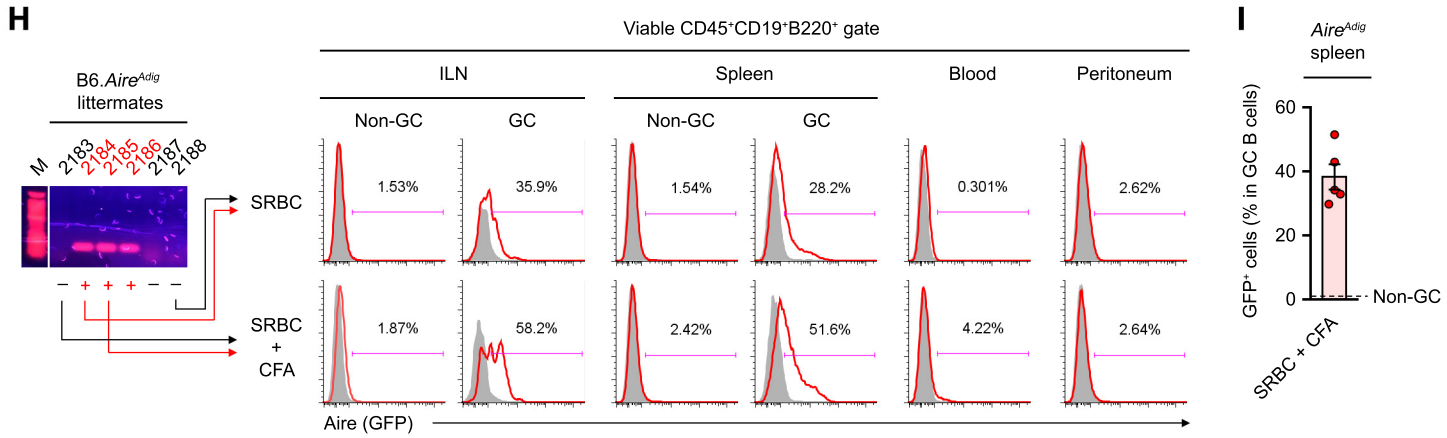

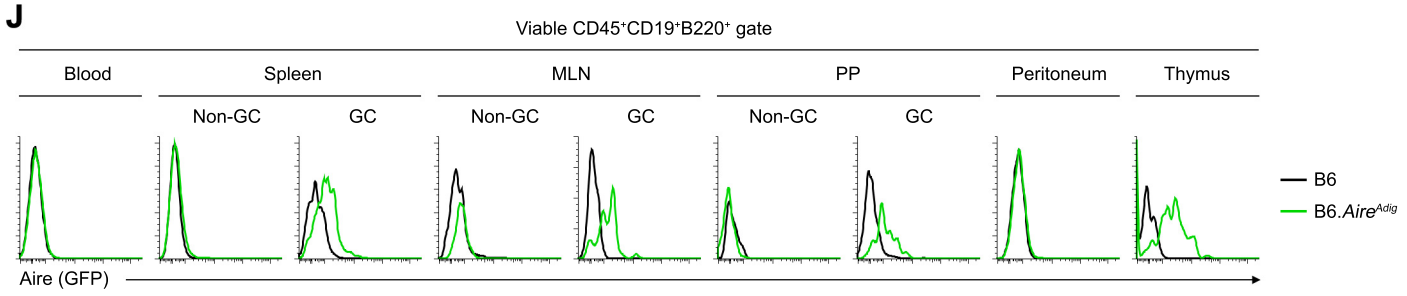

Figure S1

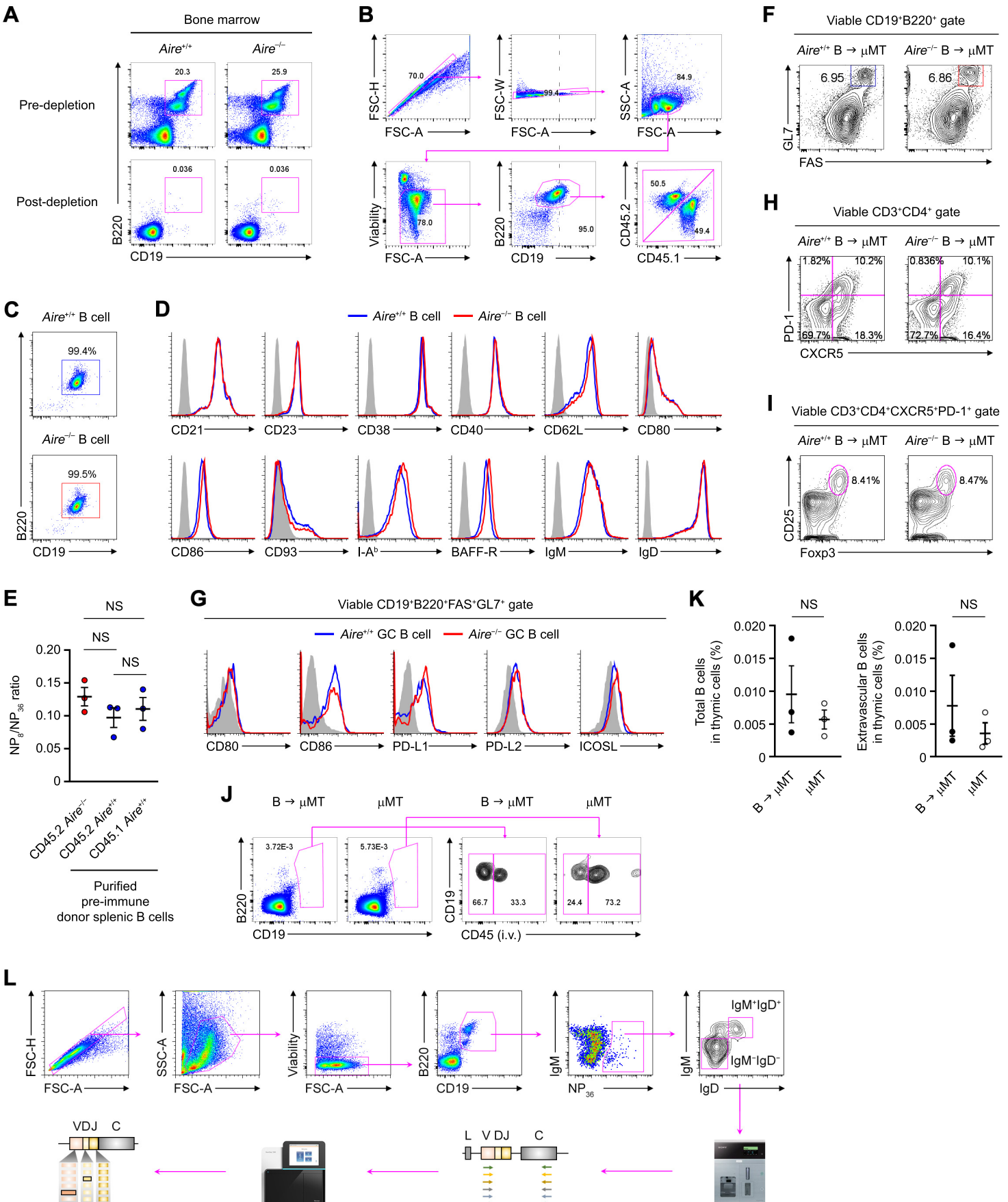

Figure S2

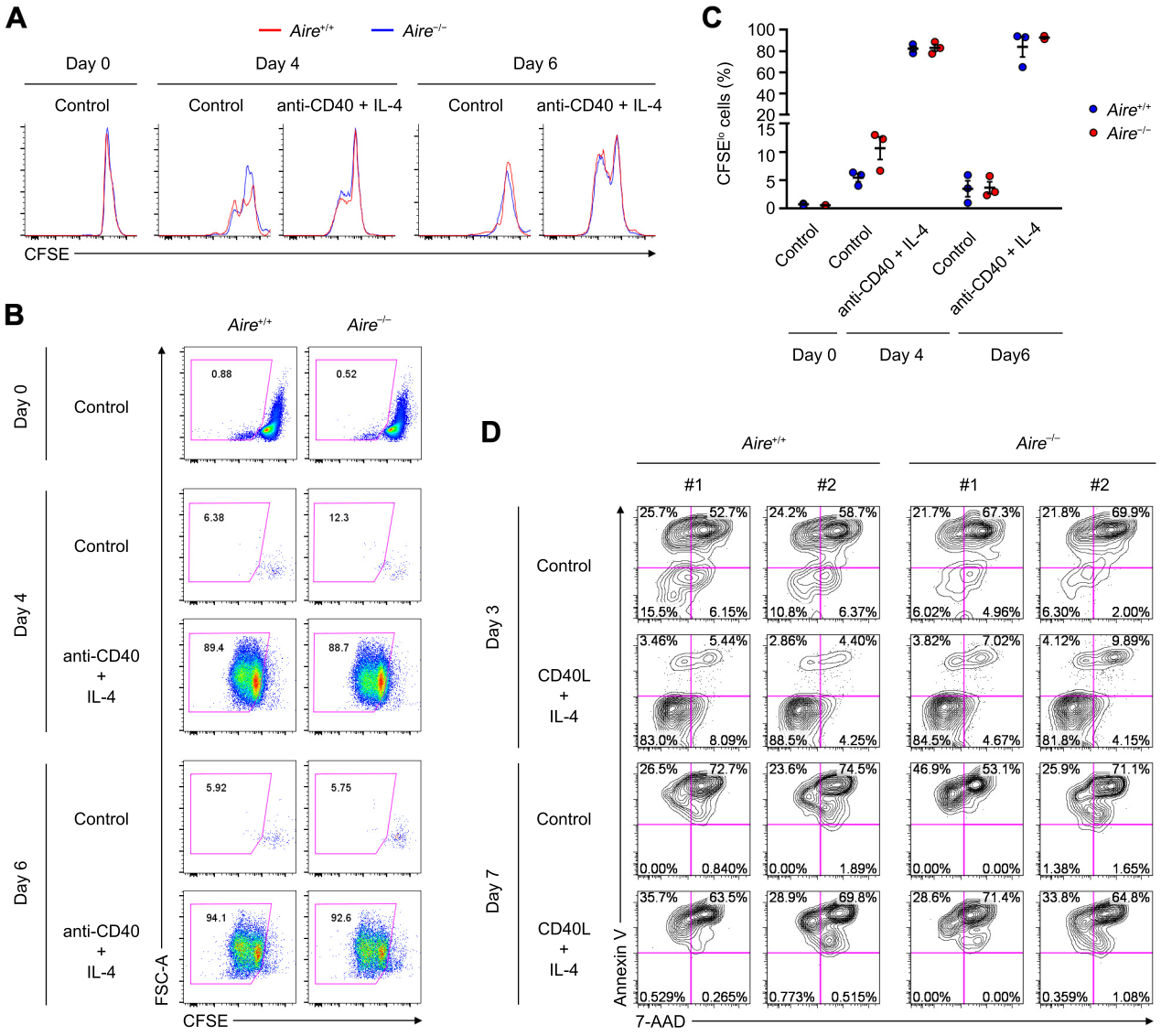

Figure S3

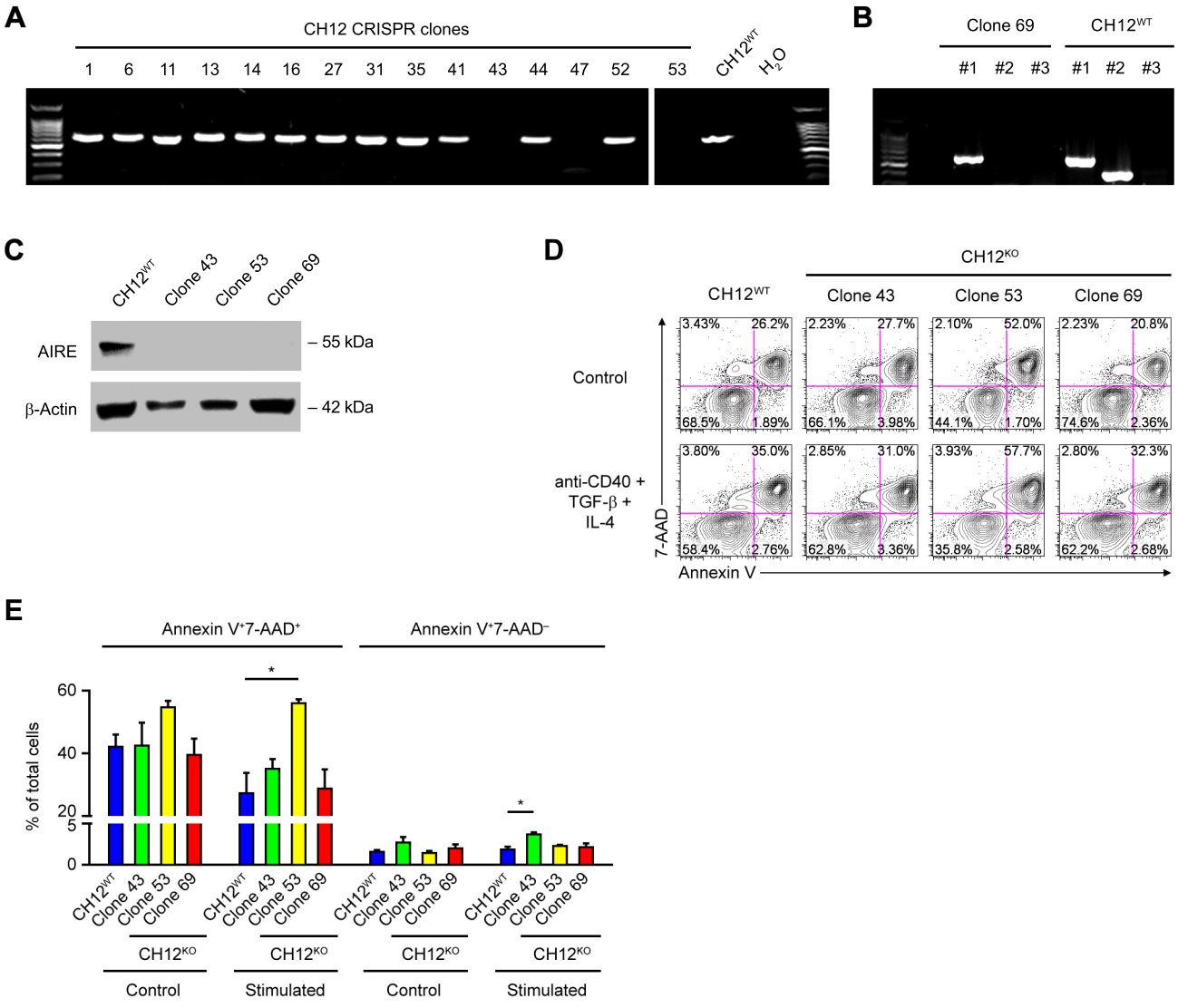

Figure S4

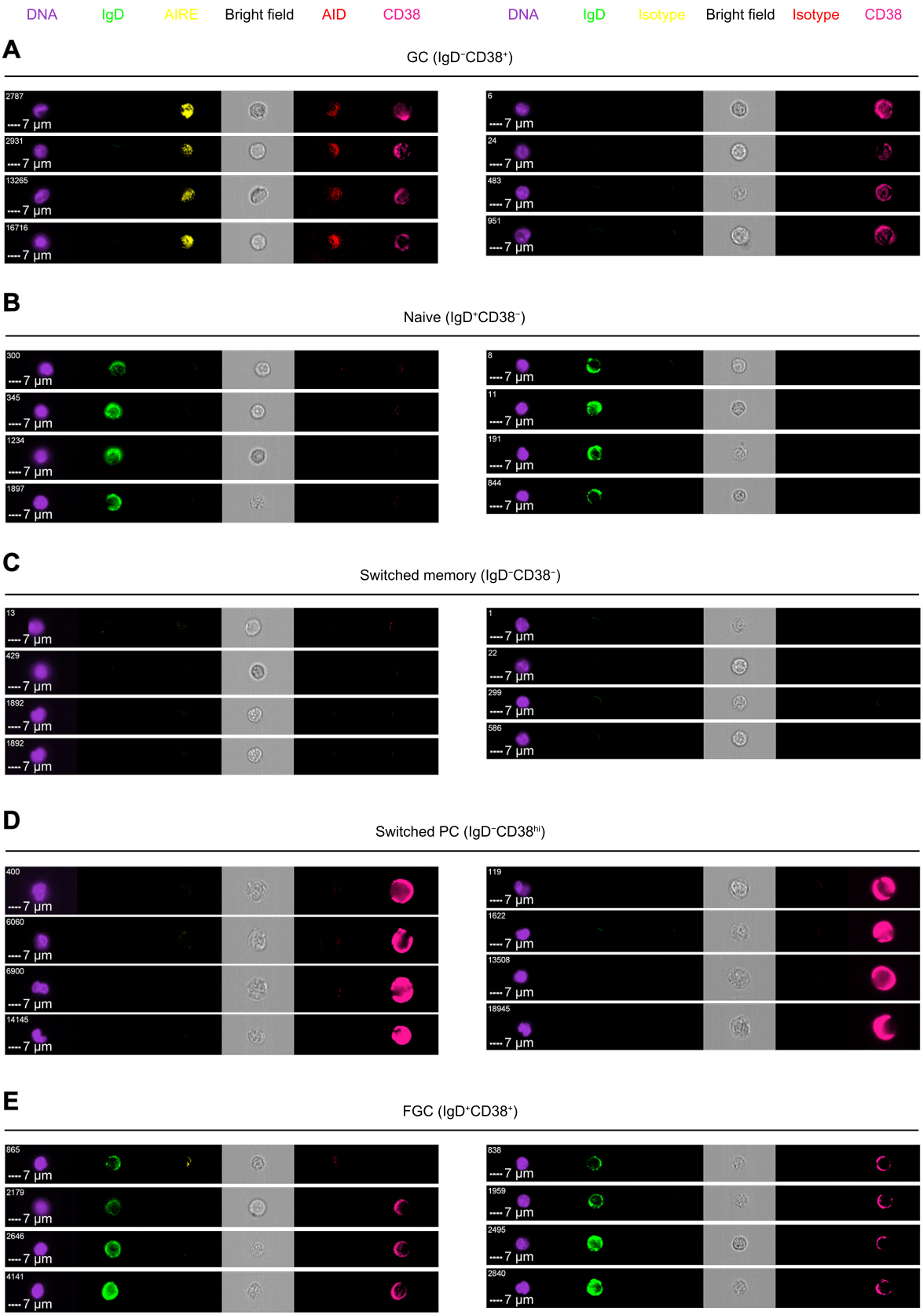

Figure S5

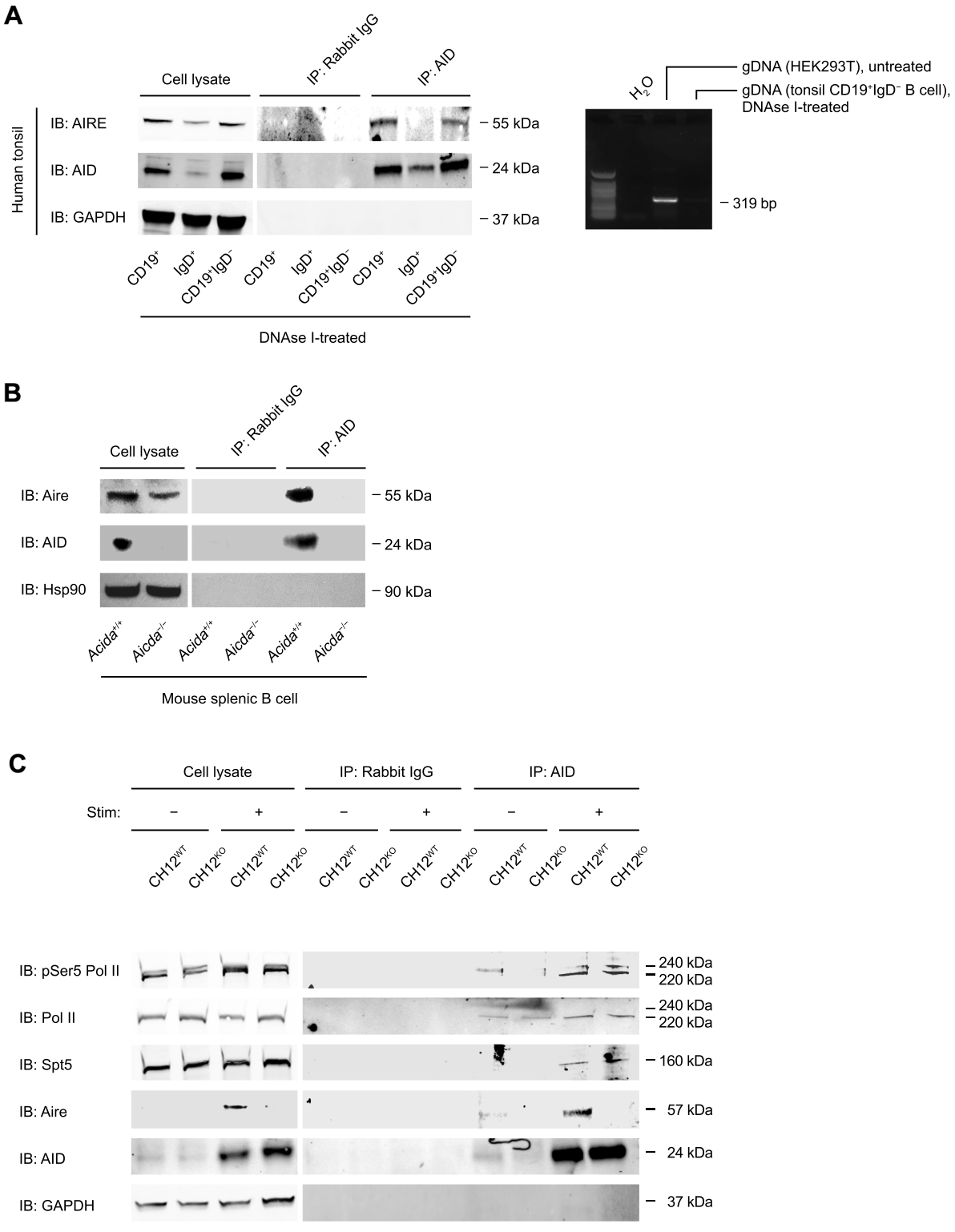

Figure S6

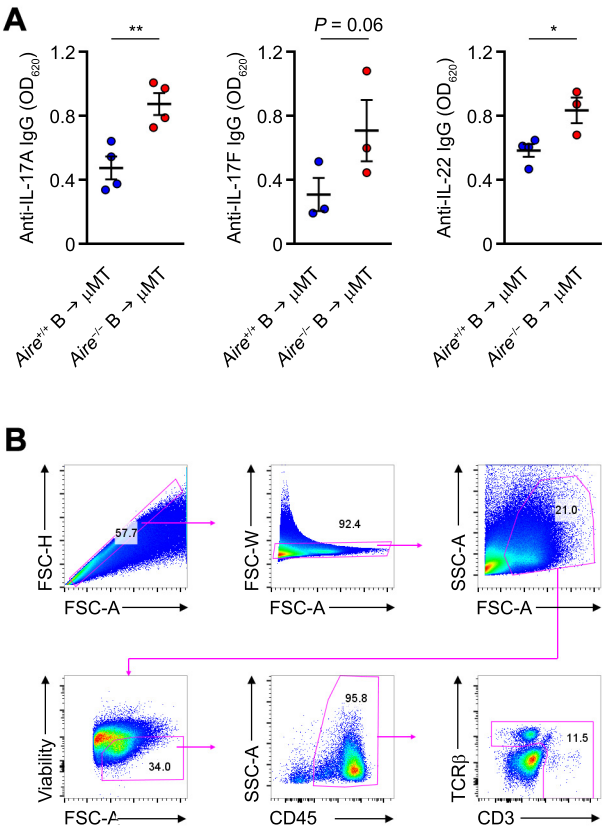

Figure S7